ELSEVIER
DEVELOPMENTS IN CLAY SCIENCE 5

HANDBOOK OF CLAY SCIENCE

SECOND EDITION

PART B: TECHNIQUES AND APPLICATIONS

EDITED BY
F. BERGAYA AND G. LAGALY

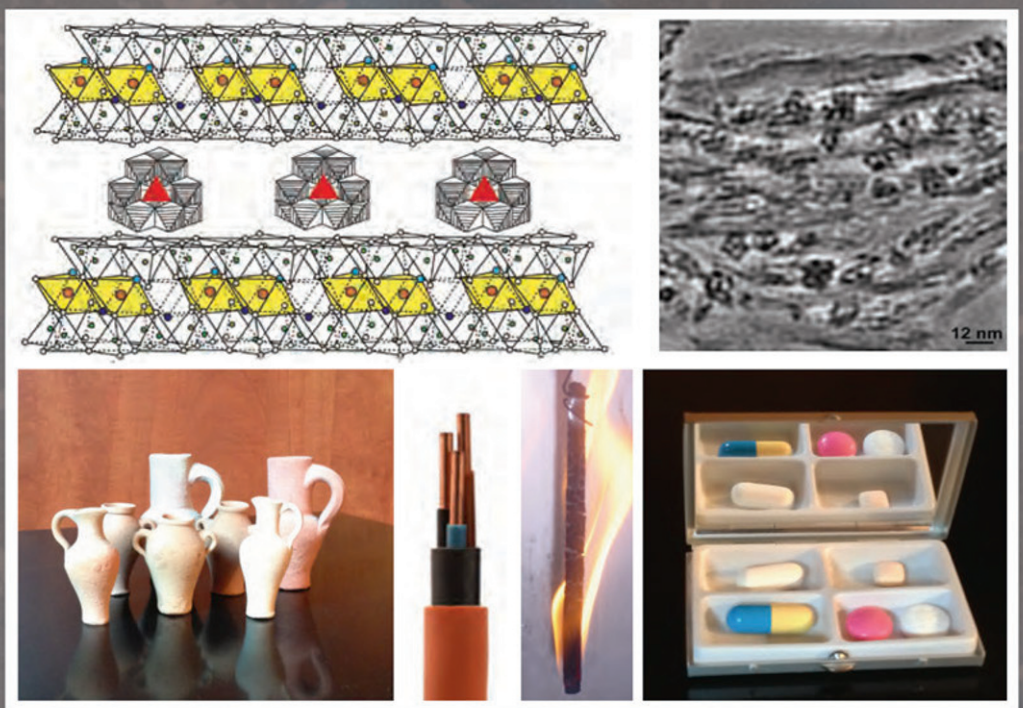

Developments in
Clay Science – Volume 5B

Handbook of Clay Science

Second Edition

Techniques and Applications

Faïza Bergaya
CRMD, CNRS-Université d'Orléans,
Orléans Cedex 2,
France

Gerhard Lagaly
Institut für Anorganische Chemie,
Christian-Albrechts-Universität zu Kiel, Kiel,
Germany

Amsterdam • Boston • Heidelberg • London • New York • Oxford
ELSEVIER Paris • San Diego • San Francisco • Singapore • Sydney • Tokyo

Chapter 2.3

X-ray Identification of Mixed-Layer Structures. Modelling of Diffraction Effects

B.A. Sakharov[a] and B. Lanson[b]

[a]*Geological Institute, Russian Academy of Sciences, Moscow, Russian Federation*

[b]*Mineralogy & Environments, ISTerre, University Grenoble 1 – CNRS, Grenoble, France*

Chapter Outline

Developments in Clay Science, Vol. 5B. http://dx.doi.org/10.1016/B978-0-08-098259-5.00005-6

Mixed-layer structures are remarkable examples of the order/disorder observed in natural (e.g. clay minerals and layered oxides) and synthetic (e.g. carbons, layered double hydroxides, layered dichalcogenides, and high-temperature superconductors) lamellar crystals. Mixed-layer structures consist in the alternation either of layers exhibiting contrasting structures, compositions, and basal distances or of layers having similar basal distances but differing by their internal structures or stacking mode, that is exhibiting different layer displacement or rotation between consecutive layers. The different layer types can co-exist in variable proportions within the crystal and define a variety of layer stacking sequences.

Two main categories of mixed-layer structures can be singled out depending on the actual distribution of interstratified layer types. The first corresponds to regular structures in which different layer types alternate periodically, usually along the axis perpendicular to the layer plane (the c^*-axis). When they were naturally occurring, such mixed-layer structures were often given mineral names, as they had strictly periodic structures and were also often considered as distinct phases. Chlorites and corrensite are two examples of such structures that can be described as regular talc–brucite and chlorite–smectite, respectively. Within the material chemistry community, these regular alternations of different layer types are known as the 'staging' phenomenon, the nth staging corresponding to the systematic occurrence of a given layer type at every nth layer (Fogg et al., 1998; Ijdo and Pinnavaia, 1998). When the different layer types have the same structure but differ in their layer displacement, their regular alternation defines polytypic variants of a given mineral/species.

In the second type of mixed-layer structures, the different layer types either alternate at random or tend to some sort of ordering (avoiding, for example, the existence of pairs of the minor layer type) or segregation (clustering layers of a given type). In this case, and if interstratified layers have significantly different thicknesses and structures, the resulting reflection positions do not obey Bragg's law but form a non-rational series ($d_{001} \neq l \times d_{00l}$) leading to an apparent lack of physical meaning for the observed peak positions. The second type of mixed-layer structures also includes structures in which the respective thicknesses of interstratified layers are multiples of each other (e.g. chlorite–serpentine). In this case, the positions of reflections corresponding to the mixed-layer structure form a rational series, and the identification of the interstratified character of the structure then requires a more detailed analysis of peak position, profiles (especially width), and relative intensities for different reflections (Moore and Reynolds, 1997; Drits, 2003). Finally, the second type of mixed-layer structures includes structures in which interstratified layers have approximately the same thickness but distinct structures or layer displacement. In this case, only the positions of non-basal reflections are affected. These reflections form non-rational series as basal reflections for mixed-layer structures in which interstratified layers have significantly different thicknesses and structures. Within this last type of mixed-layer structures, additional variety can arise from the possible incommensurability of the interstratified layers within the **a**–**b** plane.

The sustained interest in mixed-layer structures arises from their reactivity, which is reinforced by their anisotropic character. In particular, the intercalation properties of lamellar compounds, including clay minerals, have drawn the attention of the material chemistry community for the last few decades with the view to prepare polyfunctional materials. Similarly, the reactivity of natural layered silicates in response to their environmental conditions was thoroughly investigated both for its potential ability to record temperature and/or pressure paleo-conditions, and for assessing the possible impact of these minerals on their environment, in particular in the context of waste storage. Lanson (2011) recently reviewed the efforts dedicated to the structural characterization of mixed-layer structures, essentially using X-ray diffraction (XRD) in the fields of materials chemistry and (clay) mineralogy (layered silicates, layered oxides, and layered double hydroxides). This author stressed the necessity of a direct quantitative comparison between experimental and calculated XRD patterns to determine the crystal chemistry of mixed-layer structures. He also showed that mixed-layer structures containing three, or more, layer types may be extremely common, the main reasons for their scarce description in the literature being the lack of adapted calculation routines.

This chapter thus proposes a thorough description of theoretical concepts allowing the calculation of diffraction effects from mixed-layer structures with any layer types and ordering parameters using the matrix formalism. It also includes algorithms allowing a comprehensive determination of the probability parameters required to describe layer stacking in mixed-layer structures. Finally, all recent developments that have proved to be necessary to fit XRD data from mixed-layer structures (fluctuations of layer thickness, presence of inter-crystalline defects, contrasting nature of crystal external edges, etc.) are described, and the equations necessary for the calculation of induced diffraction effects derived.

2.3.1 DIFFRACTION INVESTIGATION OF MIXED-LAYER STRUCTURES

2.3.1.1 Diffraction Fundamentals

A scattering entity may be considered as an ensemble of elementary scatterers or atoms, with an individual scattering power.[1] When interacting with the primary X-ray beam, these elementary scatterers act as a source of scattered waves. According to the kinematic theory of diffraction, the wavelength of these secondary waves is unaffected by the scattering, and their amplitude is much lower than that of the primary waves. Secondary waves are scattered in all directions, their

1. The scattering power of an atom, particle, or object is the amplitude ratio of X-rays scattered in a given direction and with a given wavelength by this element to that scattered by a free electron. The scattering power of an atom is known as its 'atomic scattering amplitude' and expressed in electron units.

relative phases in a given direction depending on the mutual arrangement of elementary scatterers in the scattering entity. Constructive, or destructive, interferences of secondary waves induce a modulation of the diffracted intensity as a function of the direction considered. Figure 2.3.1A shows two elementary scatterers, one at the origin of the coordinate system (in C) and the other shifted by vector **r** (in B). The directions of incident and scattered waves are indicated by the unit vectors $\mathbf{k}_0$ and **k**, respectively. The distances covered by the waves scattered at the origin and at the end of vector **r** differ in their length: $\Delta = (AB - CD) = -[(\mathbf{k} - \mathbf{k}_0) \cdot \mathbf{r}]$, where $[(\mathbf{k} - \mathbf{k}_0) \cdot \mathbf{r}]$ is the scalar product of the two vectors. The path difference between the two waves determines their phase shift: $\varphi = \frac{2\pi}{\lambda}\Delta = -\frac{2\pi}{\lambda}[(\mathbf{k} - \mathbf{k}_0) \cdot \mathbf{r}]$.

Waves scattered at the origin (in C) are thus ahead of phase by φ compared to those scattered at the end of vector **r** (in B). Vector $\mathbf{s} = (\mathbf{k} - \mathbf{k}_0)/\lambda$ is defined symmetrically with respect to the incident and diffracted beams (Fig. 2.3.1B), thus leading to $s = 2 \sin \theta/\lambda$, θ being half of the diffraction angle. The scalar

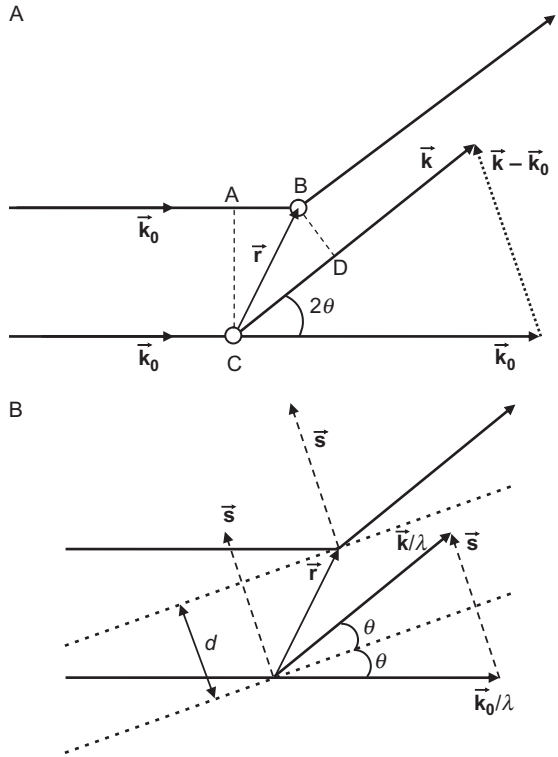

FIGURE 2.3.1 (A) Schematic representation of incident ($\mathbf{k}_0$) and diffracted (**k**) beams for two elementary scatterers located at the origin and at the end of vector **r** (C and B, respectively). (B) Definition of vector $\mathbf{s} = (\mathbf{k} - \mathbf{k}_0)/\lambda$ and of the path difference between waves diffracted by planes perpendicular to **s** and located in C and B.

product ($\mathbf{s}\cdot\mathbf{r}$) implies that the phase shift is related solely to the component of **r** along the **s** direction. The component of **r** perpendicular to the **s** direction does not contribute to the phase shift, and all elementary scatterers located along the dotted lines on Fig. 2.3.1B thus share a common phase term, and diffraction may be considered as the reflection of X-rays by the set of planes shown by these lines. Vector **s** is perpendicular to these reflecting planes, and the path difference between waves diffracted by these planes can be expressed as

$$[(\mathbf{k}-\mathbf{k}_0)\cdot\mathbf{r}] = \lambda(\mathbf{s}\cdot\mathbf{r}) = \lambda|\mathbf{s}||\mathbf{r}|\cos(\mathbf{s}\cdot\mathbf{r}) = 2d\sin\theta,$$

where $d = |\mathbf{r}|\cos(\mathbf{s}\cdot\mathbf{r})$ is the interplanar distance (d-value). When the value of this path difference is a multiple of λ, that is, when $2d\sin\theta = n\lambda$ (Bragg's law), interferences of secondary waves are constructive and the sum of their amplitudes is maximum.

Thus, if f_j is the scattering power of the atom whose position is defined by vector $\mathbf{r}_j$, its scattered amplitude is

$$f_j \exp -2\pi i\left(\mathbf{s}\cdot\mathbf{r}_j\right) \tag{2.3.1}$$

and the amplitude of waves scattered by a set of atoms can be written as

$$A(\mathbf{s}) = \sum_j f_j \exp -2\pi i\left(\mathbf{s}\cdot\mathbf{r}_j\right) \tag{2.3.2}$$

To obtain a dimensionless term in the exponential, the dimensions of **s** and **r** are reciprocal. If the distribution of scatterers is described by **r** in the real space, then the scattered amplitude $A(\mathbf{s})$ can be described by vector **s** in the reciprocal space. In turn, the intensity of the scattered waves is the product of $A(\mathbf{s})$ and its conjugate value, that is,

$$I(\mathbf{s}) = A(\mathbf{s})A^*(\mathbf{s}) = \sum_i \sum_j f_i f_j \exp -2\pi i\left[\mathbf{s}\cdot\left(\mathbf{r}_j - \mathbf{r}_i\right)\right]. \tag{2.3.3}$$

Equation (2.3.3) allows the calculation of diffraction effects arising from a set of atoms if their scattering powers and mutual arrangement are known. Scattering centres may be not only atoms but also a set of scatterers. For example, the concept of a crystal lattice is often used to describe diffraction by crystalline materials. According to this concept, each of the lattice nodes has a scattering power corresponding to the unit cell. In this case, f_j should be replaced in Eq. (2.3.2) by the scattering power of the unit cell, named structure amplitude (F), and vector $\mathbf{r}_j$ defines the origin of the jth unit cell. The structure amplitude can be written as $F(\mathbf{s}) = \sum_i f_i \exp -2\pi i(\mathbf{s}\cdot\mathbf{r}_i)$, the sum over i being limited to a single unit cell.

2.3.1.2 Calculation of Diffraction Effects from Mixed-Layer Structures

It will be assumed hereafter that layers constitutive of mixed-layer structures have a two-dimensional (2D) periodicity. Mixed-layer structures can thus be considered as one-dimensionally (1D) disordered structures in which layers

differing by their thickness and/or scattering power alternate along the perpendicular to the layer plane with different degrees of order/disorder. Diffraction effects will be calculated first for a single layer, then for a set of layers (crystal), and finally for a set of crystals (powder sample).

The single layer has an orthogonal unit cell with parameters a, b, and c_0, the **a** and **b** lattice vectors being defined within the layer plane while c_0 represents the layer thickness or the layer-to-layer distance in a crystal. The origin of the nth unit cell in the layer is located at $\mathbf{r}_n = n_1\mathbf{a} + n_2\mathbf{b}$. Similarly, the position of the jth atom in this unit cell is at $\mathbf{r}_j = x_j\mathbf{a} + y_j\mathbf{b} + z_j\mathbf{c}_0$, x_j, y_j, with z_j being the relative coordinates of this atom in the unit cell. The position of any atom in the layer may thus be determined from the sum of vectors $\mathbf{r}_n$ and $\mathbf{r}_j$, while, according to Eq. (2.3.1), the amplitude of X-rays scattered by this atom can be written as:

$$f_j \exp - 2\pi i\left[\mathbf{s}\cdot\left(\mathbf{r}_n + \mathbf{r}_j\right)\right].$$

In turn, the amplitude of X-rays scattered by a single layer can be obtained by summing this amplitude over all j atoms of the unit cell and over all unit cells of the layer: that is,

$$\begin{aligned} A(\mathbf{s}) &= \frac{1}{\Omega}\sum_{n_1}\sum_{n_2}\sum_{j} f_j \exp - 2\pi i\left[\mathbf{s}\cdot\left(\mathbf{r}_n + \mathbf{r}_j\right)\right] \\ &= \frac{1}{\Omega}\sum_{n_1}\sum_{n_2} \exp - 2\pi i(\mathbf{s}\cdot\mathbf{r}_n)\sum_{j} f_j \exp - 2\pi i\left(\mathbf{s}\cdot\mathbf{r}_j\right), \end{aligned} \tag{2.3.4}$$

the double sum over n_1 and n_2 being normalized by the surface area of the unit cell within the **a**–**b** plane (Ω).

It is then convenient to define vector **s** in the coordinate system of the reciprocal lattice. Vectors **a***, **b***, and **c*** are reciprocal of **a**, **b**, and **c** in the real space: that is, $(\mathbf{a}\cdot\mathbf{a}^*) = (\mathbf{b}\cdot\mathbf{b}^*) = (\mathbf{c}\cdot\mathbf{c}^*) = 1$ and $(\mathbf{a}\cdot\mathbf{b}^*) = (\mathbf{b}\cdot\mathbf{a}^*) = (\mathbf{a}\cdot\mathbf{c}^*) = (\mathbf{c}\cdot\mathbf{a}^*) = (\mathbf{b}\cdot\mathbf{c}^*) = (\mathbf{c}\cdot\mathbf{b}^*) = 0$. The axes of the reciprocal coordinate system are thus perpendicular to the planes of the coordinate system in the real space. If α, β, and γ are the coordinates of **s** in the reciprocal space ($\mathbf{s} = \alpha\mathbf{a}^* + \beta\mathbf{b}^* + \gamma\mathbf{c}^*$), then

$$(\mathbf{r}_n\cdot\mathbf{s}) = n_1\alpha + n_2\beta \quad \text{and} \quad \left(\mathbf{r}_j\cdot\mathbf{s}\right) = x_j\alpha + y_j\beta + z_j\gamma. \tag{2.3.5}$$

By combining Eqs. (2.3.4) and (2.3.5):

$$A(\alpha,\beta,\gamma) = \frac{1}{\Omega}\sum_{n_1}\sum_{n_2} \exp - 2\pi i(n_1\alpha + n_2\beta)\sum_{j} f_j \exp - 2\pi i\left(x_j\alpha + y_j\beta + z_j\gamma\right). \tag{2.3.6}$$

The amplitude of X-rays scattered by a single layer is thus a function of the α, β, and γ coordinates of vector **s** in the reciprocal space. If this layer is rectangular with an extension of N_1 and N_2 unit cells along the **a** and **b** axes, respectively, the first two sums in Eq. (2.3.6) are geometric progressions with common ratios equal to exp-$2\pi i\alpha$ and exp-$2\pi i\beta$, respectively, and Eq. (2.3.6) can be expressed as

$$A(\alpha,\beta,\gamma)=\frac{1}{\Omega}\frac{\sin\pi N_1\alpha}{\sin\pi\alpha}\frac{\sin\pi N_2\beta}{\sin\pi\beta}\exp-\pi i[(N_1-1)\alpha+(N_2-1)\beta]$$
$$\sum_j f_j\exp-2\pi i\left(x_j\alpha+y_j\beta+z_j\gamma\right).$$

In turn, the intensity, normalized to a unit cell, of X-rays scattered by atoms of this layer becomes

$$I(\alpha,\beta,\gamma)=\frac{\Omega}{\sigma}A^*(\alpha,\beta,\gamma)A(\alpha,\beta,\gamma)$$
$$=\frac{1}{\Omega\sigma}\frac{\sin^2\pi N_1\alpha}{\sin^2\pi\alpha}\frac{\sin^2\pi N_2\beta}{\sin^2\pi\beta}\left|\sum_j f_j\exp-2\pi i\left(x_j\alpha+y_j\beta+z_j\gamma\right)\right|^2, \quad (2.3.7)$$

where σ is the surface area of the layer in the **a**–**b** plane.

In this equation, the product $\frac{\sin^2\pi N_1\alpha}{\sin^2\pi\alpha}\frac{\sin^2\pi N_2\beta}{\sin^2\pi\beta}$ is the interference function $\Phi(\alpha,\beta)$ and depends on the size and shape of the layer, while the squared expression is the structure factor of a unit cell $|F(\alpha,\beta,\gamma)|^2$.

For high values of N_1 and N_2 ($\sim10^3$–10^4), the interference function exhibits the major maxima for integer values $\alpha=h$, $\beta=k$, while the intensity decreases rapidly when $\alpha\neq h$ and $\beta\neq k$. If α, β, and γ are expressed as $h+X$, $k+Y$, and Z, respectively, Eq. (2.3.7) may be written as

$$I_{hk}(X,Y,Z)=\frac{1}{\Omega\sigma}\Phi_{hk}(X,Y)|F_{hk}(X,Y,Z)|^2.$$

In the reciprocal space, the intensity maxima are thus located along the rods parallel to the **c***-axis and crossing the reciprocal lattice at hk nodes (Fig. 2.3.2). Within the X, Y range over which the interference function ($\Phi_{hk}(X,Y)$) is intense, the structure factor ($|F_{hk}(X,Y,Z)|^2$) varies slowly and may be satisfactorily approximated by $|F_{hk}(Z)|^2$, leading to the following expression for the intensity distribution within hk rods:

$$I_{hk}(X,Y,Z)=\frac{1}{\Omega\sigma}\Phi_{hk}(X,Y)|F_{hk}(Z)|^2. \quad (2.3.8)$$

The intensity distribution within a rod is thus described by two independent functions, namely, the structure factor $|F_{hk}(Z)|^2$ along a rod and the interference function $\Phi_{hk}(X,Y)$ across that rod. Because only waves scattered by planes parallel to the layer surface are involved, the sole rod with $h=0$ and $k=0$ needs to be considered for the calculation of basal reflection intensity. In this case, the amplitude of X-rays scattered by one layer is proportional to the product of the structure amplitude $F(Z)$ and the shape factor $D(X,Y)$.[2]

2. The shape factor $D(X,Y)$ is the Fourier transform of the layer shape function $g(x,y)$,which is equal to 1 and 0 within and outside the layer, respectively (Ewald, 1940).

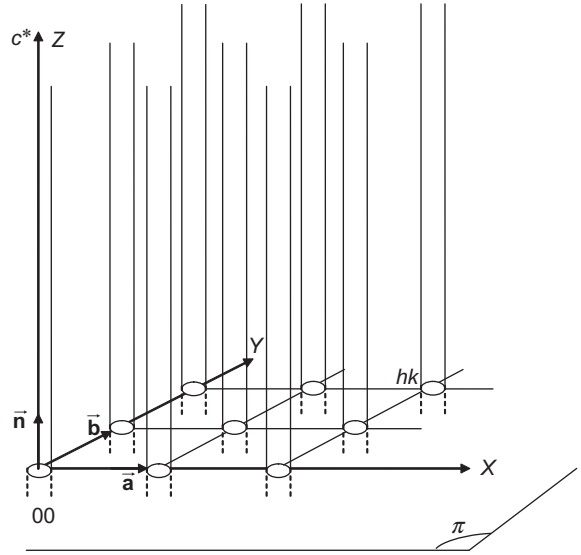

FIGURE 2.3.2 Schematic intensity distribution in the reciprocal space for a single layer. Intensity maxima are located along the rods parallel to the **c***-axis and crossing the reciprocal lattice at *hk* nodes.

$$A(X,Y,Z) = \frac{1}{\Omega} F(Z) D(X,Y) \quad \text{with} \quad F(Z) = \sum_j K_j f_j \exp - 2\pi i z_j Z,$$

where z_j is the coordinate along the normal to the layer of the jth atom in the unit cell (in Å); K_j is the occupancy of the z_j position by the j atoms; and Z is the coordinate in the reciprocal space along **c*** (in $Å^{-1}$).

The function $D(X,Y)$ depends on the size and shape of the layer. It is reasonable to assume that in a crystal, all layers have the same shape and size in the **a**–**b** plane. Consequently, the terms $D(X,Y)$ are similar for all layers and may be omitted in the following developments. A mixed-layer crystal with N layers may thus be considered as a column parallel to the **c***-axis (or to the Z direction) and consisting of N unit cells of different types with a common basis. To calculate the intensity of waves scattered by such a column along Z, it is convenient to choose the origin of the coordinate system on the lower surface of the crystal and to number layers from bottom to top (Fig. 2.3.3). The position of the mth layer in the crystal is thus defined by vector $\mathbf{r}_m$. X-rays scattered by the unit cell of the mth layer are thus ahead of phase with respect to those scattered by the unit cell at the origin of the coordinate system, and their amplitude is

$$F_m(Z) \exp - 2\pi i Z r_m, \tag{2.3.9}$$

where F_m is the structure amplitude of the unit cell for the mth layer, and r_m the distance from the origin of the crystal to the origin of the mth layer.

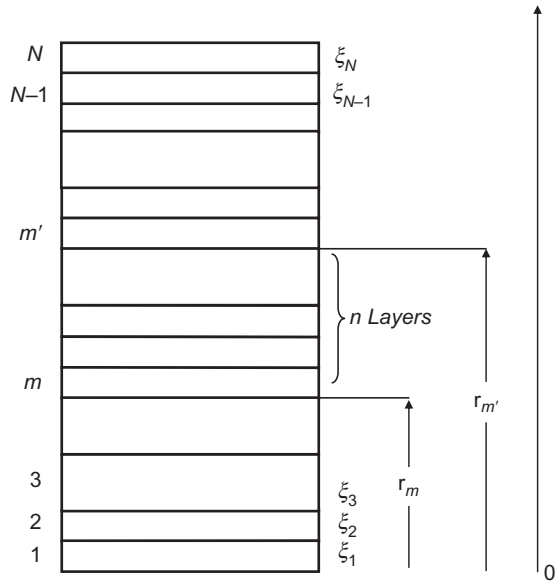

FIGURE 2.3.3 Schematic representation of a mixed-layer crystal composed of N layers (or unit cells), labelled from 1 to N from bottom to top. The position of the mth layer (or unit cell) in the crystal is defined by vector $\mathbf{r}_m$ and its thickness is ξ_m.

The summation of Eq. (2.3.9) over all unit cells of the column is the amplitude of waves scattered by the whole crystal:

$$A(Z) = \sum_{m=1}^{N} F_m(Z) \exp -2\pi i Z r_m \tag{2.3.10}$$

Equation (2.3.10) may be further modified by introducing the phase shift $\varphi_i = -2\pi Z \xi_i$ between the ith and $(i+1)$th layers, which depends on the layer thickness (ξ_i), as

$$\begin{aligned} A(Z) = F_1 + F_2 \exp i\varphi_1 + F_3 \exp i(\varphi_1 + \varphi_2) + \cdots \\ + F_N \exp i(\varphi_1 + \varphi_2 + \cdots + \varphi_{N-1}) \end{aligned} \tag{2.3.11}$$

F_1, F_2, ..., F_N being the structure amplitudes of the first, second, ..., and Nth layers, and φ_1, φ_2, ..., φ_{N-1} the phase shifts induced by the thicknesses of the first, second, ..., and $(N-1)$th layers (ξ_1, ξ_2, ..., and ξ_{N-1}, respectively).

The intensity of the diffracted waves is the product of this structure amplitude and its conjugate value (Wilson, 1949a):

$$
\begin{aligned}
I(Z) = A^*(Z)A(Z) = {} & F_1^*F_1 + F_2^*F_2 + \cdots + F_N^*F_N \\
& + F_1^*F_2 \exp i\varphi_1 + F_2^*F_3 \exp i\varphi_2 + \cdots + F_{N-1}^*F_N \exp i\varphi_{N-1} + \text{conjugate} \\
& + F_1^*F_3 \exp i(\varphi_1 + \varphi_2) + F_2^*F_4 \exp i(\varphi_2 + \varphi_3) + \cdots \\
& + F_{N-2}^*F_N \exp i(\varphi_{N-2} + \varphi_{N-1}) + \text{conjugate} \\
& + F_1^*F_N \exp i(\varphi_1 + \varphi_2 + \cdots + \varphi_{N-1}) + \text{conjugate}
\end{aligned}
\tag{2.3.12}
$$

The different terms of Eq. (2.3.12) are arranged in the way that the products of structure amplitudes are calculated for single layers in the first line, for layer pairs in the second line, layer triplets in the third line, etc. Terms of the first line thus correspond to the contribution to intensity of waves diffracted by single layers. Terms of the second line and their conjugates correspond to the contribution to intensity of waves diffracted by pairs of adjacent layers taking into account the path difference between rays scattered by external layers of each pair, etc. The last term and its conjugate value are the contribution to intensity of waves diffracted by the crystal's outer layers taking into account the path difference between scattered rays. The intensity of X-rays diffracted by a lamellar crystal thus sums the contributions from individual layers and those from the two external layers in all possible subsequences consisting of two, three, ..., $(N-1)$, N layers, taking into account the distance between these external layers.

In mixed-layer structures, the occurrence probability of a layer with a given nature (structure amplitude) and thickness as the first, second, ..., and Nth layers, which are needed in Eq. (2.3.12), is defined by a set of probability parameters. If the probability of finding an s-type layer ($s = 1, 2, \ldots, T$) at position q ($q = 1, 2, \ldots, N$) is w_s, the intensity of waves diffracted by this layer is $w_s F_s^* F_s$. For a mixed-layer structure with T layer types, $\sum_{s=1}^{T} w_s = 1$, and the average intensity of waves diffracted by layer q in a crystal can be expressed as

$$
\sum_{s=1}^{T} w_s F_s^* F_s = \overline{F_0^* F_0}, \tag{2.3.13}
$$

where the index 0 indicates that this average intensity is calculated for a single layer. It is possible to hypothesize that w_s does not depend on q and that Eq. (2.3.13) is valid for all layers. Consequently, the intensity of waves diffracted, independently of each other, by all individual layers in a crystal is equal to

$$
N \sum_{s=1}^{T} w_s F_s^* F_s = N\ \overline{F_0^* F_0}. \tag{2.3.14}
$$

By analogy with the second line of Eq. (2.3.12), the contribution to intensity of waves diffracted by an *st* pair of layers can be calculated by defining the probability w_{st} to find a pair of s and t layers in positions q and $(q+1)$, respectively:

$$w_{st}F_s^*F_t \exp i\varphi_s + \text{conjugate} = 2\text{Re}w_{st}F_s^*F_t \exp i\varphi_s, \tag{2.3.15}$$

where Re is the real part of the complex.

As for the contribution of single layers, $\sum_{s=1}^{T}\sum_{t=1}^{T} w_{st} = 1$, and the average intensity of X-rays scattered by pairs of adjacent layers in positions q and $(q+1)$ can be written as

$$2\text{Re}\sum_{s=1}^{T}\sum_{t=1}^{T} w_{st}F_s^*F_t \exp i\varphi_s = 2\text{Re}\ \overline{F_0^*F_1 \exp i\{\varphi\}_1}, \tag{2.3.16}$$

where F_1 is the structure amplitude of the nearest neighbour layer of the F_0 layer, and $\{\varphi\}_1$ the phase shift induced by the layer-to-layer distance between their origins (thickness of the F_0 layer). As for the contribution of single layers, Eq. (2.3.16) is assumed to be valid for all $(N-1)$ layer pairs in a crystal consisting of N layers, and the total contribution to intensity of waves diffracted by pairs of adjacent layers can be expressed as

$$2\text{Re}(N-1)\sum_{s=1}^{T}\sum_{t=1}^{T} w_{st}F_s^*F_t \exp i\varphi_s = 2\text{Re}(N-1)\ \overline{F_0^*F_1 \exp i\{\varphi\}_1}. \tag{2.3.17}$$

A similar logic can be used to calculate the contribution to intensity of a layer sequence in which s and t layers occur as nth nearest neighbours ($n = 2, 3, \ldots, (N-1)$), that is, in position q and $q+n$, respectively:

$$\begin{aligned} &w_{sh_1h_2\ldots h_{n-1}t}F_s^*F_t \exp i\left(\varphi_s + \varphi_{h_1} + \varphi_{h_2} + \cdots + \varphi_{h_{n-1}}\right) + \text{conjugate} \\ &\quad = 2\text{Re}w_{sh_1h_2\ldots h_{n-1}t}F_s^*F_t \exp i\left(\varphi_s + \varphi_{h_1} + \varphi_{h_2} + \cdots + \varphi_{h_{n-1}}\right) \end{aligned} \tag{2.3.18}$$

where $w_{sh_1h_2\ldots h_{n-1}t}$ is the occurrence probability of the $sh_1h_2\ldots h_{n-1}t$ layer sequence, $\varphi_s, \varphi_{h_1}, \varphi_{h_2}, \ldots, \varphi_{h_{n-1}}$ the phase shifts induced by the corresponding layer thicknesses $\xi_s, \xi_{h_1}, \xi_{h_2}, \ldots \xi_{h_{n-1}}$.

Again, $\sum_{s=1}^{T}\sum_{h_1=1}^{T}\sum_{h_2=1}^{T}\cdots\sum_{h_{n-1}=1}^{T}\sum_{t=1}^{T} w_{sh_1h_2\ldots h_{n-1}t} = 1$, and the average intensity of waves diffracted by a $(n+1)$ layer sequence with s and t layers in positions q and $(q+n)$ is

$$\begin{aligned} &2\text{Re}\sum_{s=1}^{T}\sum_{h_1=1}^{T}\sum_{h_2=1}^{T}\cdots\sum_{h_{n-1}=1}^{T}\sum_{t=1}^{T} w_{sh_1h_2\ldots h_{n-1}t}F_s^*F_t \\ &\exp i\left(\varphi_s + \varphi_{h_1} + \varphi_{h_2} + \cdots + \varphi_{h_{n-1}}\right) = 2\text{Re}\ \overline{F_0^*F_n \exp i\{\varphi\}_n} \end{aligned} \tag{2.3.19}$$

For a given value of n, the index q may vary from 1 to $(N-n)$ as there are $(N-n)$ sequences of $(n+1)$ layers in an N-layer crystal. Equation (2.3.19) is valid for all these sequences, and the total contribution to intensity of waves diffracted by sequences of $(n+1)$ layers can be expressed as

$$2\mathrm{Re}(N-n)\sum_{s=1}^{T}\sum_{h_1=1}^{T}\sum_{h_2=1}^{T}\cdots\sum_{h_{n-1}=1}^{T}\sum_{t=1}^{T}w_{sh_1h_2\ldots h_{n-1}t}F_s^*F_t$$
$$\exp i\left(\varphi_s+\varphi_{h_1}+\varphi_{h_2}+\cdots+\varphi_{h_{n-1}}\right)$$
$$=2\mathrm{Re}(N-n)\ \overline{F_0^*F_n\exp i\{\varphi\}_n} \tag{2.3.20}$$

Index n may vary from 1 (layer pairs) to $(N-1)$, the $n=0$ case corresponding to individual layers (Eq. 2.3.14).

The summation of Eq. (2.3.20) for n values ranging from 1 to $(N-1)$ allows calculating the contribution to intensity of all layer sequences in a crystal, that is,

$$2\mathrm{Re}\sum_{n=1}^{N-1}(N-n)\sum_{s=1}^{T}\sum_{h_1=1}^{T}\sum_{h_2=1}^{T}\cdots\sum_{h_{n-1}=1}^{T}\sum_{t=1}^{T}w_{sh_1h_2\ldots h_{n-1}t}F_s^*F_t$$
$$\exp i\left(\varphi_s+\varphi_{h_1}+\varphi_{h_2}+\cdots+\varphi_{h_{n-1}}\right)$$
$$=2\mathrm{Re}\sum_{n=1}^{N-1}(N-n)\ \overline{F_0^*F_n\exp i\{\varphi\}_n} \tag{2.3.21}$$

The total intensity of diffracted waves is obtained by taking into account the contributions of individual layers (Eq. 2.3.14).

$$I=N\sum_{s=1}^{T}w_sF_s^*F_s+2\mathrm{Re}\sum_{n=1}^{N-1}(N-n)\sum_{s=1}^{T}\sum_{h_1=1}^{T}\sum_{h_2=1}^{T}\cdots\sum_{h_{n-1}=1}^{T}\sum_{t=1}^{T}w_{sh_1h_2\ldots h_{n-1}t}F_s^*F_t$$
$$\exp i\left(\varphi_s+\varphi_{h_1}+\varphi_{h_2}+\cdots+\varphi_{h_{n-1}}\right)$$
$$=N\overline{F_0^*F_0}+2\mathrm{Re}\sum_{n=1}^{N-1}(N-n)\ \overline{F_0^*F_n\exp i\{\varphi\}_n} \tag{2.3.22}$$

A periodic structure is a specific case of Eq. (2.3.22) with $T=1$, $F_s=F_{h_1}=F_{h_2}=\cdots=F_{h_{n-1}}=F_t=F$, $\varphi_s=\varphi_{h_1}=\varphi_{h_2}=\cdots=\varphi_{h_{n-1}}=\varphi$, and $w_s=w_{sh_1}=\cdots=w_{sh_1h_2\cdots h_{n-1}t}=1$, leading to a simplified expression of the diffracted intensity, as

$$I(Z)=F^*F\left\{N+2\mathrm{Re}\sum_{n=1}^{N-1}(N-n)\exp in\varphi\right\}$$
$$=F^*(Z)F(Z)\left\{N+2\mathrm{Re}\sum_{n=1}^{N-1}(N-n)\exp 2\pi iZn\xi\right\}$$
$$=|F(Z)|^2\frac{\sin^2\pi NZ\xi}{\sin^2\pi Z\xi}=|F(Z)|^2G(Z) \tag{2.3.23}$$

In this case, the intensity distribution along the Z-axis is the product of the structure factor of the unit cell $|F(Z)|^2$ and of the interference function $G(Z)$. For a mixed-layer structure, the occurrence probabilities of the different layer sequences introduced in Eq. (2.3.22) remain to be determined.

2.3.2 STATISTICAL DESCRIPTION OF LAYER STACKING IN MIXED-LAYER STRUCTURES

The intensity of X-rays diffracted by a single crystal (Eq. 2.3.12) can be calculated as the sum of the contributions from individual layers, layer pairs, layer triplets, and so on. For periodic crystals, the expression is much simplified (Eq. 2.3.23), whereas for a mixed-layer structure, the occurrence probability of the different layer sequences introduced in Eq. (2.3.22) should be determined. In addition, natural mixed-layer structures usually occur as finely dispersed powders whose individual crystals differ by the number, content, and distribution of the different layer types. Diffraction by such an ensemble of crystals can be described statistically, the frequency of individual layers, layer pairs, layer triplets, etc. being described by a set of probability parameters. The Markovian model is widely used for this purpose (Hendricks and Teller, 1942; Wilson, 1942; Jagodzinski, 1949a,b,c, 1954; Méring, 1950; Kakinoki and Komura, 1952, 1954a; MacEwan, 1958; Allegra, 1961, 1964; Reynolds, 1967, 1980; Drits and Sakharov, 1976; Bethke and Altaner, 1986; Drits and Tchoubar, 1990), as it allows calculating the occurrence probability of any layer sequence. These sequences may be composed of one, two, three, ... layers whose positions in the crystal are known. The Markovian model allows also taking into account different order–disorder models with the common Reichweite parameter S and a reduced set of probability parameters for each S value.

The Markovian model assumes that the probability of finding a given layer type at a given position in the crystal only depends on the nature of its neighbours. The essential parameter of the various order–disorder models used to describe layer stacking is the number of layers that influence the occurrence probability of a layer type at a given position. This parameter is the 'short-range order factor', or 'Reichweite', S, and was first introduced by Jagodzinski (1949a,b,c, 1954). For random layer stacking, the occurrence probability of a layer at a given position does not depend on adjacent layers and $S=0$. If this probability depends on a unique preceding layer, then $S=1$, and, when the occurrence probability of a layer in position n depends on layers with positions $(n-1)$, $(n-2)$, ..., $(n-m)$, then $S=m$. Here, n and m are the numbers of layers in an arbitrary but fixed direction along the layer stack, and S can only have integer values (Lanson, 2011). The following section essentially reviews the set of probability parameters required to describe thoroughly layer stacking for different values of the S parameter, and the logical procedures to determine them.

2.3.2.1 Occurrence Probability of Any Layer Sequence

2.3.2.1.1 Randomly Interstratified (S = 0) Mixed-Layer Structures with Two Layer Types (T = 2)

If the alternation of A and B layers is random ($S=0$), the occurrence probability of layer type i ($i=A$, B) at a given position in the crystal does not

depend on the adjacent layers and is equal to its abundance w_i, with the following relation:

$$w_A + w_B = 1 \tag{2.3.24}$$

The occurrence probability of any layer sequence is then equal to the product of the relative abundances of its building layers, that is,

$$\begin{aligned}
&w_{AA} = w_A^2, w_{AB} = w_{BA} = w_A w_B, w_{BB} = w_B^2\\
&w_{AAA} = w_A^3, w_{AAB} = w_{ABA} = w_{BAA} = w_A^2 w_B, w_{ABB} = w_{BAB} = w_{BBA} = w_A w_B^2, w_{BBB} = w_B^3\\
&w_{AAAA} = w_A^4, w_{AAAB} = w_{AABA} = w_{ABAA} = w_{BAAA} = w_A^3 w_B\\
&w_{AABB} = w_{ABAB} = w_{ABBA} = w_{BAAB} = w_{BABA} = w_{BBAA} = w_A^2 w_B^2\\
&w_{BBBA} = w_{BBAB} = w_{BABB} = w_{ABBB} = w_A w_B^3, w_{BBBB} = w_B^4, \text{etc.}
\end{aligned}$$

As for the relative abundances of elementary layers, the occurrence probabilities of the different layer pairs, triplets, etc., are linked by specific relations:

$$\begin{aligned}
&w_{AA} + w_{AB} + w_{BA} + w_{BB} = 1\\
&w_{AAA} + w_{AAB} + w_{ABA} + w_{ABB} + w_{BAA} + w_{BAB} + w_{BBA} + w_{BBB} = 1, \text{etc.}
\end{aligned} \tag{2.3.25}$$

2.3.2.1.2 Mixed-Layer Structures with S = 1 and Two Layer Types (T = 2)

When $S = 1$, the occurrence probability of a j-type layer at a given position depends on the nature of the preceding layer i. In addition to the relative abundance parameters w_A and w_B, a new set of junction probability coefficients (p_{AA}, p_{AB}, p_{BA}, p_{BB}) is necessary to determine the occurrence probability of a layer sequence. The p_{ij} ($i, j = A, B$) parameter describes the probability of finding a j-type layer after an i-type one. With these two sets of parameters, the occurrence probability of any layer sequence can be described as follows:

$$\begin{aligned}
&w_{AA} = w_A p_{AA}, w_{AB} = w_A p_{AB}, w_{BA} = w_B p_{BA}, w_{BB} = w_B p_{BB}\\
&w_{AAA} = w_A p_{AA} p_{AA}, w_{AAB} = w_A p_{AA} p_{AB}, w_{ABA} = w_A p_{AB} p_{BA}, \ldots, w_{BBB} = w_B p_{BB} p_{BB}\\
&w_{AAAA} = w_A p_{AA} p_{AA} p_{AA}, w_{AAAB} = w_A p_{AA} p_{AA} p_{AB}, w_{AABA} = w_A p_{AA} p_{AB} p_{BA},\\
&\qquad w_{ABAA} = w_A p_{AB} p_{BA} p_{AA},\\
&w_{AABB} = w_A p_{AA} p_{AB} p_{BB}, w_{ABAB} = w_A p_{AB} p_{BA} p_{AB}, \ldots, w_{BBBB} = w_B p_{BB} p_{BB} p_{BB}, \text{etc.}
\end{aligned}$$

2.3.2.1.3 Mixed-Layer Structures with S ≥ 2 and T = 2

For a mixed-layer structure with $S = 2$, the probability of finding a k-type layer at a given position depends on the nature of the preceding layer pair ij. In addition to the relative abundances w_i and junction probabilities p_{ij}, a new set of junction probabilities p_{ijk} ($i, j, k = A, B$) is needed to describe the

layer stacking sequence. The p_{ijk} coefficients define the probability of finding a k-type layer following an ij layer pair. In turn,

$$w_{AA} = w_A p_{AA}, w_{AB} = w_A p_{AB}, w_{BA} = w_B p_{BA}, w_{BB} = w_B p_{BB}$$

as in the $S = 1$ case, and

$$w_{AAA} = w_A p_{AA} p_{AAA}, w_{AAB} = w_A p_{AA} p_{AAB}, w_{ABA} = w_A p_{AB} p_{ABA}, \ldots, w_{BBB} = w_B p_{BB} p_{BBB}$$

$$w_{AAAA} = w_A p_{AA} p_{AAA} p_{AAA}, w_{AAAB} = w_A p_{AA} p_{AAA} p_{AAB},$$

$$w_{AABA} = w_A p_{AA} p_{AAB} p_{ABA}, w_{ABAA} = w_A p_{AB} p_{ABA} p_{BAA},$$

$$w_{AABB} = w_A p_{AA} p_{AAB} p_{ABB}, w_{ABAB} = w_A p_{AB} p_{ABA} p_{BAB}, \ldots,$$

$$w_{BBBB} = w_B p_{BB} p_{BBB} p_{BBB}, \text{etc.}$$

Mixed-layer structures with $S = 3$ can be described with the same guidelines after the introduction of an additional set of junction probabilities p_{ijkl} defining the probability of finding an l-type layer after an ijk layer triplet:

$$w_{AA} = w_A p_{AA}, w_{AB} = w_A p_{AB}, w_{BA} = w_B p_{BA}, w_{BB} = w_B p_{BB}$$

$$w_{AAA} = w_A p_{AA} p_{AAA}, w_{AAB} = w_A p_{AA} p_{AAB}, w_{ABA} = w_A p_{AB} p_{ABA}, \ldots, w_{BBB} = w_B p_{BB} p_{BBB}$$

$$w_{AAAA} = w_A p_{AA} p_{AAA} p_{AAAA}, w_{AAAB} = w_A p_{AA} p_{AAA} p_{AAAB},$$

$$w_{AABA} = w_A p_{AA} p_{AAB} p_{AABA}, w_{ABAA} = w_A p_{AB} p_{ABA} p_{ABAA},$$

$$w_{AABB} = w_A p_{AA} p_{AAB} p_{AABB}, \ldots,$$

$$w_{BAAA} = w_B p_{BA} p_{BAA} p_{BAAA}, \ldots, w_{BBBB} = w_B p_{BB} p_{BBB} p_{BBBB}$$

2.3.2.1.4 Mixed-Layer Structures: General Case

The same guidelines can be used to determine the occurrence probabilities of the different layer sequences for a mixed-layer structure consisting of T layer types. These probabilities are systematically linked by the following relations:

$$\sum_{i=1}^{T} w_i = 1, \sum_{i=1}^{T}\sum_{j=1}^{T} w_{ij} = 1, \sum_{i=1}^{T}\sum_{j=1}^{T}\sum_{k=1}^{T} w_{ijk} = 1, \ldots, \text{etc.} \qquad (2.3.26)$$

Accordingly, a randomly interstratified mixed-layer structure ($S = 0$) appears as a specific case ($p_{ij} = w_j$) of mixed-layer structures with $S = 1$. Similarly, a mixed-layer structure with $S = 1$ is a specific case of a mixed-layer structure with $S = 2$ where $p_{ijk} = p_{jk}, \ldots$ which can be written as $(S = 0) \in (S = 1) \in (S = 2) \cdots$ using the mathematical formalism. Despite misleading uses in the literature, the Reichweite parameter S defines only the extent of the influence of a given layer, but provides no indication as to the nature of this influence, which is characterized by junction probabilities. For $S > 0$,

these junction probabilities can be varied to describe mixed-layer structures with a tendency to either layer ordering, or layer segregation.

The complete calculation of occurrence probabilities for the different layer sequences in mixed-layer structures with $S = m$ requires the junction probability parameters $w_i, p_{ij}, p_{ijk}, \ldots, p_{ijk\cdots l}$, where the number of indexes $ijk\cdots l$ is equal to $(m+1)$, to be known. When using the Markovian model, specific relationships link w and p parameters, and only a fraction of them are independent. The following section describes these relations and lists the sets of independent probability parameters for mixed-layer structures with different values of S and T.

2.3.2.2 Determination of Independent Probability Parameters

2.3.2.2.1 Randomly Interstratified Mixed-Layer Structures (S = 0)

As described above, the occurrence probability of any layer sequence in a two-component mixed-layer structure with $S = 0$ is equal to $w_A^{n_A} w_B^{n_B}$, n_A and n_B being the numbers of A and B layers, respectively, in this sequence. From Eq. (2.3.24), a two-component ($T = 2$) mixed-layer structure randomly interstratified is thus fully described by one of the coefficients w_A or w_B. From Eq. (2.3.26), the number of independent probability coefficients is $(T-1)$ for a randomly interstratified mixed-layer structure consisting of T layer types. The relative abundance of the first layer type, for example may be defined without restrictions within the [0, 1] range, but the range available for the other occurrence probability parameters depends on the values of the previously defined coefficients. For example, the relative abundance of the second layer type should be defined within the range $[0, (1-w_1)]$, that of the third layer type within the range $[0, (1-w_1-w_2)]$,... and $w_T = 1 - \sum_{i=1}^{T-1} w_i$.

2.3.2.2.2 Mixed-Layer Structures with S = 1 and T = 2

In this case, the six probability parameters (w_A, w_B, p_{AA}, p_{AB}, p_{BA}, p_{BB}) required to characterize thoroughly the mixed-layer structure are linked by the following relations:

$$w_A + w_B = 1, \quad p_{AA} + p_{AB} = 1, \quad \text{and} \quad p_{BA} + p_{BB} = 1 \tag{2.3.27}$$

The first relation is obvious, the other two meaning that a given layer (A or B) is followed by either an A or a B layer, which is also evident for a two-component mixed-layer structure. In addition, the six probability parameters are related by the following relations:

$$w_A = w_A p_{AA} + w_B p_{BA}, \quad \text{and} \quad w_B = w_A p_{AB} + w_B p_{BB} \tag{2.3.28}$$

The products $w_A p_{AA}$ and $w_B p_{BA}$ describe the occurrence probabilities of AA and BA pairs, that is w_{AA} and w_{BA}, respectively, whereas the overall relations assert that a given layer (A or B, respectively) follows either an A or a B layer in a two-component mixed-layer structure. By combining the second relation

of Eq. (2.3.27) ($p_{AB}=1-p_{AA}$) with the first of Eq. (2.3.28) [$w_A(1-p_{AA})=w_Bp_{BA}$], it is possible to deduce that

$$w_Ap_{AB}=w_Bp_{BA},\quad or\quad w_{AB}=w_{BA} \tag{2.3.29}$$

The four relations in Eqs. (2.3.27) and (2.3.29) thus reduce to two the number of independent probability parameters required to characterize thoroughly a mixed-layer structure with $S=1$ and $T=2$. One of these parameters should be w_A or w_B. If w_A is chosen and if $w_A>w_B$, then Eq. (2.3.29) leads to

$$p_{AB}=\frac{w_B}{w_A}p_{BA}=\frac{w_B}{w_A}(1-p_{BB})\quad\text{and}\quad\frac{w_B}{w_A}\leq 1 \tag{2.3.30}$$

It is thus convenient to choose p_{BA} or p_{BB} as the second independent probability parameter, as there are no restrictions on the value of either, which can range from 0 to 1. If p_{BB} is chosen as the second independent parameter, all other probability parameters can be calculated as

$$w_B=1-w_A,p_{BA}=1-p_{BB},p_{AB}=\frac{1-w_A}{w_A}(1-p_{BB}),p_{AA}=1-\frac{1-w_A}{w_A}(1-p_{BB}) \tag{2.3.31}$$

2.3.2.2.3 *Ordering and Segregation in Mixed-Layer Structures with S=1 and T=2*

Among mixed-layer structures with $S=1$, two main types can be differentiated depending on the relative values of the w_A and p_{AA} probability parameters. For example, when $p_{AA}>w_A$, the occurrence of AA pairs is favoured compared to random interstratification; A layers are thus clustered and the mixed-layer structure is said to be segregated. On the other hand, when $p_{AA}<w_A$, the occurrence of AB and BA pairs is favoured compared to random interstratification, and interstratification is considered to be ordered. As proposed first by Sato (1965), the degree of segregation, or of ordering, may be described from the last relation in Eq. (2.3.31):

$$p_{BB}=\frac{w_A}{1-w_A}p_{AA}+1-\frac{w_A}{1-w_A} \tag{2.3.32}$$

and the derived Fig. 2.3.4.

Equation (2.3.32) indicates that p_{BB} and p_{AA} are linearly correlated for a given w_A value. Mixed-layer structures with a given w_A value are thus located along straight lines originating from the upper right corner of the diagram in Fig. 2.3.4. Both p_{AA} and p_{BB} axes correspond to mixed-layer structures with the maximum possible degree of ordering (MPDO), which corresponds to $p_{BB}=0$ when $w_A\geq w_B$ or to $p_{AA}=0$ for $w_A\leq w_B$ ($S=1$). The physical mixture of periodic crystals composed either of A or of B layers corresponds to the upper right corner of the diagram with $p_{AA}=p_{BB}=1$ (Fig. 2.3.4). The specific case of randomly interstratified mixed-layer structures ($S=0$) corresponds to

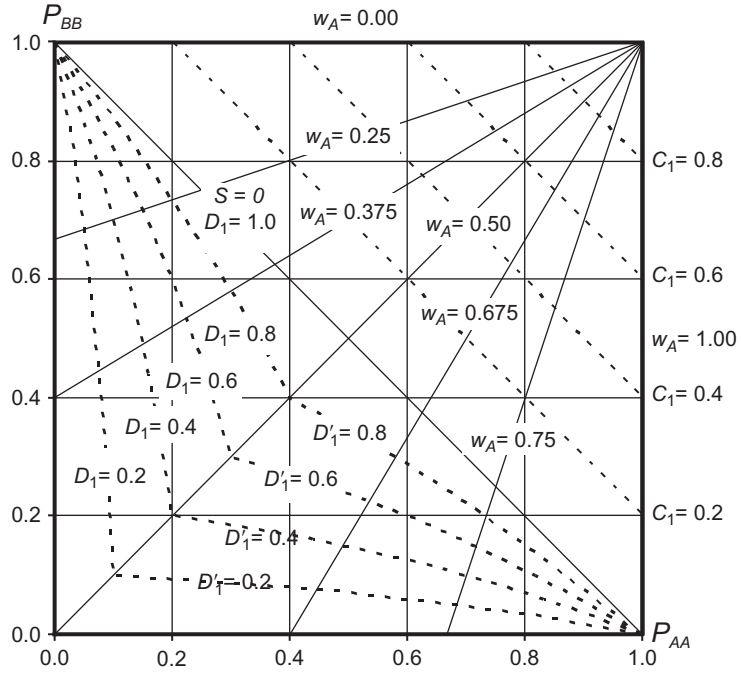

FIGURE 2.3.4 Junction probability diagram for two-component mixed-layer structures with $S=1$. See text for details. *Adapted from Drits and Sakharov (1976).*

the line where $p_{ij}=w_j$, that is to the straight line linking the upper left and lower right corners of the diagram in Fig. 2.3.4. The domain above this diagonal, that is, towards the physical mixture point at the upper right corner, corresponds to mixed-layer structures with a tendency to segregation, whereas the domain below this diagonal corresponds to partial ordering. The lower left corner with $w_A=w_B=0.5$ and $p_{AA}=p_{BB}=0$ corresponds to the periodic $ABAB\ldots$ layer sequence with a 1:1 ratio between A and B layers.

Cesari et al. (1965) defined simple parameters to characterize the degree of ordering, or of segregation, in two-component mixed-layer structures with $S=1$. In the first case, the parameter aims at quantifying the degree of randomness (or disorder) in the stacking of A and B layers, and can be defined as

$$D_1 = p_{AA}/w_A \quad \text{when } w_A < w_B \text{ and } 0 \le p_{AA} \le w_A \tag{2.3.33}$$

and

$$D'_1 = p_{BB}/w_B \quad \text{when } w_A > w_B \text{ and } 0 \le p_{BB} \le w_B \tag{2.3.34}$$

The index 1 of D and D' parameters indicates that the disorder parameters describe mixed-layer structures with $S=1$. Both D_1 and D'_1 parameters may vary from 0 (MPDO case, $S=1$) to 1 (random interstratification, $S=0$). Drits and Sakharov (1976) transformed Eq. (2.3.32) into

$$w_A = \frac{1 - p_{BB}}{2 - p_{AA} - p_{BB}} \tag{2.3.35}$$

and introduced this relation into Eqs. (2.3.33) and (2.3.34) to obtain

$$p_{BB} = \frac{2p_{AA} - p_{AA}^2 - D_1}{p_{AA} - D_1} \quad \text{and} \quad p_{AA} = \frac{2p_{BB} - p_{BB}^2 - D_1'}{p_{BB} - D_1'} \tag{2.3.36}$$

These two relations define the relation between the p_{AA} and p_{BB} parameters for a given degree of disorder (D_1 or D_1'), independent of w_A. If the latter parameter is varied, Eq. (2.3.36) allows drawing the dashed lines in the partial ordering domain (Fig. 2.3.4). Non-integral values of the short-range order parameter S were sometimes used to describe the degree of ordering in mixed-layer structures with $S = 1$ (Reynolds, 1988; Yuan and Bish, 2010). The use of such non-integral values should be avoided, however, and the degree of partial ordering should be described either by a specific parameter (e.g. D_1 or D_1') or by the set of independent junction probabilities as recommended by the AIPEA nomenclature committee (Bailey, 1982; Guggenheim et al., 2006).

The degree of segregation in a two-component mixed-layer structure may be defined in a similar way (Cesari et al., 1965), as

$$C_1 = 1 - \frac{1 - p_{AA}}{1 - w_A} \quad \text{when } w_A \le p_{AA} \le 1 \tag{2.3.37}$$

As in the previous case, the C_1 parameter may vary from 0 (random interstratification, $S = 0$) to 1 (physical mixture, $S = 1$). Drits and Sakharov (1976) introduced Eq. (2.3.35) into Eq. (2.3.37) to obtain a relation between the p_{AA} and p_{BB} parameters for a given degree of segregation C_1 independently of w_A:

$$p_{BB} = C_1 - p_{AA} + 1 \tag{2.3.38}$$

If w_A is varied, Eq. (2.3.38) allows drawing the dashed lines in the segregation domain (Fig. 2.3.4).

2.3.2.2.4 *Mixed-Layer Structures with S = 1 and T = 3*

For mixed-layer structures with more than two layer types, the analytical definition of independent probability parameters has not been achieved yet because of its intrinsic complexity. Even in comprehensive monographs (Cesari and Allegra, 1967; Drits and Sakharov, 1976; Drits and Tchoubar, 1990), three-component mixed layers, for example, were described only for particular cases. The same complexity exists for two-component mixed-layer structures with $S > 1$. To reduce this complexity, a priori assumptions are commonly made on junction probabilities (Drits and Sakharov, 1976; Reynolds, 1980; Bethke and Altaner, 1986; Drits and Tchoubar, 1990), thus limiting the versatility of structure models for a given set of S and T values. For example, a third layer type may be considered to randomly replace one of the two 'main' components (Newmod—three components) rather than

having its own independent set of junction probabilities. Similarly, for a two-component structure with $S=2$, MPDO is often assumed for the definition of p_{ij} junction probabilities ($p_{BB}=0$ when $w_A>w_B$), thus automatically setting some of the p_{ijk} probabilities (Drits and Tchoubar, 1990). These restrictive assumptions have been excluded in the following description of a new algorithm for the choice of independent probability coefficients. This logical process is first described for mixed-layer structures with $S=1$ and $T=3$, and then extended to any couple of T and S values.

Similar to Eqs. (2.3.27) and (2.3.28) for two-component mixed-layer structures, the following relations are valid for a three-component (A, B, and C layer types) mixed-layer structure:

$$w_A + w_B + w_C = 1 \tag{2.3.39}$$

$$\begin{cases} p_{AA} + p_{AB} + p_{AC} = 1 \\ p_{BA} + p_{BB} + p_{BC} = 1 \\ p_{CA} + p_{CB} + p_{CC} = 1 \end{cases} \tag{2.3.40}$$

$$\begin{cases} w_A = w_A p_{AA} + w_B p_{BA} + w_C p_{CA} \\ w_B = w_A p_{AB} + w_B p_{BB} + w_C p_{CB} \\ w_C = w_A p_{AC} + w_B p_{BC} + w_C p_{CC} \end{cases} \tag{2.3.41}$$

Because of Eq. (2.3.39), only two of the three relations in Eq. (2.3.41) are independent, and the 12 probability coefficients w_i and p_{ij} ($i,j=A$, B, C) are linked by six independent equations (Eqs. 2.3.39–2.3.41). Six independent probability parameters are thus to be defined, two among the w_i and four among the p_{ij} parameters. If the three relations in Eq. (2.3.40) are multiplied respectively by w_A, w_B, and w_C, respectively, the left part of these relations define the $[W_{ij}]$ matrix as $w_i p_{ij} = w_{ij}$. The right part of the relations may then be reported to the right of each line and to the top of each column, that is,

$$[W_{ij}] = \begin{array}{c|ccc|c} & w_A & w_B & w_C & \\ \hline & w_{AA} & w_{AB} & w_{AC} & w_A \\ & w_{BA} & w_{BB} & w_{BC} & w_B \\ & w_{CA} & w_{CB} & w_{CC} & w_C \end{array} \tag{2.3.42}$$

The sum of the matrix elements in each column corresponds to the right part of the relations in Eq. (2.3.41), whereas the left part of these relations is given by the occurrence probabilities reported above these columns. Equations (2.3.40) and (2.3.41) indicate that the maximum value of any matrix element in Eq. (2.3.42) is the lower of the w_i occurrence probability parameters for the line and column of this matrix element, reported to the right and above this matrix element, respectively. Let us assume, for example, a mixed-layer structure with $w_A=0.60$, $w_B=0.24$, and $w_C=0.16$, with all elements of the $[W_{ij}]$ matrix initially having null values. Any of the matrix elements can be

defined as the first independent parameter, which will be hereafter indicated with bold characters, for example, w_{AB}:

$$[W_{ij}] = \left|\begin{array}{ccc} 0.60 & 0.24 & 0.16 \\ 0 & \boldsymbol{w_{AB}} & 0 \\ 0 & 0 & 0 \\ 0 & 0 & 0 \end{array}\right| \begin{array}{c} \\ 0.60 \\ 0.24 \\ 0.16 \end{array}$$

All elements of the first row and second column being initially null, the maximum value for the w_{AB} parameter is $min(w_A, w_B) = \min(0.60, 0.24) = 0.24$, the values of w_A and w_B being those of the first row and the second column, to the right and above the matrix, respectively. On the other hand, the minimum value for w_{AB} is given by the difference between w_A (or w_B) and the sum of maximum values allowed for other elements in the first row (or the second column):

$$\begin{aligned} w_{AB}^{\min} &= \max\left\{\left(w_A - w_{AA}^{\max} - w_{AC}^{\max}\right), \left(w_B - w_{BB}^{\max} - w_{CB}^{\max}\right)\right\} \\ &= \max\{(0.60 - 0.60 - 0.16), (0.24 - 0.24 - 0.16)\} = -0.16. \end{aligned}$$

Because occurrence probabilities can take only positive values,

$$w_{AB}^{\min} = \max\left\{\left(w_A - w_{AA}^{\max} - w_{AC}^{\max}\right), \left(w_B - w_{BB}^{\max} - w_{CB}^{\max}\right), 0\right\} = 0.$$

Let us choose, for example, $w_{AB} = 0.12$. It is then possible to choose any other element of the $[W_{ij}]$ matrix as the second independent parameter following a similar procedure if this second element, for example, w_{BC}, does not belong to the first row or the second column of the matrix. The range allowed for w_{BC} values ([0, 0.16]) may be defined in a similar way:

$$\begin{aligned} w_{BC}^{\max} &= \min\{(w_B - w_{BA} - w_{BB}), (w_C - w_{AC} - w_{CC})\} \\ &= \min\{(0.24 - 0 - 0), (0.16 - 0 - 0)\} = 0.16, \end{aligned}$$

and

$$\begin{aligned} w_{BC}^{\min} &= \max\left\{\left(w_B - w_{BA}^{\max} - w_{BB}^{\max}\right), \left(w_B - w_{BB}^{\max} - w_{CB}^{\max}\right), 0\right\} \\ &= \max\{(0.24 - 0.24 - 0.12), (0.16 - 0.16 - 0.16), 0\} = 0, \end{aligned}$$

and it is possible to choose $w_{BC} = 0.024$. Any of the any remaining null elements may then be selected as the third independent probability parameter, for example w_{AA}.

$$[W_{ij}] = \left|\begin{array}{ccc} 0.60 & 0.24 & 0.16 \\ \boldsymbol{w_{AA}} & \mathbf{0.12} & 0 \\ 0 & 0 & \mathbf{0.024} \\ 0 & 0 & 0 \end{array}\right| \begin{array}{c} \\ 0.60 \\ 0.24 \\ 0.16 \end{array}$$

Extreme values of this parameter may be calculated as described above:

$$\begin{aligned} w_{AA}^{\max} &= \min\{(w_A - w_{AB} - w_{AC}), (w_A - w_{BA} - w_{CA})\} \\ &= \min\{(0.60 - 0.12 - 0), (0.60 - 0 - 0)\} = 0.48 \end{aligned}$$

More generally, the maximum value of any element in the matrix can be written as

$$w_{ij}^{\max} = \min\left\{\left(w_i - \sum_{q\neq j} w_{iq}\right), \left(w_j - \sum_{q\neq i} w_{qj}\right)\right\} \tag{2.3.43}$$

Similarly, $w_{AA}^{\min} = \max\{(w_A - w_{AB} - w_{AC}^{\max}),(w_A - w_{BA}^{\max} - w_{CA}^{\max}),0\}$.

The values of $w_{AC}^{\max}$, $w_{BA}^{\max}$, and $w_{CA}^{\max}$ need to be determined first from Eq. (2.3.43):

$$\begin{aligned} w_{AC}^{\max} &= \min\{(w_A - w_{AA} - w_{AB}),(w_C - w_{BC} - w_{CC})\} \\ &= \min\{(0.60 - 0 - 0.12),(0.16 - 0.024 - 0)\} = 0.136 \\ w_{BA}^{\max} &= \min\{(w_B - w_{BB} - w_{BC}),(w_A - w_{AA} - w_{CA})\} \\ &= \min\{(0.24 - 0 - 0.024),(0.60 - 0 - 0)\} = 0.216 \\ w_{CA}^{\max} &= \min\{(w_C - w_{CB} - w_{CC}),(w_A - w_{AA} - w_{BA})\} \\ &= \min\{(0.16 - 0 - 0),(0.60 - 0 - 0)\} = 0.16 \end{aligned}$$

and

$$\begin{aligned} w_{AA}^{\min} &= \max\left\{\left(w_A - w_{AB} - w_{AC}^{\max}\right),\left(w_A - w_{BA}^{\max} - w_{CA}^{\max}\right),0\right\} \\ &= \max\{(0.60 - 0.12 - 0.136),(0.60 - 0.216 - 0.16),0\} = 0.344 \end{aligned}$$

More generally, the minimum value of any element in the matrix can be written as

$$w_{ij}^{\min} = \max\left\{\left(w_i - \sum_{q\neq j}\left(w_{iq}^{\max} + w_{iq}\right)\right), \left(w_j - \sum_{q\neq i}\left(w_{qj}^{\max} + w_{qj}\right)\right), 0\right\} \tag{2.3.44}$$

where $w_{iq}^{\max}$, $w_{qj}^{\max}$ are the maximum possible values of null elements and w_{iq}, w_{qj} are the previously determined occurrence probabilities.

Thus, $0.344 \leq w_{AA} \leq 0.48$, and it is possible to choose $w_{AA} = 0.36$; some additional probability parameters are then determined:

$$\begin{aligned} w_{AC} &= (w_A - w_{AA} - w_{AB}) = (0.60 - 0.36 - 0.12) = 0.12 \\ w_{CC} &= (w_C - w_{AC} - w_{BC}) = (0.16 - 0.12 - 0.024) = 0.016 \end{aligned}$$

To define only the independent parameters, it is essential to calculate unknown occurrence probabilities in $[W_{ij}]$ as soon as they are fully determined. The fourth and last independent probability coefficient may then be chosen among remaining null elements, for example, w_{BA}:

$$[W_{ij}] = \left|\begin{array}{ccc|c} & 0.60 & 0.24 & 0.16 & \\ \hline \mathbf{0.36} & \mathbf{0.12} & 0.12 & 0.60 \\ \boldsymbol{w_{BA}} & 0 & \mathbf{0.024} & 0.24 \\ 0 & 0 & 0.016 & 0.16 \end{array}\right|$$

It is first necessary to define the possible range $[w_{BA}^{\min}, w_{BA}^{\max}]$ for this parameter:

$$\begin{aligned} w_{BA}^{\max} &= \min\{(w_B - w_{BB} - w_{BC}), (w_A - w_{AA} - w_{CA})\} \\ &= \min\{(0.24 - 0 - 0.024), (0.60 - 0.36 - 0)\} = 0.216 \\ w_{BA}^{\min} &= \max\{(w_B - w_{BB}^{\max} - w_{BC}), (w_A - w_{AA} - w_{CA}^{\max}), 0\} \end{aligned}$$

with

$$\begin{aligned} w_{BB}^{\max} &= \min\{(w_B - w_{BA} - w_{BC}), (w_B - w_{AB} - w_{CB})\} \\ &= \min\{(0.24 - 0 - 0.024), (0.24 - 0.12 - 0)\} = 0.12 \\ w_{CA}^{\max} &= \min\{(w_C - w_{CB} - w_{CC}), (w_A - w_{AA} - w_{BA})\} \\ &= \min\{(0.16 - 0 - 0.016), (0.60 - 0.36 - 0)\} = 0.144 \end{aligned}$$

Then, $w_{BA}^{\min} = \max\{(w_B - w_{BB}^{\max} - w_{BC}), (w_A - w_{AA} - w_{CA}^{\max}), 0\} = \max\{(0.24 - 0.12 - 0.024), (0.60 - 0.36 - 0.144), 0\} = 0.096$

Thus, $0.096 \le w_{BA} \le 0.216$, and it is possible to choose $w_{BA} = 0.12$, all other probability parameters being then determined: $w_{BB} = 0.096$, $w_{CB} = 0.024$, and $w_{CA} = 0.12$.

$$[W_{ij}] = \left|\begin{array}{ccc|c} & 0.60 & 0.24 & 0.24 & \\ \hline \mathbf{0.36} & \mathbf{0.12} & 0.12 & 0.60 \\ \mathbf{0.12} & 0.096 & \mathbf{0.024} & 0.24 \\ 0.12 & 0.024 & 0.016 & 0.16 \end{array}\right|$$

The $[P_{ij}]$ matrix of junction probabilities can then be calculated by dividing the three rows of matrix $[W_{ij}]$ by w_A, w_B, and w_C, respectively:

$$[P_{ij}] = \begin{vmatrix} 0.60 & 0.20 & 0.20 \\ 0.50 & 0.40 & 0.10 \\ 0.75 & 0.15 & 0.10 \end{vmatrix}$$

The relations in Eqs. (2.3.43) and (2.3.44) can be used to determine independent probability parameters through the same algorithm for any mixed-layer structure with $S = 1$ and arbitrary T.

2.3.2.2.5 *Mixed-Layer Structures with* S = 2, T = 2

The algorithm described in the previous section to determine independent probability parameters for mixed-layer structures with $S = 1$ and $T = 3$ can be extended to any mixed-layer structure with arbitrary S, for example, $S = 2$. In addition to the probability parameters w_i and p_{ij}, it is then necessary to define a set of p_{ijk} ($i, j, k = A, B$) junction probabilities. In this example, w_i and p_{ij} coefficients have been determined: $w_A = 0.8$, and $p_{BB} = 0.1$

Thus, $w_B = 0.2$, $p_{BA} = 0.9$, $p_{AB} = 0.225$, and $p_{AA} = 0.775$, and the occurrence probabilities of the different layer pairs may be calculated: $w_{AA} = 0.62$, $w_{AB} = w_{BA} = 0.18$, and $w_{BB} = 0.02$.

Additional independent probability coefficients are thus to be defined only among the p_{ijk} parameters that are linked by the following relations:

$$\begin{cases} p_{AAA}+p_{AAB}=1 \\ p_{ABA}+p_{ABB}=1 \\ p_{BAA}+p_{BAB}=1 \\ p_{BBA}+p_{BBB}=1 \end{cases} \tag{2.3.45}$$

$$\begin{cases} w_{AA}=w_{AA}p_{AAA}+w_{BA}p_{BAA} \\ w_{AB}=w_{AA}p_{AAB}+w_{BA}p_{BAB} \\ w_{BA}=w_{AB}p_{ABA}+w_{BB}p_{BBA} \\ w_{BB}=w_{AB}p_{ABB}+w_{BB}p_{BBB} \end{cases} \text{ or } \begin{cases} w_{AA}=w_{AAA}+w_{BAA} \\ w_{AB}=w_{AAB}+w_{BAB} \\ w_{BA}=w_{ABA}+w_{BBA} \\ w_{BB}=w_{ABB}+w_{BBB} \end{cases} \tag{2.3.46}$$

$$w_{AA}+w_{AB}+w_{BA}+w_{BB}=1 \tag{2.3.47}$$

Among the eight relations (Eqs. 2.3.45 and 2.3.46), only six are independent owing to Eqs. (2.3.28) and (2.3.47). As a consequence, only two of the eight probability coefficients p_{ijk} ($i, j, k=A, B$) are independent. To construct the $[W_{ijk}]$ matrix, the four relations in Eq. (2.3.45) are multiplied by w_{AA}, w_{AB}, w_{BA}, and w_{BB}, respectively, and these occurrence probabilities are reported to the right of and above the matrix, as in Eq. (2.3.48). When the two j indices are not identical, the value of the matrix element at the intersection of the ijth row and jkth column is necessarily null and is not reported in Eq. (2.3.48) for the sake of simplicity. When the two j indices are identical, coefficients w_{ijk} possibly take non-zero values, but it is convenient to assume all elements of the $[W_{ijk}]$ matrix having initially null values:

$$[W_{ijk}]=\left|\begin{array}{cccc|c} w_{AA} & w_{AB} & w_{BA} & w_{BB} & \\ w_{AAA} & w_{AAB} & & & w_{AA} \\ & & w_{ABA} & w_{ABB} & w_{AB} \\ w_{BAA} & w_{BAB} & & & w_{BA} \\ & & w_{BBA} & w_{BBB} & w_{BB} \end{array}\right| = \left|\begin{array}{cccc|c} 0.62 & 0.18 & 0.18 & 0.02 & \\ 0 & 0 & & & 0.62 \\ & & 0 & 0 & 0.18 \\ 0 & 0 & & & 0.18 \\ & & 0 & 0 & 0.02 \end{array}\right| \tag{2.3.48}$$

Any of the matrix elements can be defined as the first independent parameter, for example w_{ABA}. The possible range for this parameter can be defined as described in the previous section:

$$\begin{aligned} w_{ABA}^{\max} &= \min\{(w_{AB}-w_{ABB}),(w_{BA}-w_{BBA})\}=\min\{(0.18-0),(0.18-0)\} \\ &= 0.18 \end{aligned}$$

On the other hand, $w_{ABA}^{\min}$ depends on $w_{ABB}^{\max}$, and $w_{BBA}^{\max}$ which cannot exceed $w_{BB}=0.02$. Thus

$$\begin{aligned} w_{ABA}^{\min} &= \max\left\{\left(w_{AB}-w_{ABB}^{\max}\right),\left(w_{BA}-w_{BBA}^{\max}\right),0\right\} \\ &= \max\{(0.18-0.02),(0.18-0.02),0\}=0.16. \end{aligned}$$

Thus, $0.16 \leq w_{ABA} \leq 0.18$, and it is possible to choose $w_{ABA} = 0.171$, some additional probability parameters being then determined:

$$[W_{ijk}] = \left|\begin{array}{cccc|c} 0.62 & 0.18 & 0.18 & 0.02 & \\ 0 & 0 & & & 0.62 \\ & & \mathbf{0.171} & 0.009 & 0.18 \\ 0 & 0 & & & 0.18 \\ & & 0.009 & 0.011 & 0.02 \end{array}\right|$$

The fourth and last independent probability coefficient may then be chosen from among the remaining null elements, for example, w_{AAB}, and its possible range $[w_{AAB}^{\min}, w_{AAB}^{\max}]$ defined:

$$w_{AAB}^{\max} = \min\{(w_{AA} - w_{AAA}), (w_{AB} - w_{BAB})\} = \min\{(0.62 - 0), (0.18 - 0)\} = 0.18$$
$$w_{AAB}^{\min} = \max\left\{\left(w_{AA} - w_{AAA}^{\max}\right), \left(w_{AB} - w_{BAB}^{\max}\right), 0\right\} = \max\{(0.62 - 0.62), (0.18 - 0.18), 0\} = 0$$

It is possible to choose $w_{AAB} = 0.155$, and all other probability parameters can then be determined:

$$[W_{ijk}] = \left|\begin{array}{cccc|c} 0.62 & 0.18 & 0.18 & 0.02 & \\ 0.465 & \mathbf{0.155} & & & 0.62 \\ & & \mathbf{0.171} & 0.009 & 0.18 \\ 0.155 & 0.025 & & & 0.18 \\ & & 0.009 & 0.011 & 0.02 \end{array}\right|$$

The general formulas in Eqs. (2.3.43) and (2.3.44) defining the maximum and minimum values of a given matrix element for mixed-layer structures with $S = 1$ and any T value can be extended to mixed-layer structures with $S = 2$:

$$w_{ijk}^{\max} = \min\left\{\left(w_{ij} - \sum_{q \neq k} w_{ijq}\right), \left(w_{jk} - \sum_{q \neq i} w_{qjk}\right)\right\} \tag{2.3.49}$$

$$w_{ijk}^{\min} = \max\left\{\left(w_{ij} - \sum_{q \neq k}\left(w_{ijq}^{\max} + w_{ijq}\right)\right), \left(w_{jk} - \sum_{q \neq i}\left(w_{qjk}^{\max} + w_{qjk}\right)\right), 0\right\}, \tag{2.3.50}$$

w_{ijq}, w_{qjk} being the previously determined occurrence probabilities.

The $[P_{ijk}]$ matrix of junction probabilities can then be calculated by dividing the rows of matrix $[W_{ijk}]$ by the corresponding w_{ij} probabilities:

$$[P_{ijk}] = \left|\begin{array}{cccc} p_{AAA} & p_{AAB} & & \\ & & p_{ABA} & p_{ABB} \\ p_{BAA} & p_{BAB} & & \\ & & p_{BBA} & p_{BBB} \end{array}\right| = \left|\begin{array}{cccc} 0.75 & 0.25 & & \\ & & 0.95 & 0.05 \\ 0.861 & 0.139 & & \\ & & 0.45 & 0.55 \end{array}\right|$$

The same algorithm can be used for mixed-layer structures with $S=2$ and any T value. In this case, the relative proportions of the different layer types (w_i) should be defined first, and independent junction probability parameters for nearest neighbours ($S=1$, p_{ij}) next. As a third step, independent junction probabilities for next-nearest neighbours (p_{ijk}) should be defined, and the occurrence probability may then be calculated for any layer sequence in the mixed-layer structure with $S=2$.

The above algorithm may be extended to any mixed-layer structure with any values of the short-range order factor (Reichweite) S and layer type number T. In this case, the range of values allowed for any matrix element can be expressed as

$$w_{ij\cdots kl}^{\max} = \min\left\{\left(w_{ij\cdots k} - \sum_{q\neq l} w_{ij\cdots kq}\right), \left(w_{j\cdots kl} - \sum_{q\neq i} w_{qj\cdots kl}\right)\right\} \tag{2.3.51}$$

$$w_{ij\cdots kl}^{\min} = \max\left\{\left(w_{ij\cdots k} - \sum_{q\neq l}\left(w_{ij\cdots kq}^{\max} + w_{ij\cdots kq}\right)\right), \left(w_{j\cdots kl} - \sum_{q\neq i}\left(w_{qj\cdots kl}^{\max} + w_{qj\cdots kl}\right)\right), 0\right\}, \tag{2.3.52}$$

where the number of indices for probability parameters $w_{ij\cdots kl}^{\max}, w_{ij\cdots kl}^{\min}, w_{ij\cdots kq}^{\max}$, $w_{qj\cdots kl}^{\max}, w_{ij\cdots kq}, w_{qj\cdots kl}$ and $w_{ij\cdots k}, w_{j\cdots kl}$ are $S+1$ and S, respectively.

The $S=0$ case is a special one as randomly interstratified mixed-layer structures require only the definition of layer relative abundances w_i ($i=1$, 2, . . ., T), and there are $(T-1)$ independent parameters. For mixed-layer structures with $S\geq 1$, there are $(T-1)^2T^{S-1}$ independent parameters among $w_{ij\cdots k}$ coefficients with $S+1$ indices. For example, in addition to the $(T-1)$ independent w_i probability parameters, mixed-layer structures with $S=1$ require the definition of $(T-1)^2$ independent w_{ij} probability parameters. Mixed-layer structures with $S=2$ require the additional definition of $(T-1)^2T$ independent w_{ijk} probability parameters, and so on.

2.3.2.2.6 *Ordering and Segregation in Mixed-Layer Structures with* S = 2, T = 2

Drits and Sakharov (1976) proposed a plot similar to that in Fig. 2.3.4 to differentiate two-component mixed-layer structures with $S=2$ and different degrees of order/disorder in the stacking of A and B layers. For their description, these authors hypothesized that A layers were prevailing ($w_A > w_B$) and that nearest neighbour ordering ($S=1$) was characterized by maximum possible degree of ordering (MPDO, $p_{BB}=0$). In this case, $w_{AA}=w_A-w_B$, $w_{AB}=w_{BA}=w_B$, $w_{BB}=0$.

The following relations can be deduced from Eq. (2.3.46):

$$w_{AA}\ p_{AAB} = w_{BA}\ p_{BAA} \text{ or } (w_A - w_B)p_{AAB} = w_{BA}\ p_{BAA}, \text{ or}$$
$$(1 - p_{AAA}) = \frac{w_B}{w_A - w_B}(1 - p_{BAB}),$$

and the last relation can be modified to

$$p_{AAA} = \frac{w_B}{w_A - w_B} p_{BAB} + 1 - \frac{w_B}{w_A - w_B} \tag{2.3.53}$$

Equation (2.3.53) is analogous to Eq. (2.3.32) established for mixed-layer structures with $S = 1$ and correlates linearly the junction probability parameters p_{AAA} and p_{BAB} for a given w_A value (Fig. 2.3.5). Mixed-layer structures with a given w_A value are thus located along straight lines originating from the upper right corner of the diagram in Fig. 2.3.5. The relative abundance of A layers increases clockwise from the vertical line to the right of the diagram ($w_A = 0.5$) to the top horizontal line ($w_A = 1.0$), the line linking the upper right and lower left corners corresponding to $w_A = 0.667$. The physical mixture of periodic crystals composed either of A layers or of AB layer pairs corresponds to the upper right corner of the diagram with $p_{AAA} = p_{BAB} = 1$ (Fig. 2.3.5). Both p_{AAA} and p_{BAB} axes

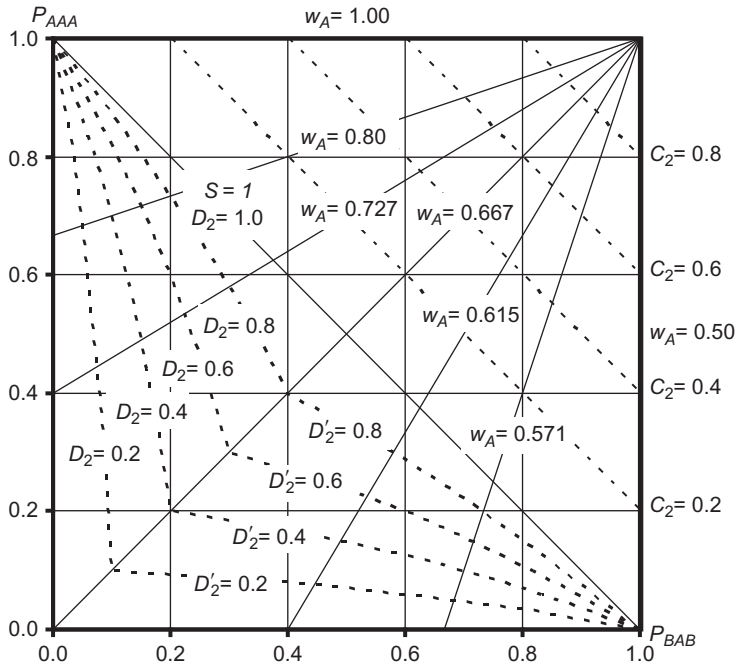

FIGURE 2.3.5 Junction probability diagram for two-component mixed-layer structures with $S = 2$, and maximum possible degree of ordering at $S = 1$ (MPDO, $w_A > w_B$ and $p_{BB} = 0$). See text for details. *Adapted from Drits and Sakharov (1976).*

correspond to mixed-layer structures with MPDO, which corresponds to $p_{BAB}=0$ when $w_A \geq 0.667$ or to $p_{AAA}=0$ for $w_A \leq 0.667$ ($S=2$). The first axis corresponds to the random interstratification of *AB* layer pairs and *AAB* layer triplets, whereas the second one corresponds to the random interstratification of *AAB* layer triplets and *A* single layers (Reynolds, 1988; Drits et al., 1994). The lower left corner with $p_{AAA}=p_{BAB}=0$ corresponds to the periodic $AABAAB\cdots$ layer sequence with a 2:1 ratio between *A* and *B* layers. The specific case of $S=1$ with MPDO but random interstratification at $S=2$ corresponds to the line where $p_{AAA}+p_{BAB}=1$, that is, to the straight line linking the upper left and lower right corners of the diagram in Fig. 2.3.5. In this case, it is possible to deduce the following relations, characteristic of $S=1$ with MPDO, using Eqs. (2.3.46) and (2.3.53):

$$p_{AAA}=\frac{w_A-w_B}{w_A}=p_{AA}, \quad \text{and} \quad p_{BAB}=\frac{w_B}{w_A}=p_{AB}$$

The domain above this diagonal that is towards the physical mixture point at the upper right corner corresponds to mixed-layer structures with a tendency to segregation of *A* layers and *AB* layer pairs, whereas the domain below this diagonal corresponds to partial ordering. Mixed-layer structures with a similar tendency to ordering at $S=2$ but with contrasting composition (relative contents of *A* and *B* layers) share the following parameters:

$$D_2=\frac{w_A}{w_B}p_{BAB} \quad \text{for} \quad 0\leq p_{BAB}\leq \frac{w_B}{w_A}, w_A \geq 2/3 \tag{2.3.54}$$

and

$$D'_2=\frac{w_A}{w_A-w_B}p_{AAA} \quad \text{for } 0\leq p_{AAA}\leq \frac{w_A-w_B}{w_A} \text{ and } 1/2\leq w_A\leq 2/3 \tag{2.3.55}$$

The index 2 of *D* and *D′* parameters indicates that the disorder parameters describe mixed-layer structures with $S=2$. Equation (2.3.53) can be transformed to

$$\frac{w_B}{w_A}=\frac{1-p_{AAA}}{2-p_{AAA}-p_{BAB}}.$$

As a consequence,

$$D_2=\frac{p_{BAB}(2-p_{AAA}-p_{BAB})}{1-p_{AAA}}, \quad \text{and } p_{AAA}=\frac{2p_{BAB}-p_{BAB}^2-D_2}{p_{BAB}-D_2}.$$

$$\text{Similarly}: \quad p_{BAB}=\frac{2p_{AAA}-p_{AAA}^2-D'_2}{p_{AAA}-D'_2}$$

The last two equations were used in Fig. 2.3.5 to draw the dashed lines corresponding to given values of the disorder parameters *D* and *D′*, that is, to mixed-layer structures with a similar tendency to ordering. Similarly, the degree of segregation of *A* layers and *AB* layer pairs in mixed-layer structures with

$S=2$ can be described by the parameter $C_2=1-[(1-p_{BAB})/(1-w_B/w_A)]$ for $\frac{w_B}{w_A}\leq p_{BAB}\leq 1$.

As a consequence, the relation $p_{BAB}=1+C_2-p_{AAA}$ allows drawing in Fig. 2.3.5 the straight dashed lines corresponding to a given degree of segregation of A layers and AB layer pairs.

2.3.3 CALCULATION OF THE INTENSITY DIFFRACTED BY MIXED-LAYER STRUCTURES: THE MATRIX FORMALISM

Using the expression in Eq. (2.3.10), Eq. (2.3.12) describing the intensity of waves diffracted by a mixed-layered crystal can be written as

$$I(Z)=A^*(Z)A(Z)=\sum_{m=1}^{N}\sum_{m'=1}^{N}F_m^*(Z)F_{m'}(Z)\exp 2\pi iZ(r_m-r_{m'}) \tag{2.3.56}$$

The terms with $m=m'$ can be written separately, whereas the relation $n=|m'-m|$ can be introduced to label the layers in $(n+1)$ layer sequences. Similarly, $|r_n|=|r_m-r_{m'}|$ and Eq. (2.3.56) can be written as

$$\begin{aligned} I(Z)&=\sum_{m=1}^{N}F_m^*(Z)F_m(Z)+\sum_{\substack{m=1\\ m\neq m'}}^{N}\sum_{m'=1}^{N}F_m^*(Z)F_{m'}(Z)\exp 2\pi iZ(r_m-r_{m'})\\ &=\sum_{m=1}^{N}F_m^*(Z)F_m(Z)+2\mathrm{Re}\sum_{n=1}^{N-1}\sum_{m=1}^{N-n}F_m^*(Z)F_{m+n}(Z)\exp 2\pi iZr_n \end{aligned} \tag{2.3.57}$$

A comparison of Eqs. (2.3.57) and (2.3.22) leads to

$$\sum_{m=1}^{N}F_m^*(Z)F_m(Z)=N\sum_{s=1}^{T}w_sF_s^*F_s=N\overline{F_o^*(Z)F_o(Z)}, \tag{2.3.58}$$

and to

$$\begin{aligned} &2Re\sum_{n=1}^{N-1}\sum_{m=1}^{N-n}F_m^*(Z)F_{m+n}(Z)\exp\ 2\pi iZr_n\\ &=2Re\sum_{n=1}^{N-1}(N-n)\sum_{s=1}^{T}\sum_{h_1=1}^{T}\sum_{h_2=1}^{T}\cdots\sum_{h_{n-1}=1}^{T}\sum_{t=1}^{T}w_{sh_1h_2\cdots h_{n-1}t}F_s^*F_t\exp i\left(\varphi_s+\varphi_{h_1}+\varphi_{h_2}+\cdots+\varphi_{h_{n-1}}\right)\\ &=2Re\sum_{n=1}^{N-1}(N-n)\overline{F_o^*(Z)F_n(Z)\exp\ 2\pi iZr_n} \end{aligned} \tag{2.3.59}$$

And the intensity diffracted by a mixed-layer crystal can be expressed as

$$I(Z)=N\overline{F_o^*(Z)F_o(Z)}+2\mathrm{Re}\sum_{n=1}^{N-1}(N-n)\overline{F_o^*(Z)F_n(Z)\exp\ 2\pi iZr_n} \tag{2.3.60}$$

This expression corresponds to the sum of the average intensity of waves diffracted by single layers and of the average intensity of waves diffracted by layers at both ends of $(n+1)$ layer sequences, taking into account the distance between these layers.

Hendricks and Teller (1942) were the first to develop a matrix formalism to calculate the intensity diffracted by 1D disordered lamellar crystals with infinite thickness and random layer stacking. Kakinoki and Komura (1952, 1954a,b) extended this approach further to mixed-layer crystals with a limited number of layers. These authors introduced also the concept of range of interaction between layers (Reichweite) proposed by Jagodzinski (1949a,b,c). Another approach, which is based on the direct summation of the contributions to diffracted intensity from waves scattered by all possible layer subsequences in crystals, was also developed for the calculation of XRD patterns from mixed-layer structures (Reynolds, 1967, 1980). The matrix formalism was refined by Allegra (1961, 1964), before its interest became evident with the onset of computer simulation of XRD patterns (Sato, 1969a,b; Drits and Sakharov, 1976; Plançon, 1981; Sakharov et al., 1982a,b, 1983; Drits and Tchoubar, 1990). Contrary to direct summation, the matrix formalism allows, indeed, the straightforward calculation of the contributions of n layer sequences to diffracted intensity if these contributions are known for $(n-1)$ layer sequences. In addition, the matrix formalism is extremely versatile as it sets no limitations on the number of layer types in mixed-layer structures or on the actual extent of the short-range order factor (Reichweite; Sakharov et al., 1982a,b, 1983; Drits and Tchoubar, 1990). Using a notation consistent with this chapter, the intensity of X-rays diffracted by a mixed-layer crystal (Kakinoki and Komura, 1952, 1954a,b) can be expressed as

$$I = NSpur[V][W] + 2\mathrm{Re}\sum_{n=1}^{N-1}(N-n)Spur[V][W][Q]^n \qquad (2.3.61)$$

where $[V]$ is a matrix containing the products of the structure amplitudes $F_i^* F_j$ of the ith and jth layer types, respectively; $[W]$ is the diagonal matrix of occurrence probabilities for single layers, layer pairs, triplets, and so on; $[Q]$ is the square matrix containing the products of the junction probability parameter and the corresponding phase term; and *Spur* is the trace of the resulting matrix, that is, the sum of its diagonal elements.

The order of matrices $[V]$, $[W]$, and $[Q]$ depends, together with the location of their elements, on the number T of layer types present in the mixed-layer structure and its Reichweite parameter S. It is shown in the following sections that Eqs. (2.3.60) and (2.3.61) are equivalent and describe identical diffraction effects.

2.3.3.1 Mixed-Layer Structures with $S=1$ or $S=0$, and $T=2$

If A and B layers alternate in a mixed-layer structure with $S=1$, the above matrices can be written as

$$[V]=\begin{vmatrix} F_A^*F_A & F_B^*F_A \\ F_A^*F_B & F_B^*F_B \end{vmatrix},[W]=\begin{vmatrix} w_A & \\ & w_B \end{vmatrix},[Q]=\begin{vmatrix} p_{AA}\exp i\varphi_A & p_{AB}\exp i\varphi_A \\ p_{BA}\exp i\varphi_B & p_{BB}\exp i\varphi_B \end{vmatrix} \tag{2.3.62}$$

and it is possible to deduce

$$NSpur[V][W]=N\left(w_AF_A^*F_A+w_BF_B^*F_B\right)=\sum_{s=1}^{T}w_sF_s^*F_s \tag{2.3.63}$$

The first term of Eq. (2.3.61) is thus equivalent to Eq. (2.3.58). In addition

$$\begin{aligned}
&2\mathrm{Re}\sum_{n=1}^{N-1}(N-n)Spur[V][W][Q]^n \\
&\quad=\left.\begin{aligned}&2\mathrm{Re}(N-1)\left[w_Ap_{AA}F_A^*F_A\exp i\varphi_A+w_Bp_{BA}F_B^*F_A\exp i\varphi_B\right.\\&\left.+w_Ap_{AB}F_A^*F_B\exp i\varphi_A+w_Bp_{BB}F_B^*F_B\exp i\varphi_B\right]\\&=2\mathrm{Re}(N-1)\sum_{s=1}^{T}\sum_{t=1}^{T}w_sp_{st}F_s^*F_t\exp i\varphi_s\end{aligned}\right\}\ \text{for}\ n=1,\\
&\quad=\left.\begin{aligned}&2\mathrm{Re}(N-2)\left[w_Ap_{AA}p_{AA}F_A^*F_A\exp i(\varphi_A+\varphi_A)\right.\\&+w_Bp_{BA}p_{AA}F_B^*F_A\exp i(\varphi_B+\varphi_A)+w_Ap_{AB}p_{BA}F_A^*F_A\exp i(\varphi_A+\varphi_B)\\&+w_Bp_{BB}p_{BA}F_B^*F_A\exp i(\varphi_B+\varphi_B)+w_Ap_{AA}p_{AB}F_A^*F_B\exp i(\varphi_A+\varphi_A)\\&+w_Bp_{BA}p_{AB}F_B^*F_B\exp i(\varphi_B+\varphi_A)+w_Ap_{AB}p_{BB}F_A^*F_B\exp i(\varphi_A+\varphi_B)\\&\left.+w_Bp_{BB}p_{BB}F_B^*F_B\exp i(\varphi_B+\varphi_B)\right]\\&=2\mathrm{Re}(N-2)\sum_{s=1}^{T}\sum_{h_1}^{T}\sum_{t=1}^{T}w_sp_{sh_1}p_{h_1t}F_s^*F_t\exp i\varphi_s\end{aligned}\right\}\ \text{for}\ n=2,\ \text{etc.}
\end{aligned} \tag{2.3.64}$$

The second term of Eq. (2.3.61) is thus equivalent to Eq. (2.3.59) for all values of n and for $T=2$. For mixed-layer structures with $S=0$, Eq. (2.3.61) is unchanged, the junction probabilities in matrix $[Q]$ being $p_{AA}=p_{BA}=w_A$ and $p_{AB}=p_{BB}=w_B$.

2.3.3.2 Mixed-Layer Structures with $S=1$ and $T=3$

If A, B, and C layers alternate in a mixed-layer structure with $S=1$, matrices $[V]$, $[W]$, and $[Q]$ can be written as

$$[V]=\begin{vmatrix} F_A^*F_A & F_B^*F_A & F_C^*F_A \\ F_A^*F_B & F_B^*F_B & F_C^*F_B \\ F_A^*F_C & F_B^*F_C & F_C^*F_C \end{vmatrix},[W]=\begin{vmatrix} w_A & & \\ & w_B & \\ & & w_C \end{vmatrix},\ \text{and}$$

$$[Q]=\begin{vmatrix} p_{AA}\exp i\varphi_A & p_{AB}\exp i\varphi_A & p_{AC}\exp i\varphi_A \\ p_{BA}\exp i\varphi_B & p_{BB}\exp i\varphi_B & p_{BC}\exp i\varphi_B \\ p_{CA}\exp i\varphi_C & p_{CB}\exp i\varphi_C & p_{CC}\exp i\varphi_C \end{vmatrix}$$

As for two-component mixed-layer structures, it is possible to demonstrate that Eqs. (2.3.60) and (2.3.61) are equivalent.

2.3.3.3 Mixed-Layer Structures with $S=2$ and $T=2$

If A and B layers alternate in a mixed-layer structure with $S=2$, matrices $[V]$, $[W]$, and $[Q]$ can be written as

$$[V]=\begin{vmatrix} F_A^*F_A & F_A^*F_A & F_B^*F_A & F_B^*F_A \\ F_A^*F_A & F_A^*F_A & F_B^*F_A & F_B^*F_A \\ F_A^*F_B & F_A^*F_B & F_B^*F_B & F_B^*F_B \\ F_A^*F_B & F_A^*F_B & F_B^*F_B & F_B^*F_B \end{vmatrix}, [W]=\begin{vmatrix} w_{AA} & & & \\ & w_{AB} & & \\ & & w_{BA} & \\ & & & w_{BB} \end{vmatrix},$$

and

$$[Q]=\begin{vmatrix} p_{AAA}\exp i\varphi_A & p_{AAB}\exp i\varphi_A & & \\ p_{BAA}\exp i\varphi_B & p_{BAB}\exp i\varphi_B & & \\ & & p_{ABA}\exp i\varphi_A & p_{ABB}\exp i\varphi_A \\ & & p_{BBA}\exp i\varphi_B & p_{BBB}\exp i\varphi_B \end{vmatrix} \quad (2.3.65)$$

Equation (2.3.61) can then be calculated for different values of n:

$$\begin{aligned} NSpur[V][W] &= N\left(w_{AA}F_A^*F_A + w_{AB}F_A^*F_A + w_{BA}F_B^*F_B + w_{BB}F_B^*F_B\right) \\ &= N\left(w_AF_A^*F_A + w_BF_B^*F_B\right) = \sum_{s=1}^{T} w_sF_sF_s^* \quad \text{for } n=0, \end{aligned}$$

$$\left.\begin{aligned} &2\mathrm{Re}\sum_{n=1}^{N-1}(N-n)Spur[V][W][Q]^n \\ &\quad = 2\mathrm{Re}(N-1)\left[w_{AA}p_{AAA}F_A^*F_A\exp i\varphi_A + w_{BA}p_{BAA}F_B^*F_A\exp i\varphi_B\right. \\ &\quad + w_{AA}p_{AAB}F_A^*F_A\exp i\varphi_A + w_{BA}p_{BAB}F_B^*F_A\exp i\varphi_B \\ &\quad + w_{AB}p_{ABA}F_A^*F_B\exp i\varphi_A + w_{BB}p_{BBA}F_B^*F_A\exp i\varphi_B \\ &\quad \left. + w_{AB}p_{ABB}F_A^*F_B\exp i\varphi_A + w_{BB}p_{BBB}F_B^*F_A\exp i\varphi_B\right] \\ &\quad = 2\mathrm{Re}(N-1)\left[w_Ap_{AA}F_A^*F_A\exp i\varphi_A + w_Bp_{BA}F_B^*F_A\exp i\varphi_B\right. \\ &\quad \left. + w_Ap_{AB}F_A^*F_B\exp i\varphi_A + w_Bp_{BB}F_B^*F_B\exp i\varphi_B\right] \\ &\quad = 2\mathrm{Re}(N-1)\sum_{s=1}^{T}\sum_{t=1}^{T}w_sp_{st}F_s^*F_t\exp i\varphi_s \end{aligned}\right\} \text{for } n=1,$$

$$
\begin{aligned}
&2\mathrm{Re}\sum_{n=1}^{N-1}(N-n)Spur[V][W][Q]^n \\
&=2\mathrm{Re}(N-2)\left[w_{AA}p_{AAA}p_{AAA}F_A^*F_A\exp i\left(\varphi_A+\varphi_A\right)+w_{BA}p_{BAA}p_{AAA}F_B^*F_A\exp i\left(\varphi_B+\varphi_A\right)\right. \\
&+w_{AB}p_{ABA}p_{BAA}F_A^*F_A\exp i\left(\varphi_A+\varphi_B\right)+w_{BB}p_{BBA}p_{BAA}F_B^*F_A\exp i\left(\varphi_B+\varphi_B\right) \\
&+w_{AA}p_{AAA}p_{AAB}F_A^*F_A\exp i\left(\varphi_A+\varphi_A\right)+w_{BA}p_{BAA}p_{AAB}F_B^*F_A\exp i\left(\varphi_B+\varphi_A\right) \\
&+w_{AB}p_{ABA}p_{BAB}F_A^*F_A\exp i\left(\varphi_A+\varphi_B\right)+w_{BB}p_{BBA}p_{BAB}F_B^*F_A\exp i\left(\varphi_B+\varphi_B\right) \\
&+w_{AA}p_{AAB}p_{ABA}F_A^*F_B\exp i\left(\varphi_A+\varphi_A\right)+w_{BA}p_{BAB}p_{ABA}F_B^*F_B\exp i\left(\varphi_B+\varphi_A\right) \\
&+w_{AB}p_{ABB}p_{BBA}F_A^*F_B\exp i\left(\varphi_A+\varphi_B\right)+w_{BB}p_{BBB}p_{BBA}F_B^*F_B\exp i\left(\varphi_B+\varphi_B\right) \\
&+w_{AA}p_{AAB}p_{ABB}F_A^*F_B\exp i\left(\varphi_A+\varphi_A\right)+w_{BA}p_{BAB}p_{ABB}F_B^*F_B\exp i\left(\varphi_B+\varphi_A\right) \\
&\left.+w_{AB}p_{ABB}p_{BBB}F_A^*F_B\exp i\left(\varphi_A+\varphi_B\right)+w_{BB}p_{BBB}p_{BBB}F_B^*F_B\exp i\left(\varphi_B+\varphi_B\right)\right] \\
&=2\mathrm{Re}(N-2)\left[w_Ap_{AA}p_{AAA}F_A^*F_A\exp i\left(\varphi_A+\varphi_A\right)+w_Bp_{BA}p_{BAA}F_B^*F_A\exp i\left(\varphi_B+\varphi_A\right)\right. \\
&+w_Ap_{AB}p_{ABA}F_A^*F_A\exp i\left(\varphi_A+\varphi_B\right)+w_Bp_{BB}p_{BBA}F_B^*F_A\exp i\left(\varphi_B+\varphi_B\right) \\
&+w_Ap_{AA}p_{AAB}F_A^*F_B\exp i\left(\varphi_A+\varphi_A\right)+w_Bp_{BA}p_{BAB}F_B^*F_B\exp i\left(\varphi_B+\varphi_A\right) \\
&\left.+w_Ap_{AB}p_{ABB}F_A^*F_B\exp i\left(\varphi_A+\varphi_B\right)+w_Bp_{BB}p_{BBB}F_B^*F_B\exp i\left(\varphi_B+\varphi_B\right)\right] \\
&=2\mathrm{Re}(N-2)\sum_{s=1}^{T}\sum_{h_1}^{T}\sum_{t=1}^{T}w_sp_{sh_1}p_{h_1t}F_s^*F_t\exp i\varphi_s
\end{aligned}
\quad \left.\begin{array}{l} \\ \\ \\ \\ \\ \\ \\ \\ \\ \\ \\ \\ \\ \\ \\ \\ \end{array}\right\} \text{for } n=2, \text{ etc.}
$$

As for mixed-layer structures with $S=1$, it is possible to demonstrate that Eqs. (2.3.60) and (2.3.61) are equivalent.

2.3.3.4 Mixed-Layer Structures with $S=2$ and $T=3$

If A, B, and C layers alternate in a mixed-layer structure with $S=2$, matrices $[V]$, $[W]$, and $[Q]$ become

$$
[V]=\begin{vmatrix}
F_A^*F_A & F_A^*F_A & F_A^*F_A & F_B^*F_A & F_B^*F_A & F_B^*F_A & F_C^*F_A & F_C^*F_A & F_C^*F_A \\
F_A^*F_A & F_A^*F_A & F_A^*F_A & F_B^*F_A & F_B^*F_A & F_B^*F_A & F_C^*F_A & F_C^*F_A & F_C^*F_A \\
F_A^*F_A & F_A^*F_A & F_A^*F_A & F_B^*F_A & F_B^*F_A & F_B^*F_A & F_C^*F_A & F_C^*F_A & F_C^*F_A \\
F_A^*F_B & F_A^*F_B & F_A^*F_B & F_B^*F_B & F_B^*F_B & F_B^*F_B & F_C^*F_B & F_C^*F_B & F_C^*F_B \\
F_A^*F_B & F_A^*F_B & F_A^*F_B & F_B^*F_B & F_B^*F_B & F_B^*F_B & F_C^*F_B & F_C^*F_B & F_C^*F_B \\
F_A^*F_B & F_A^*F_B & F_A^*F_B & F_B^*F_B & F_B^*F_B & F_B^*F_B & F_C^*F_B & F_C^*F_B & F_C^*F_B \\
F_A^*F_C & F_A^*F_C & F_A^*F_C & F_B^*F_C & F_B^*F_C & F_B^*F_C & F_C^*F_C & F_C^*F_C & F_C^*F_C \\
F_A^*F_C & F_A^*F_C & F_A^*F_C & F_B^*F_C & F_B^*F_C & F_B^*F_C & F_C^*F_C & F_C^*F_C & F_C^*F_C \\
F_A^*F_C & F_A^*F_C & F_A^*F_C & F_B^*F_C & F_B^*F_C & F_B^*F_C & F_C^*F_C & F_C^*F_C & F_C^*F_C
\end{vmatrix},
$$

$$[W]=\begin{vmatrix} w_{AA} & & & & & & & & \\ & w_{AB} & & & & & & & \\ & & w_{AC} & & & & & & \\ & & & w_{BA} & & & & & \\ & & & & w_{BB} & & & & \\ & & & & & w_{BC} & & & \\ & & & & & & w_{CA} & & \\ & & & & & & & w_{CB} & \\ & & & & & & & & w_{CC} \end{vmatrix}$$

and

$$[Q]=\begin{vmatrix} p_{AAA}\varphi_A & p_{AAB}\varphi_A & p_{AAC}\varphi_A & & & & & & \\ & & & p_{ABA}\varphi_A & p_{ABB}\varphi_A & p_{ABC}\varphi_A & & & \\ & & & & & & p_{ACA}\varphi_A & p_{ACB}\varphi_A & p_{ACC}\varphi_A \\ p_{BAA}\varphi_B & p_{BAB}\varphi_B & p_{BAC}\varphi_B & & & & & & \\ & & & p_{BBA}\varphi_B & p_{BBB}\varphi_B & p_{BBC}\varphi_B & & & \\ & & & & & & p_{BCA}\varphi_B & p_{BCB}\varphi_B & p_{BCC}\varphi_B \\ p_{CAA}\varphi_C & p_{CAB}\varphi_C & p_{CAC}\varphi_C & & & & & & \\ & & & p_{CBA}\varphi_C & p_{CBB}\varphi_C & p_{CBC}\varphi_C & & & \\ & & & & & & p_{CCA}\varphi_C & p_{CCB}\varphi_C & p_{CCC}\varphi_C \end{vmatrix},$$

φ_j being equivalent to $\exp i\varphi_j$.

2.3.3.5 Mixed-Layer Structures with $S \geq 3$ and $T \geq 2$

If A and B layers alternate in a mixed-layer structure with $S=3$, matrices $[V]$, $[W]$, and $[Q]$ become

$$[V]=\begin{vmatrix} F_A^*F_A & F_A^*F_A & F_A^*F_A & F_A^*F_A & F_B^*F_A & F_B^*F_A & F_B^*F_A & F_B^*F_A \\ F_A^*F_A & F_A^*F_A & F_A^*F_A & F_A^*F_A & F_B^*F_A & F_B^*F_A & F_B^*F_A & F_B^*F_A \\ F_A^*F_A & F_A^*F_A & F_A^*F_A & F_A^*F_A & F_B^*F_A & F_B^*F_A & F_B^*F_A & F_B^*F_A \\ F_A^*F_A & F_A^*F_A & F_A^*F_A & F_A^*F_A & F_B^*F_A & F_B^*F_A & F_B^*F_A & F_B^*F_A \\ F_A^*F_B & F_A^*F_B & F_A^*F_B & F_A^*F_B & F_B^*F_B & F_B^*F_B & F_B^*F_B & F_B^*F_B \\ F_A^*F_B & F_A^*F_B & F_A^*F_B & F_A^*F_B & F_B^*F_B & F_B^*F_B & F_B^*F_B & F_B^*F_B \\ F_A^*F_B & F_A^*F_B & F_A^*F_B & F_A^*F_B & F_B^*F_B & F_B^*F_B & F_B^*F_B & F_B^*F_B \\ F_A^*F_B & F_A^*F_B & F_A^*F_B & F_A^*F_B & F_B^*F_B & F_B^*F_B & F_B^*F_B & F_B^*F_B \end{vmatrix},$$

$$[W]=\begin{vmatrix} w_{AAA} & & & & & & & \\ & w_{AAB} & & & & & & \\ & & w_{ABA} & & & & & \\ & & & w_{ABB} & & & & \\ & & & & w_{BAA} & & & \\ & & & & & w_{BAB} & & \\ & & & & & & w_{BBA} & \\ & & & & & & & w_{BBB} \end{vmatrix},$$

and

$$[Q]=\begin{vmatrix} p_{AAAA}\varphi_A & p_{AAAB}\varphi_A & & & & & & \\ & & p_{AABA}\varphi_A & p_{AABB}\varphi_A & & & & \\ & & & & p_{ABAA}\varphi_A & p_{ABAB}\varphi_A & & \\ & & & & & & p_{ABBA}\varphi_A & p_{ABBB}\varphi_A \\ p_{BAAA}\varphi_B & p_{BAAB}\varphi_B & & & & & & \\ & & p_{BABA}\varphi_B & p_{BABB}\varphi_B & & & & \\ & & & & p_{BBAA}\varphi_B & p_{BBAB}\varphi_B & & \\ & & & & & & p_{BBBA}\varphi_B & p_{BBBB}\varphi_B \end{vmatrix}.$$

The same logical process can be used for any set of S and T values, Eqs. (2.3.60) and (2.3.61) being equivalent in all cases.

2.3.3.6 Periodic Structures ($T=1$)

When the crystal contains a single type of layer with a given scattering amplitude $F(Z)$ and layer thickness ξ, the expression of matrices $[V]$, $[W]$, and $[Q]$ becomes $F^*(Z)F(Z)$, 1, and $\exp-2\pi iZ\xi$, respectively, and Eq. (2.3.61) is equivalent to Eq. (2.3.23).

2.3.4 INTENSITY DIFFRACTED BY A POWDER OF CRYSTALS WITH CONTRASTING NUMBERS OF LAYERS

Equation (2.3.61) is valid for a set of crystals all of which have the same number of layers (N), whereas powder samples obviously include crystals with contrasting numbers of layers. If the relative abundances of crystals with 1, 2, ..., N layers are noted $F(1)$, $F(2)$, ..., $F(N)$, respectively, the overall intensity diffracted by the powder may be written as the weighted ($\sum_{m=1}^{N}F(m)=1$) sum of the intensities scattered by crystals with 1, 2, ..., N layers, that is,

$$I=I_1+I_2+\cdots+I_N, \quad \text{with}$$

$$I_1=F(1)[1SpurVW] \quad \text{for crystals with 1 layer,}$$

$$I_2=F(2)[2SpurVW+2\mathrm{Re}\{1SpurVWQ\}] \quad \text{for crystals with 2 layers,}$$

$$I_3 = F(3)\left[3SpurVW + 2\mathrm{Re}\left\{2SpurVWQ + 1SpurVWQ^2\right\}\right]$$

for crystals with 3 layers, …,

and

$$I_N = F(N)\left[NSpurVW + 2\mathrm{Re}\left\{(N-1)SpurVWQ + \ldots + 1SpurVWQ^{N-1}\right\}\right]$$

for crystals with N layers.

Thus

$$\begin{aligned} I = & \sum_{m=1}^{N} mF(m)SpurVW \\ & + 2\mathrm{Re}\left\{\sum_{m=2}^{N}(m-1)F(m)SpurVWQ + \cdots\right. \\ & \left. + \sum_{m=N}^{N}(m-(N-1))F(m)SpurVWQ^{N-1}\right\} \\ & = \overline{N}SpurVW + 2\mathrm{Re}\sum_{n=1}^{N-1}\sum_{m=n+1}^{N}(m-n)F(m)SpurVWQ^n \end{aligned} \quad (2.3.66)$$

where $\overline{N} = \sum_{m=1}^{N} mF(m)$ is the average number of layers in the crystals.

Equations (2.3.61) and (2.3.66) differ only by the weight of the $SpurVW$ and $SpurVWQ^n$ terms, which are N and $c_n = (N-n)$, respectively, in Eq. (2.3.61), and $\overline{N}$ and $c_n = \sum_{m=n+1}^{N}(m-n)F(m)$, respectively, in Eq. (2.3.66).

2.3.4.1 Lognormal Distributions of Crystal Thickness

In nature, the distribution of occurrence probabilities of crystals with contrasting numbers of layers $F(m)$ with $m = 1, 2, \ldots, N$ can have distinct shapes (Eberl et al., 1998), the thickness distribution of so-called illite fundamental particles in natural illite and illite–smectite being essentially lognormal in shape (Eberl et al., 1990; Srodon et al., 2000).

$$F(m) = \frac{1}{\sqrt{2\pi}\beta m}\exp -\frac{(\ln m - \alpha)^2}{2\beta^2} \quad (2.3.67)$$

In addition, Drits et al. (1997c, 1998) have derived a unique relation linking the α and β^2 parameters of the coherent scattering domain (CSD) size lognormal distribution reported for these clay minerals to the average thickness of the crystals ($\overline{N}$): that is, $\alpha = 0.9485\ln\overline{N} - 0.017$ and $\beta^2 = 0.1032\ln\overline{N} + 0.034$

A lognormal distribution of CSD sizes, with the above α and β^2 parameters, allowed a satisfactory fitting of the XRD data of various periodic and mixed-layer clay minerals (Drits et al., 1997b, 2002a,b, 2004; Sakharov et al., 1999a, b; Lindgreen et al., 2000, 2002, 2008; Claret et al., 2004; McCarty et al.,

2004, 2008, 2009; Ferrage et al., 2005b, 2007, 2011b; Inoue et al., 2005; Lanson et al., 2009). With the lognormal distribution, the contribution of very thick crystals to the diffracted intensity becomes rapidly insignificant because of their negligible proportion, and the maximum number of layers in crystals (N_{max}) may be set to $\sim 5\overline{N}$ for practical purposes.

2.3.4.2 Ergun's Model

Ergun (1970) proposed a model in which the intensity is diffracted by large defective domains rather than by small CSD diffracting incoherently with respect to each other. Although this model corresponds essentially to the current concept of defective megacrystals (see Section 2.3.7), Reynolds (1985) adapted it in his well-known Newmod program to propose an alternative model of CSD size distribution. According to this 'defect-broadening' model, the probability of finding a defect-free domain in a crystal with N layers decreases exponentially when the size of this domain is increased, owing to the occurrence of random stacking faults along the Z direction. Equation (2.3.61) then becomes

$$I = NSpur[V][W] + 2\mathrm{Re}\sum_{n=1}^{N-1}(N-n)\exp(-n/\delta)Spur[V][W][Q]^n \qquad (2.3.68)$$

where $\exp(-n/\delta)$ is the probability of finding a defect-free sequence of $(n+1)$ layers; δ is the parameter controlling the shape of the distribution and corresponds to the average size of defect-free domains, expressed as a number—possibly non-integral—of layers; and N is the total number of layers in a crystal.

According to Reynolds (1985), realistic reflection profiles can be obtained for clay minerals by using a crystal size $N \approx 5\delta$. The above expression of the 'defect-broadening' model can be converted to a CSD size distribution $F(m)$, with $m = 1, 2, \ldots, N$, by assuming at first that $\exp(-1/\delta) = q$. If Eq. (2.3.68) is multiplied by $\dfrac{\overline{N}}{N}$, its comparison with Eq. (2.3.66) leads to

$$\frac{\overline{N}}{N}(N-n)q^n = \sum_{m=n+1}^{N}(m-n)F(m) \quad \text{with } n = 0,1,2,\ldots,N-1 \qquad (2.3.69)$$

In the above summations over m (Eq. 2.3.69), it is possible to subtract the summation for $n = k+1$ from that for $n = k$ [$k = 0, 1, \ldots, (N-1)$]. By doing so twice, it is possible to show that

$$F(m) = \frac{\overline{N}}{N}q^{m-1}\left[(N-m+1) - 2(N-m)q + (N-m-1)q^2\right] \quad \text{with}$$
$$m = 1,2,\ldots,N-1$$

and

$$F(m) = \frac{\overline{N}}{N}q^{m-1}\left[(N-m+1) - 2(N-m)q\right] \quad \text{for } m = N.$$

The 'defect-broadening' model thus corresponds to the following distribution of CSD sizes:

$$F(m) = (1-q)q^{m-1}\left[1 + [mq - (m-1)]\frac{\overline{N}}{N}\right] \quad \text{with } m = 1,2,\ldots,N-1 \quad (2.3.70)$$

and

$$F(N) = \frac{\overline{N}}{N}q^{N-1} \quad (2.3.71)$$

In Eq. (2.3.70), the expression within the square brackets is the correction factor for the finite crystal thickness, whereas for infinite crystals

$$F(m) = (1-q)q^{m-1} \quad \text{with} \quad \sum_{m=1}^{\infty} F(m) = (1-q)\frac{1}{(1-q)} = 1, \text{ as } N \to \infty.$$

To perceive its physical meaning, q can be expressed as a function of $\overline{N}$ and N. Subtracting the relation for $n=1$ from that for $n=0$ in Eq. (2.3.69), it is possible to obtain $q = \dfrac{N(\overline{N}-1)}{(N-1)\overline{N}}$.

In this model, structural defects coincide systematically with interlayer spacings, and $\overline{N}$ can be associated with the mean number of layers in one CSD. Hence, $\dfrac{N}{\overline{N}}$ and $(N-1)$ are the total number of CSD and the total number of interlayer spaces in a crystal, and $(\overline{N}-1)$ is the number of defect-free interlayer spaces in one CSD, respectively; $\dfrac{N}{\overline{N}}(\overline{N}-1)$ is the total number; and $\dfrac{N(\overline{N}-1)}{\overline{N}(N-1)} = q$ is the mean fraction (relative number) of defect-free interlayer spaces in a crystal, respectively. For a given value of fixed $\overline{N} = \delta$, values of q resulting from this hypothesis can differ slightly from that calculated directly from $\exp(-1/\delta) = q$ and depend on N. For example, $q = 0.818731$ for $\delta = 5$, whereas $q = 0.816327$ assuming $\overline{N} = 5$ and $N = 50$, or $q = 0.818605$ for $\overline{N} = 5$ and $N = 44$. As a consequence, the parameter δ can be expressed as

$$\delta = -\frac{1}{\ln q} = \frac{1}{\ln\left[\overline{N}(N-1)\right] - \ln\left[N(\overline{N}-1)\right]} = \frac{1}{\ln\frac{(N-1)}{N} - \ln\frac{(\overline{N}-1)}{\overline{N}}}.$$

2.3.5 INFLUENCE OF SMALL VARIATIONS OF LAYER THICKNESS (LAYER-TO-LAYER DISTANCE)

The possible variation of the layer-to-layer distance has long been recognized for clay minerals (Kodama et al., 1971), and was, for example, related to the incomplete filling of K^+-deficient muscovite interlayer space. More recently, such variations were evidenced in smectites (Ferrage et al., 2005a,b, 2010) and in smectite-containing mixed-layer structures (Drits et al., 1997b, 2002b; Sakharov et al., 1999a; Lindgreen et al., 2000; Drits, 2003), and their influence on XRD patterns was shown to be non-negligible. To model the

influence of such fluctuations of the layer-to-layer distance in a periodic crystal ($T=1$), it is convenient to consider at first that this parameter follows a normal distribution about a mean value ξ_0. The occurrence probability of layers with a thickness ξ is therefore

$$\Psi(\xi)=\frac{1}{\sqrt{2\pi}\Delta}\exp-\frac{(\xi-\xi_0)^2}{2\Delta^2} \tag{2.3.72}$$

where Δ is the variance of the distribution, and the average value of the phase term corresponding to layer thickness ξ is

$$\begin{aligned}\int_{-\infty}^{+\infty}\Psi(\xi)\exp(-2\pi iZ\xi)\,\mathrm{d}\xi&=\frac{1}{\sqrt{2\pi}\Delta}\int_{-\infty}^{+\infty}\exp-\frac{(\xi-\xi_0)^2}{2\Delta^2}\exp(-2\pi iZ\xi)\,\mathrm{d}\xi\\&=\exp(-2\pi iZ\xi_0)\exp-2(\pi Z\Delta)^2\end{aligned} \tag{2.3.73}$$

2.3.5.1 Defects of the First Type

Depending on the nature of the interactions between the layers and on the physical reasons for the translations' variations, layer thickness fluctuations were shown to be of two types (Guinier, 1964; Drits and Tchoubar, 1990). In the first type, fluctuations follow a unique law for any layer pair, and this law thus describes both short- and long-range order in a layer stack. As a result, the total translation between two nth nearest-neighbour layers is equal to n times the average translation and can be expressed as $\xi_n=(n-1)\xi_0+\xi$, with $\Psi(\xi_n)=\Psi(\xi)$, whatever the value of n, although the translation may vary from one layer pair to the other.The initial expression of Eq. (2.3.23) then becomes

$$\begin{aligned}I(Z)&=\int_{-\infty}^{+\infty}\Psi(\xi)F(Z)F^*(Z)\left\{N+2\ \mathrm{Re}\sum_{n=1}^{N-1}(N-n)\exp-2\pi iZ\xi_n\right\}d\xi\\&=F(Z)F^*(Z)\left\{\begin{array}{l}N\displaystyle\int_{-\infty}^{+\infty}\Psi(\xi)d\xi\\+2\ \mathrm{Re}\displaystyle\sum_{n=1}^{N-1}(N-n)\int_{-\infty}^{+\infty}\Psi(\xi)\exp[-2\pi iZ(n-1)\xi_0]\exp(-2\pi iZ\xi)d\xi\end{array}\right\}\\&=F(Z)F^*(Z)\left\{\begin{array}{l}N\displaystyle\int_{-\infty}^{+\infty}\Psi(\xi)d\xi\\+2\ \mathrm{Re}\displaystyle\sum_{n=1}^{N-1}(N-n)\exp[-2\pi iZ(n-1)\xi_0]\int_{-\infty}^{+\infty}\Psi(\xi)\exp(-2\pi iZ\xi)d\xi\end{array}\right\}\\&=F(Z)F^*(Z)\left\{N+\exp-2(\pi Z\Delta)^2 2\ \mathrm{Re}\sum_{n=1}^{N-1}(N-n)\exp-2\pi iZn\xi_0\right\}\end{aligned} \tag{2.3.74}$$

where $\int_{-\infty}^{+\infty}\Psi(\xi)\,d\xi = 1$.

For a mixed-layer structure whose elementary layers are affected by such fluctuations of the first type, the exponential factor $\exp -2(\pi Z\Delta)^2$ is introduced in Eq. (2.3.61) ahead of the real part of the summation, as in Eq. (2.3.74). Reflection intensity is thus decreased by this type of defect, and the influence increases with Z (or the diffraction angle).

2.3.5.2 Defects of the Second Type

In the second type of fluctuations, there is no long-range correlation between the defects, and the total translation between two nth nearest-neighbour layers is no longer equal to n times the average translation. According to Guinier (1964), this type of defect results, for example, from crystal growth when new structural fragments are added to the crystal, leading to a loss of long-range order in the structure, the loss increasing when new fragments are added. As a result, the total translation between two nth nearest-neighbour layers is equal to $\xi_n = n\xi$, with $\Psi(\xi_n) = [\Psi(\xi)]^n$. The initial expression of Eq. (2.3.23) then becomes

$$\begin{aligned} I(Z) &= \int_{-\infty}^{+\infty}\Psi(\xi)F(Z)F^*(Z)\left\{N + 2\mathrm{Re}\sum_{n=1}^{N-1}(N-n)\exp -2\pi i Z\xi_n\right\}d\xi \\ &= F(Z)F^*(Z)\left\{N\int_{-\infty}^{+\infty}\Psi(\xi)\,d\xi + 2\mathrm{Re}\sum_{n=1}^{N-1}(N-n)\int_{-\infty}^{+\infty}\Psi(\xi_n)\exp(-2\pi i Z n\xi)\,d\xi\right\} \\ &= F(Z)F^*(Z)\left\{N + 2\mathrm{Re}\sum_{n=1}^{N-1}(N-n)\exp(-2\pi i Z n\xi_0)\exp -2n(\pi Z\Delta)^2\right\} \end{aligned} \tag{2.3.75}$$

In contrast to Eq. (2.3.74), the exponential factor $\exp -2n(\pi Z\Delta)^2$ is included in the summation of Eq. (2.3.75), and depends on n. In a mixed-layer structure, elementary layers may exhibit different fluctuations of their layer thickness, and Eq. (2.3.12), which describes the intensity of waves diffracted by a mixed-layer crystal as the sum of contributions from single layers, layer pairs, layer triplets and so on, thus becomes

$$\sum_i w_i F_i F_i^* \int_{-\infty}^{+\infty}\Psi_i(\xi)\,d\xi = \sum_i w_i F_i F_i^* \quad \text{for single layers,}$$

$$\begin{aligned} &\sum_i\sum_j w_i p_{ij} F_i F_j^* \int_{-\infty}^{+\infty}\Psi_i(\xi)\exp -(2\pi i Z\xi)\,d\xi \\ &= \sum_i\sum_j w_i p_{ij} F_i F_j^* \exp -(2\pi i Z\xi_i)\exp -2(\pi Z\Delta_i)^2 \quad \text{for layer pairs,} \end{aligned}$$

$$\sum_i \sum_j \sum_k w_i p_{ij} p_{ijk} F_i F_k^* \int_{-\infty}^{+\infty} \Psi_i(\xi) \exp -(2\pi i Z \xi) \mathrm{d}\xi \int_{-\infty}^{+\infty} \Psi_j(\xi) \exp -(2\pi i Z \xi) \mathrm{d}\xi$$
$$= \sum_i \sum_j \sum_k w_i p_{ij} p_{ijk} F_i F_k^* \exp -\left[2\pi i Z\left(\xi_i + \xi_j\right)\right]$$
$$\exp -2\pi^2 Z^2 \left(\Delta_i^2 + \Delta_j^2\right) \quad \text{for layer triplets, so on.}$$

In turn, each $Q_{jkl\ldots}$ element of the $[Q]$ matrix in Eq. (2.3.61) will incorporate an exponential term $\exp -(a_j + ib_j)$ where $a_j = 2(\pi Z \Delta_j)^2$ and $b_j = 2\pi Z \xi_j$, Δ_j being the variance of the normal layer thickness distribution for j-type layers. As a consequence, defects of the second type also increasingly reduce reflection intensity with increasing values of Z, but, in addition, their impact depends on n (the effect of both types of defects on the diffracted intensity distribution is described in Appendix A3).

2.3.6 INFLUENCE OF THE OUTER SURFACE LAYERS OF CRYSTALS

The occurrence on the outer basal surfaces of crystals of layers with a structure or composition different from that of the 'core' layers is another possible disruption of crystal periodicity. Until recently, the influence of such defects on calculated XRD patterns was assumed to be minor, and no specific effort was made to integrate their description in programs allowing the calculation of diffraction effects from mixed-layer structures. As a result, outer crystal surfaces were not described specifically in these programs. In Newmod, the outer surface layers were 'naked' 2:1 layers (Reynolds, 1985), whereas early versions of the programs developed by the groups in Orléans (France) and Moscow (Russia) were meant for asymmetrical crystals with all interlayer species on one side of the crystal, or more generally for outer surface layers (OSL) similar to the 'core' layers (Plançon, 1981; Sakharov et al., 1982a,b, 1983). However, high-resolution transmission electron microscopy (HRTEM) revealed that OSL may differ in nature from the 'core' layers. Illite crystals may terminate with a kaolinite layer (Tsipursky et al., 1992), whereas kaolinite crystals may have pyrophyllite or smectite layers as surface terminations (Ma and Eggleton, 1999). Kogure et al. (2001) also reported cronstedtite crystals exhibiting chlorite OSL. As clay minerals often exhibit very minute crystal sizes, the possible impact of these specific OSL on the diffracted intensity thus becomes a relevant question, a formalism allowing these effects to be taken into account (Sakharov et al., 2004b) is therefore described.

Let us first consider a periodic structure with a 'core' of N identical layers and two OSL, whose structure factors are F, F_b, and F_t, respectively (Fig. 2.3.6). OSL at the bottom and top of the crystal, labelled b and t, respectively, can be considered as two layers in addition to the N 'core' layers of the crystal. From Eq. (2.3.12), the intensity of X-rays diffracted by a crystal corresponds to (i) the contribution from all individual layers and (ii) the

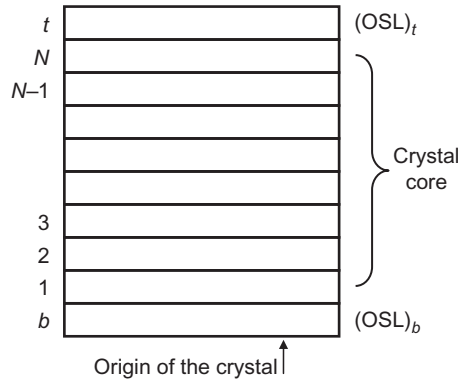

FIGURE 2.3.6 Schematic representation of a crystal with an N-layer core and $(OSL)_b$ and $(OSL)_t$ layers at the bottom and top, respectively, of the crystal.

contribution to intensity from the two external layers in all possible subsequences consisting of two, three, . . ., $(N-1)$, N layers, taking into account the phase shift between these external layers. Thus

$$
\begin{aligned}
I = A^*A = {} & F_b^*F_b + \left\{F_1^*F_1 + F_2^*F_2 + \cdots + F_N^*F_N\right\} + F_t^*F_t \\
& + [F_b^*F_1 \exp i\varphi_b + \{F_1^*F_2 \exp i\varphi_1 + F_2^*F_3 \exp i\varphi_2 + \cdots \\
& + F_{N-1}^*F_N \exp i\varphi_{N-1}\} + F_N^*F_t \exp i\varphi_N] + \text{conjugate} \\
& + [F_b^*F_2 \exp i(\varphi_b + \varphi_1) + \{F_1^*F_3 \exp i(\varphi_1 + \varphi_2) + F_2^*F_4 \exp i(\varphi_2 + \varphi_3) + \cdots \\
& + F_{N-2}^*F_N \exp i(\varphi_{N-2} + \varphi_{N-1})\} \quad + F_{N-1}^*F_t \exp i(\varphi_{N-1} + \varphi_N)] + \text{conjugate} \\
& \vdots \\
& + [F_b^*F_{N-1} \exp i(\varphi_b + \varphi_1 + \cdots + \varphi_{N-2}) \\
& + \left\{F_1^*F_N \exp i(\varphi_1 + \varphi_2 + \cdots + \varphi_{N-1})\right\} \\
& + F_2^*F_t \exp i(\varphi_2 + \varphi_3 + \cdots + \varphi_N)] + \text{conjugate} \\
& + \begin{bmatrix} F_b^*F_N \exp i(\varphi_b + \varphi_1 + \cdots + \varphi_{N-1}) \\ + F_1^*F_t \exp i(\varphi_1 + \varphi_2 + \cdots + \varphi_N) \end{bmatrix} + \text{conjugate} \\
& + \left[F_b^*F_t \exp i(\varphi_b + \varphi_1 + \varphi_2 + \cdots + \varphi_N)\right] + \text{conjugate}
\end{aligned}
\tag{2.3.76}
$$

φ_b being the phase shift induced by the thickness of the lower OSL.

The sum of the terms between curly brackets corresponds to the contribution of the crystal N-layer core to the intensity, while the other terms correspond to the contribution of the two additional OSL. As all core layers are identical, $F_1 = F_2 = \cdots = F_N = F$ and $\varphi_1 = \varphi_2 = \cdots = \varphi_N = \varphi$. If the different terms of Eq. (2.3.76) are grouped as a function of the number of layers between outer layers ($F_i^*F_j$) in layer sequences ($i, j = b, 1, 2, \ldots, N, t$), then

$$I = \left(NF^*F + F_b^*F_b + F_t^*F_t\right) + 2\mathrm{Re}\left\{\sum_{n=1}^{N-1}\left[(N-n)F^*F + F_b^*F\exp i\varphi_b + F^*F_t\exp i\varphi\right]\exp in\varphi + F_b^*F\exp i\varphi_b + F^*F_t\exp i\varphi + F_b^*F_t\exp i\varphi_b\exp iN\varphi\right\} \quad (2.3.77)$$

A similar approach may be used for mixed-layer structures with the following matrix formalism:

$$I = Spur\left[N[V] + \left[V_b'\right] + \left[V_t'\right]\right][W] + 2\mathrm{Re}Spur\left\{\sum_{n=1}^{N-1}[(N-n)[V][W] + [V_b][W][Q_b] + [V_t][W][Q_t]][Q]^n + [V_b][W][Q_b] + [V_t][W][Q_t] + [V'][W][Q_b][Q_t]^N\right\} \quad (2.3.78)$$

Matrices $[V]$, $[W]$, and $[Q]$ are identical to those in Eq. (2.3.61), whereas matrices $[V']$, $[V_b]$, $[V_t]$, $[V_b']$, and $[V_t']$ correspond to products of structure amplitudes for core, bottom, and top layers; $[Q_b]$ contains the products of junction probability parameters and the phase term induced by the thickness of the OSL at the bottom of the crystal; and $[Q_t]$ contains the products of junction probability parameters and the phase term induced by the thickness of the N core layers (Fig. 2.3.6). Compared to Eq. (2.3.61), Eq. (2.3.78) contains all the terms describing diffraction effects from the core layers and additional terms describing the contribution of the two OSL and of their interactions with each core layer. When using the matrix formalism, a mixed-layer structure with T layer types may admit T types of OSL as crystal bottoms and tops owing to intrinsic limitations, and Eq. (2.3.78) may be used to describe mixed-layer structures differing from the occurrence probabilities of their OSL, as described in the next section.

2.3.6.1 Model I: Occurrence and Junction Probabilities of OSL are Identical to Those of the Core Layers

One may consider at first a two-component mixed-layer structure in which A and B layers are interstratified with $S = 1$, with two layer types possibly occurring on the crystal's outer basal surfaces. Although the OSL may differ from the core layers, it is convenient to label them Ab and Bb for the bottom layers and At and Bt for the top ones, and it is possible to write the following relations:

$$w_{Ab} + w_{Bb} = 1,\ p_{AbA} + p_{AbB} = 1,\ p_{BbA} + p_{BbB} = 1,$$

and

$$w_{At}+w_{Bt}=1,\ p_{AAt}+p_{ABt}=1,\ p_{BAt}+p_{BBt}=1.$$

Model I considers that these occurrence and junction probability parameters are identical to those of core A and B layers:

$$w_{Ab}=w_{At}=w_A,\ w_{Bb}=w_{Bt}=w_B,\ p_{AbA}=p_{AAt}=p_{AA},\ p_{AbB}=p_{ABt}=p_{AB},\cdots,\text{ and } p_{BbB}=p_{BBt}=p_{BB}.$$

In this case, the expression of matrices $[V]$, $[W]$, and $[Q]$ is given by Eq. (2.3.62), and that of the additional matrices present in Eq. (2.3.78) are

$$[V'_b]=\begin{vmatrix} F^*_{Ab}F_{Ab} & \\ & F^*_{Bb}F_{Bb}\end{vmatrix},\ [V'_t]=\begin{vmatrix} F^*_{At}F_{At} & \\ & F^*_{Bt}F_{Bt}\end{vmatrix},$$

$$[V_b]=\begin{vmatrix} F^*_{Ab}F_A & F^*_{Bb}F_A \\ F^*_{Ab}F_B & F^*_{Bb}F_B\end{vmatrix},[V_t]=\begin{vmatrix} F^*_{A}F_{At} & F^*_{B}F_{At} \\ F^*_{A}F_{Bt} & F^*_{B}F_{Bt}\end{vmatrix},$$

$$[V']=\begin{vmatrix} F^*_{Ab}F_{At} & F^*_{Bb}F_{At} \\ F^*_{Ab}F_{Bt} & F^*_{Bb}F_{Bt}\end{vmatrix},$$

$$[Q_b]=\begin{vmatrix} p_{AbA}\exp i\varphi_{Ab} & p_{AbB}\exp i\varphi_{Ab} \\ p_{BbA}\exp i\varphi_{Bb} & p_{BbB}\exp i\varphi_{Bb}\end{vmatrix}=\begin{vmatrix} p_{AA}\exp i\varphi_{Ab} & p_{AB}\exp i\varphi_{Ab} \\ p_{BA}\exp i\varphi_{Bb} & p_{BB}\exp i\varphi_{Bb}\end{vmatrix},$$

and

$$[Q_t]=\begin{vmatrix} p_{AAt}\exp i\varphi_A & p_{ABt}\exp i\varphi_A \\ p_{BAt}\exp i\varphi_B & p_{BBt}\exp i\varphi_B\end{vmatrix}=\begin{vmatrix} p_{AA}\exp i\varphi_A & p_{AB}\exp i\varphi_A \\ p_{BA}\exp i\varphi_B & p_{BB}\exp i\varphi_B\end{vmatrix}$$

where F_{Ab}, F_{At}, F_{Bb}, and F_{Bt} are the structure amplitudes of Ab, At, Bb, and Bt OSL, with φ_{Ab} and φ_{Bb} being the phase shifts corresponding to the thickness of Ab and Bb OSL, respectively.

For a mixed-layer structure with $S=2$, the expressions of matrices $[V]$, $[W]$, and $[Q]$ are given by Eq. (2.3.65), whereas those of the additional matrices present in Eq. (2.3.78) are

$$[V'_b]=\begin{vmatrix} F^*_{Ab}F_{Ab} & & & \\ & F^*_{Ab}F_{Ab} & & \\ & & F^*_{Bb}F_{Bb} & \\ & & & F^*_{Bb}F_{Bb}\end{vmatrix},\ [V'_t]=\begin{vmatrix} F^*_{At}F_{At} & & & \\ & F^*_{At}F_{At} & & \\ & & F^*_{Bt}F_{Bt} & \\ & & & F^*_{Bt}F_{Bt}\end{vmatrix},$$

$$[V_b]=\begin{vmatrix} F^*_{Ab}F_A & F^*_{Ab}F_A & F^*_{Bb}F_A & F^*_{Bb}F_A \\ F^*_{Ab}F_A & F^*_{Ab}F_A & F^*_{Bb}F_A & F^*_{Bb}F_A \\ F^*_{Ab}F_B & F^*_{Ab}F_B & F^*_{Bb}F_B & F^*_{Bb}F_B \\ F^*_{Ab}F_B & F^*_{Ab}F_B & F^*_{Bb}F_B & F^*_{Bb}F_B\end{vmatrix},[V_t]=\begin{vmatrix} F^*_{A}F_{At} & F^*_{A}F_{At} & F^*_{B}F_{At} & F^*_{B}F_{At} \\ F^*_{A}F_{At} & F^*_{A}F_{At} & F^*_{B}F_{At} & F^*_{B}F_{At} \\ F^*_{A}F_{Bt} & F^*_{A}F_{Bt} & F^*_{B}F_{Bt} & F^*_{B}F_{Bt} \\ F^*_{A}F_{Bt} & F^*_{A}F_{Bt} & F^*_{B}F_{Bt} & F^*_{B}F_{Bt}\end{vmatrix},$$

$$[V'] = \begin{vmatrix} F^*_{Ab}F_{At} & F^*_{Ab}F_{At} & F^*_{Bb}F_{At} & F^*_{Bb}F_{At} \\ F^*_{Ab}F_{At} & F^*_{Ab}F_{At} & F^*_{Bb}F_{At} & F^*_{Bb}F_{At} \\ F^*_{Ab}F_{Bt} & F^*_{Ab}F_{Bt} & F^*_{Bb}F_{Bt} & F^*_{Bb}F_{Bt} \\ F^*_{Ab}F_{Bt} & F^*_{Ab}F_{Bt} & F^*_{Bb}F_{Bt} & F^*_{Bb}F_{Bt} \end{vmatrix},$$

$$[Q_b] = \begin{vmatrix} p_{AAA}\exp i\varphi_{Ab} & p_{AAB}\exp i\varphi_{Ab} & & \\ & & p_{ABA}\exp i\varphi_{Ab} & p_{ABB}\exp i\varphi_{Ab} \\ p_{BAA}\exp i\varphi_{Bb} & p_{BAB}\exp i\varphi_{Bb} & & \\ & & p_{BBA}\exp i\varphi_{Bb} & p_{BBB}\exp i\varphi_{Bb} \end{vmatrix},$$

and

$$[Q_t] = \begin{vmatrix} p_{AAA}\exp i\varphi_{A} & p_{AAB}\exp i\varphi_{A} & & \\ & & p_{ABA}\exp i\varphi_{A} & p_{ABB}\exp i\varphi_{A} \\ p_{BAA}\exp i\varphi_{B} & p_{BAB}\exp i\varphi_{B} & & \\ & & p_{BBA}\exp i\varphi_{B} & p_{BBB}\exp i\varphi_{B} \end{vmatrix}$$

The same logic can be used to determine the expression of the new matrices for mixed-layer structures with $T \geq 2$ and/or with $S \geq 2$.

2.3.6.2 Model II: Occurrence Probabilities of OSL Depend on the Nature of the Previous Layer

According to this model, the nature of the OSL is controlled by that of the adjacent layer, and for a mixed-layer structure with $T = 2$ and $S = 1$

$$p_{AbA} = p_{BbB} = 1 (\text{or } p_{AbB} = p_{BbA} = 1), \quad \text{and} \quad p_{AAt} = p_{BBt} = 1 (\text{or } p_{ABt} = p_{BAt} = 1).$$

In this case, the expression of matrices $[Q_b]$ and $[Q_t]$ from Eq. (2.3.78) is

$$[Q_b] = \begin{vmatrix} \exp i\varphi_{Ab} & \exp i\varphi_{Ab} \\ \exp i\varphi_{Bb} & \exp i\varphi_{Bb} \end{vmatrix}, [Q_t] = \begin{vmatrix} \exp i\varphi_{A} & \exp i\varphi_{A} \\ \exp i\varphi_{B} & \exp i\varphi_{B} \end{vmatrix}.$$

2.3.6.3 Model III: Systematic Occurrence of a Given OSL Type at a Given End of the Crystals

According to this model, the same type of OSL is systematically present at a given end of the crystals, and only two types (b and t) of OSL may occur. For a mixed-layer structure with $T = 2$ and $S = 1$, the expressions of the additional matrices present in Eq. (2.3.78) are

$$[V'_b] = \begin{vmatrix} F^*_bF_b & \\ & F^*_bF_b \end{vmatrix}, [V'_t] = \begin{vmatrix} F^*_tF_t & \\ & F^*_tF_t \end{vmatrix}, [V_b] = \begin{vmatrix} F^*_bF_A & F^*_bF_A \\ F^*_bF_B & F^*_bF_B \end{vmatrix},$$

$$[V_t] = \begin{vmatrix} F^*_AF_t & F^*_BF_t \\ F^*_AF_t & F^*_BF_t \end{vmatrix},$$

$$[V'] = \begin{vmatrix} F_b^* F_t & F_b^* F_t \\ F_b^* F_t & F_b^* F_t \end{vmatrix}, [Q_b] = \begin{vmatrix} \exp i\varphi_b & \exp i\varphi_b \\ \exp i\varphi_b & \exp i\varphi_b \end{vmatrix}, \text{ and } [Q_t] = \begin{vmatrix} \exp i\varphi_A & \exp i\varphi_A \\ \exp i\varphi_B & \exp i\varphi_B \end{vmatrix}.$$

2.3.7 INFLUENCE OF INTER-CRYSTALLINE DEFECTS: MEGACRYSTALS

For lamellar compounds, coherent scattering domains can be seen as a crystal volume exhibiting layer parallelism and 2D periodicity within the layer plane. Following this definition, interstratification of different layer types, even of incommensurate layers, thus has no influence on the size of the CSD perpendicular to the layer plane. On the other hand, the crystal size may differ from the size of the CSD, as crystals are commonly composed mosaic blocks that are slightly misoriented with respect to each other (Guinier, 1964) and thus act as CSD, scattering X-rays independently. Accordingly, the sizes of CSD determined from the analysis of diffraction line profiles (e.g. Drits et al., 1997c) are often smaller than the particle sizes determined by other techniques such as small-angle X-ray scattering (SAXS), transmission electron microscopy (TEM), or HRTEM. For example, the XRD analysis of the Rupsroth beidellite revealed an average CSD size of ~15 layers (Besson, 1980), whereas a simultaneous SAXS study indicated crystals with up to 400 layers (Pons, 1980). Comparison of XRD patterns calculated with the common hypothesis of a set of CSD all having small sizes (Fig. 2.3.7A; Section 2.3.4) with those collected on natural and synthetic clay mineral samples revealed a similar tendency, with frequent discrepancies over the low-angle region ($2\theta < 4$–6° Cu Kα). The intensity calculated at low angle is commonly higher than the experimental one (Fig. 2.3.8), indicating the need for larger CSD sizes, despite high-quality fits over the high-angle region (McCarty et al., 2009). Two models are described hereafter that allow concealing this apparent discrepancy.

2.3.7.1 Model I (Plançon, 2002)

Plançon (2002) proposed a model in which a sample is composed of 'quasi-crystals' or megacrystals whose average size is larger than that of the CSD in the usual model (Fig. 2.3.7B). These megacrystals contain layer types identical to those in the usual XRD model. Their relative proportion and their stacking sequences are also identical to those in the usual models. However, adjacent parallel layers may be shifted with respect to each other along the c^*-axis, thus creating 'pores', according to an adjustable probability, and the ξ-spacing between i-type and j-type layers can take n_{ij} values, instead of one in the usual model. The presence of 'pore' defects affects the phase terms that depend on the distance between layers, but does not modify the structure

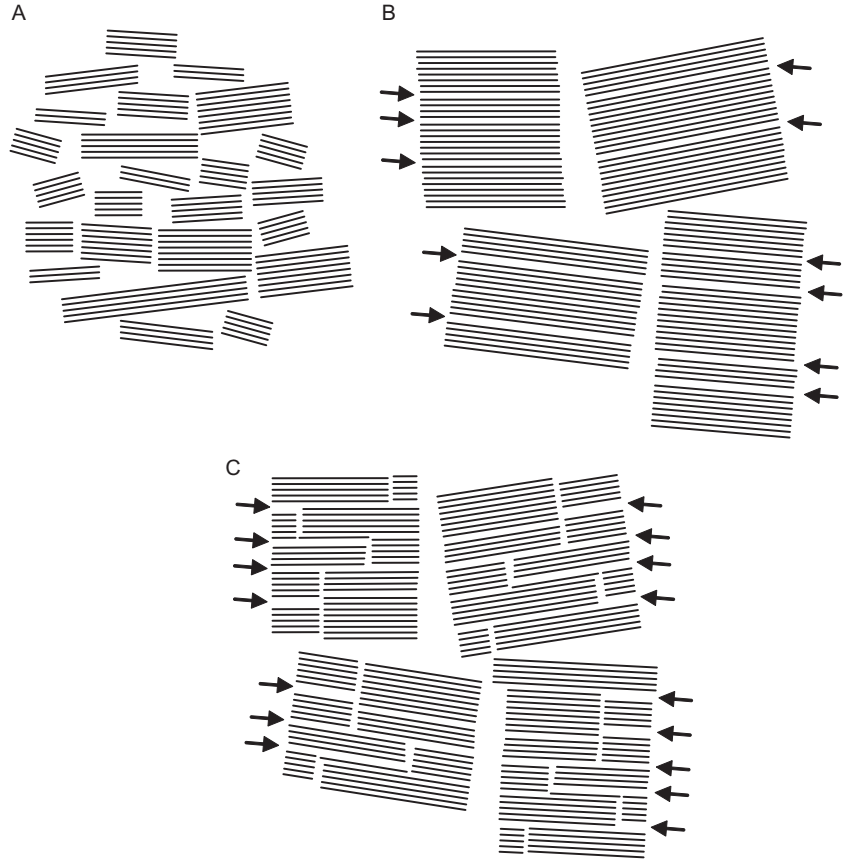

FIGURE 2.3.7 Schematic representation of a sample consisting either (A) of a set of coherent scattering domains (CSD), or (B and C) of a set of megacrystals. Additional distances may occur between parallel layers to create pores (Plançon, 2002; B), or between aggregated CSD (Sakharov, 2005; C).

amplitude of individual layers. In Eq. (2.3.61) of the diffracted intensity, only elements of the $[Q]$ matrix should thus be modified as follows: $Q_{ij}(Z) = \sum_{q=1}^{n_{ij}} p_{ijq} \exp(2\pi i Z \xi_{ijq})$, with p_{ijq} being the occurrence probability of the qth spacing, ξ_{ijq}, among the n_{ij} possible values $\left(\sum_{q=1}^{n_{ij}} p_{ijq} = p_{ij}\right)$.

If the smallest of the n_{ij} possible spacings is labelled ξ_i, that is, if ξ_i is the smallest possible thickness of an i-type layer, any ξ_{ijq} spacing can be written as $\xi_{ijq} = \xi_i + \Delta\xi_{ijq}$ with $\Delta\xi_{ijq} \geq 0$. If the occurrence probability of an additional distance $\Delta\xi_{ijq}$ between i- and j-type layers is denoted $p(\Delta\xi_{ijq})$, then $p_{ijq} = p_{ij}$ $p(\Delta\xi_{ijq})$, with $\sum_{q=1}^{n_{ij}} p(\Delta\xi_{ijq}) = 1$, and the $Q_{ij}(Z)$ terms can be written as

$$Q_{ij}(Z) = p_{ij} \exp(2\pi i Z \xi_i) \sum_{q=1}^{n_{ij}} p\left(\Delta\xi_{ijq}\right) \exp\left(2\pi i Z \Delta\xi_{ijq}\right).$$

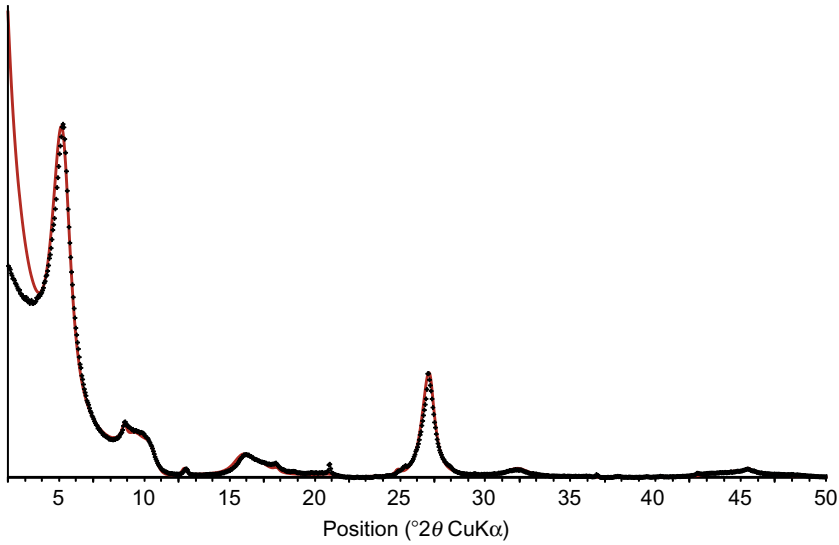

FIGURE 2.3.8 Simulation of the XRD pattern for Gulf Coast sample #496-002. Black crosses are experimental data collected on an oriented preparation of the Ca-saturated and ethylene glycol solvated <2-μm size fraction, the solid overplot being the calculated profile. The calculated profile includes the contributions of an illite-expandable, discrete smectite, illite, and kaolinite (68:28:2:2). The mixed-layer structure is composed of illite (9.98 Å), Exp_1 (16.95 Å), and Exp_2 (12.90 Å) layers (65:32:3), randomly interstratified ($S=0$). *Adapted from McCarty et al. (2008).*

In the new model, $Q_{ij}(Z)$ terms differ from those in the usual model by the factor $\sum_{q=1}^{n_{ij}} p(\Delta\xi_{ijq})\exp(2\pi i Z\Delta\xi_{ijq})$ that characterizes the deviation from the 'normal' layer spacings. Additional distances $\Delta\xi_{ijq}$ disrupt the coherence of waves scattered by different layers, the loss of coherence depending on the diffraction angle (Plançon, 2002), the coherence of diffracted waves, or the apparent size of CSD, and increasing with decreasing 2θ angles. Additional distances are systematically positive and much lower than the normal ξ_i spacing ($0 \leq \Delta\xi_{ijq} < \xi_i$). The structure is thus equivalent to a mixed-layer structure in which layers with similar structure amplitude and $\xi_{ijq} > \xi_i$ spacing occur together with the 'normal' layers, and a significant positional shift, towards lower angles, is thus expected for high-angle reflections compared to the usual model (Plançon, 2002). This positional shift is expected to occur even for periodic structures, in contradiction with experimental data, and this alternative model is likely inappropriate for the description of natural samples.

2.3.7.2 Model II (Sakharov, 2005)

As an alternative to model I, it is possible to consider that CSD, or mosaic blocks, with a size distribution identical to that of the usual model are aggregated to form megacrystals (Fig. 2.3.7C). If these CSD are arranged in such a way that their

layers are strictly parallel from one domain to the other and there is no distortion (additional, positive or negative, distances) between these domains, the resulting XRD pattern corresponds to a large monocrystal equivalent in size to the megacrystal. If the coherence of waves diffracted by the different CSD is lost because of their arrangement in the megacrystal, then the resulting XRD pattern corresponds to the usual model. The coherence of waves diffracted of the different CSD can vary steadily between these two extreme cases.

A comprehensive description of this alternative model requires the definition of inter-crystalline defects, of their occurrence frequency in a megacrystal, and of the associated phase shifts for the calculation of their impact on the diffracted intensity. For this purpose, it is convenient to consider first a large megacrystal consisting of defect-free parallel CSD. In this case, defects are located only in between OSL of different CSD and can be defined as the additional distances between adjacent CSD, independent of the other inter-crystalline distances. The additional distances between adjacent CSD can be positive or negative but are much smaller than the CSD sizes. The latter condition implies that the distance fluctuation is of the second type described in Section 2.3.5. If M is the total number of layers in a megacrystal, and N and $\overline{N}$ the maximum and average numbers of layers, respectively, in a CSD, then $(M-1)$ is the maximum number of defects, $M/\overline{N}$ the number of CSD, $((M/\overline{N})-1)$ the mean number of defects, and $\left[(M/\overline{N})-1\right]/(M-1)$ the occurrence probability of defects in this megacrystal. In a sequence of $(n+1)$ layers, n is both the number of layers adjacent to a layer arbitrarily chosen as the origin and the maximum number of defects in this sequence. Defects being randomly distributed, it is possible to deduce that $n\left[(M/\overline{N})-1\right]/(M-1)$ is the number of defects in this $(n+1)$ layer sequence, and $(M-n)n\left[M/\overline{N}-1\right]/(M-1)$ the total number of defects in all $(n+1)$ layer sequences, $(M-n)$ being the number of $(n+1)$ layer sequences in a megacrystal with M layers. If c_n is the number of defect-free $(n+1)$ layer sequences (see later), that is, of sequences of $(n+1)$ layers from the same CSD, the number of defective $(n+1)$ layer sequences is $[(M-n)-c_n]$, and the average number of defects in each of these sequences is $k_n=\left[(M-n)n\left(M-\overline{N}\right)\right]/\left[(M-1)\overline{N}(M-n-c_n)\right]$.

If N_1, N_2, …, N_N are the numbers of CSD with 1, 2, …, and N layers, respectively, in a megacrystal with M layers, then $N_1\times 1+N_2\times 2+\cdots+N_N\times N=M$. Similarly, if the occurrence probabilities of these CSD are $F(1)$ $[F(1)=N_1/\sum_{n=1}^{N}N_n]$, $F(2)$, …, and $F(N)$, respectively, then $\sum_{n=1}^{N}nF(n)=\overline{N}$, with $\sum_{n=1}^{N}F(n)=1$, and $N_1=rF(1)$, $N_2=rF(2)$, …, and $N_N=rF(N)$, r being the number of CSD $(M/\overline{N})$. As a consequence c_n can be defined as

$$c_n=\begin{cases}\dfrac{M}{\overline{N}}\displaystyle\sum_{m=n+1}^{N}(m-n)F(m), & \text{if } n<N\\ 0, & \text{if } n\geq N\end{cases}.$$

The definition of phase shifts corresponding to different distributions of arbitrary distances between CSD is described in the following sections.

2.3.7.2.1 Exponential Distribution of Defects Between CSD

It is convenient to hypothesize at first that all layers in the CSD of a mega-crystal are identical with a common layer-to-layer distance equal to ξ_0, and that $\Delta\xi$ distances between adjacent and parallel CSD follow the exponential law $W(\Delta\xi) = \begin{cases} \lambda\exp(-\lambda\Delta\xi), & \Delta\xi \geq 0 \\ 0, & \Delta\xi < 0 \end{cases}$

where $\Delta\overline{\xi} = 1/\lambda$, with λ the decay rate of the distribution and

$$\int_0^\infty W(\Delta\xi)\mathrm{d}(\Delta\xi) = 1.$$

The average phase term for two layers separated by such a defect depends on the $(\xi_0 + \Delta\xi)$ distance between these layers, and can be expressed as

$$\int_0^\infty W(\Delta\xi)\exp[-2\pi iz(\xi_0+\Delta\xi)]\mathrm{d}(\Delta\xi) = \lambda\exp(-2\pi iz\xi_0)\int_0^\infty \exp(-2\pi iz\Delta\xi)\exp(-\lambda\Delta\xi)\mathrm{d}(\Delta\xi)$$

$$= \lambda\exp(-2\pi iz\xi_0)\int_0^\infty \exp[(-2\pi iz-\lambda)\Delta\xi]\mathrm{d}(\Delta\xi) = \exp(-2\pi iz\xi_0)\frac{\lambda}{\lambda+2\pi iz}$$

$$= \frac{1-2\pi iz\Delta\overline{\xi}}{1+4\pi^2z^2\Delta\overline{\xi}^2}\exp(-2\pi iz\xi_0) = [A+iB]\exp(-2\pi iz\xi_0)$$

$$\text{where } A = \frac{1}{1+4\pi^2z^2\Delta\overline{\xi}^2}, \quad \text{and} \quad B = \frac{-2\pi z\Delta\overline{\xi}}{1+4\pi^2z^2\Delta\overline{\xi}^2}$$

The presence of one defect in a layer sequence thus induces the multiplication of the phase term by the additional $(A + iB)$ factor, this factor becoming $(A + iB)^{k_n}$ in the presence of k_n defects.

2.3.7.2.2 Normal (Gaussian) Distribution of Defects Between CSD

A normal distribution of $\Delta\xi$ distances between adjacent and parallel CSD can be expressed as $W(\Delta\xi) = \frac{1}{\sqrt{2\pi}\sigma}\exp\left[-\frac{\Delta\xi^2}{2\sigma^2}\right]$, where $\Delta\xi = \xi - \xi_0$, ξ_0 being the layer-to-layer distance within CSD, ξ the distance between adjacent CSD, and σ the standard deviation of $\Delta\xi$. In this specific case, no assumption is made as to the nature of OSL, and negative $\Delta\xi$ values are thus allowed.

The average value of the phase term for such a distribution can be expressed as

$$\int_{-\infty}^{\infty} W(\xi)\exp(-2\pi iZ\xi)\mathrm{d}\xi = \exp(-2\pi iZ\xi_0)\exp\left(-2\pi^2Z^2\sigma^2\right).$$

In contrast to the exponential distribution, this expression for a normal distribution of distances between CSD contains only the real part of the additional factor, that is, $A = \exp(-2\pi^2Z^2\sigma^2)^{k_n}$ when k_n defects are present.

2.3.7.2.3 Semi-Normal Distribution of Defects Between CSD

If only half of the previous normal distribution is considered, either negative or positive additional distances ($\Delta\xi = \xi - \xi_0$) between adjacent CSD are taken into account, and the distribution takes the following forms:

For $\xi \geq \xi_0$:

$$W(\Delta\xi) = \begin{cases} \dfrac{\sqrt{2}}{\sqrt{\pi}\sigma} \exp\left[-\dfrac{\Delta\xi^2}{2\sigma^2}\right] & \text{for} \Delta\xi \geq 0 \\ 0 & \text{for} \Delta\xi < 0 \end{cases}.$$

The average value of the phase term for such a distance distribution becomes

$$\int_0^\infty W(\Delta\xi)\exp[-2\pi i Z(\xi_0 + \Delta\xi)]\,\mathrm{d}(\Delta\xi)$$

$$= \sqrt{\frac{2}{\pi}}\frac{1}{\sigma}\int_0^\infty \exp\left[-\frac{\Delta\xi^2}{2\sigma^2}\right]\exp(-2\pi i Z\xi_0)\exp(-2\pi i Z\Delta\xi)\,\mathrm{d}(\Delta\xi)$$

$$= \exp(-2\pi i Z\xi_0)\left\{\exp\left(-2\pi^2\sigma^2Z^2\right) + i\left[-\frac{2}{\sqrt{\pi}}\exp\left(-2\pi^2\sigma^2Z^2\right)\int_0^{\alpha/2}\exp\left(t^2\right)\mathrm{d}t\right]\right\}$$

with $\alpha/2 = \sqrt{2}\pi Z\sigma$. In this case, the A and B factors multiplying the phase term become $\exp(-2\pi^2\sigma^2Z^2)$, and $-\dfrac{2}{\sqrt{\pi}}\exp(-2\pi^2\sigma^2Z^2)\int_0^{\alpha/2}\exp(t^2)\,\mathrm{d}t$, respectively.

For $\xi \leq \xi_0$:

$$W(\Delta\xi) = \begin{cases} \dfrac{\sqrt{2}}{\sqrt{\pi}\sigma} \exp\left[-\dfrac{\Delta\xi^2}{2\sigma^2}\right] & \text{for} \Delta\xi \leq 0 \\ 0 & \text{for} \Delta\xi > 0 \end{cases}$$

The average value of the phase term for such a distance distribution becomes

$$\int_0^\infty W(\Delta\xi)\exp[-2\pi i Z(\xi_0 + \Delta\xi)]\,\mathrm{d}(\Delta\xi)$$

$$= \sqrt{\frac{2}{\pi}}\frac{1}{\sigma}\int_{-\infty}^0 \exp\left[-\frac{\Delta\xi^2}{2\sigma^2}\right]\exp(-2\pi i Z\xi_0)\exp(-2\pi i Z\Delta\xi)\,\mathrm{d}(\Delta\xi)$$

$$= \exp(-2\pi i Z\xi_0)\left\{\exp\left(-2\pi^2\sigma^2Z^2\right) + i\left[\frac{2}{\sqrt{\pi}}\exp\left(-2\pi^2\sigma^2Z^2\right)\int_0^{\alpha/2}\exp\left(t^2\right)\mathrm{d}t\right]\right\}$$

with $\alpha/2 = \sqrt{2}\pi Z\sigma$. In this case, the A and B factors multiplying the phase term become $\exp(-2\pi^2\sigma^2Z^2)$, and $\frac{2}{\sqrt{\pi}}\exp(-2\pi^2\sigma^2Z^2)\int_0^{\alpha/2}\exp(t^2)\,\mathrm{d}t$, respectively.

2.3.7.2.4 Uniform Distribution of Defects Between CSD

A uniform distribution of additional distances ($\Delta\xi = \xi - \xi_0$) between adjacent CSD can be expressed as $W(\Delta\xi) = 1/(\xi_{\max} - \xi_0)$, with $\xi_{\max}$ the maximum possible distance between two adjacent CSD. The average value of the phase term for such a distance distribution becomes

$$\begin{aligned}
&\int_0^{\xi_{\max}-\xi_0} W(\Delta\xi)\exp[-2\pi iZ(\xi_0+\Delta\xi)]d(\Delta\xi) \\
&= \frac{1}{\xi_{\max}-\xi_0}\int_0^{\xi_{max}-\xi_0} \exp(-2\pi iZ\xi_0)\exp(-2\pi iZ\Delta\xi)d(\Delta\xi) \\
&= \exp(-2\pi iZ\xi_0)\left\{\frac{\sin 2\pi Z(\xi_{\max}-\xi_0)}{2\pi Z(\xi_{\max}-\xi_0)} + i\frac{\cos 2\pi Z(\xi_{\max}-\xi_0)-1}{2\pi Z(\xi_{\max}-\xi_0)}\right\}
\end{aligned}$$

In this case, the A and B factors multiplying the phase term become $\frac{\sin 2\pi Z(\xi_{\max}-\xi_0)}{2\pi Z(\xi_{\max}-\xi_0)}$ and $\frac{\cos 2\pi Z(\xi_{\max}-\xi_0)-1}{2\pi Z(\xi_{\max}-\xi_0)}$, respectively.

2.3.7.2.5 Overall Intensity Equation

If different layer types are interstratified in an M-layer megacrystal, the diffracted intensity can be deduced from Eq. (2.3.61) as

$$I_M = MSpur[V][W] + 2\mathrm{Re}\sum_{n=1}^{N-1}(M-n)Spur[V][W][Q]^n \tag{2.3.79}$$

The first term of the equation corresponds to the contribution to intensity of waves diffracted by individual layers, whereas the second term corresponds to the contribution of sequences with 2, 3, ..., M layers. If the megacrystal contains inter-crystalline defects, the second term of Eq. (2.3.79) is split in two terms corresponding to the intensity contributions from defect-free and defective layer sequences, respectively, that is,

$$\begin{aligned}
I_M &= MSpur[V][W] + 2\mathrm{Re}\sum_{n=1}^{M-1}\left[c_n + (M-n-c_n)(A+iB)^{k_n}\right]Spur[V][W][Q]^n \\
&= MSpur[V][W] + 2\mathrm{Re}\sum_{n=1}^{M-1}\left[Mc_n^* + \left(M-n-Mc_n^*\right)(A+iB)^{k_n}\right]Spur[V][W][Q]^n
\end{aligned} \tag{2.3.80}$$

$$\text{where } c_n^* = \begin{cases} \frac{1}{N}\sum_{m=n+1}^{N}(m-n)F(m), & \text{if } n < N \\ 0, & \text{if } n \geq N \end{cases}.$$

Megacrystals are most likely also distributed in size. If minimum and maximum sizes of the megacrystals are labelled M_{min} and M_{max}, respectively, the megacrystal size distribution may be described by occurrence probability coefficients $G(M_{min}), G(M_{min}+1), \ldots G(M_{max})$, with $\sum_{M=M_{min}}^{M_{max}} G(M) = 1$, and $\overline{M} = \sum_{M=M_{min}}^{M_{max}} MG(M)$. Equation (2.3.80) then becomes

$$
\begin{aligned}
I &= \sum_{M=M_{min}}^{M_{max}} G(M) I_M = \sum_{M=M_{min}}^{M_{max}} G(M) M Spur[V][W] \\
&\quad + 2\mathrm{Re} \sum_{M=M_{min}}^{M_{max}} G(M) \sum_{n=1}^{M-1} \left[Mc_n^* + (M-n-Mc_n^*)(A+iB)^{k(n,M)} \right] Spur[V][W][Q]^n \\
&= \overline{M} Spur[V][W] + 2\mathrm{Re} \sum_{M=M_{min}}^{M_{max}} G(M) \sum_{n=1}^{M_{min}-1} \left[Mc_n^* + (M-n-Mc_n^*)(A+iB)^{k(n,M)} \right] Spur[V][W][Q]^n \\
&\quad + 2\mathrm{Re} \sum_{M=M_{min}}^{M_{max}} G(M) \sum_{n=M_{min}}^{M_{max}-1} (M-n)(A+iB)^{k(n,M)} Spur[V][W][Q]^n \\
&= \overline{M} Spur[V][W] + 2\mathrm{Re} \sum_{n=1}^{M_{min}-1} \left[\overline{M} c_n^* + \sum_{M=M_{min}}^{M_{max}} G(M)(M-n-Mc_n^*)(A+iB)^{k(n,M)} \right] Spur[V][W][Q]^n \\
&\quad + 2\mathrm{Re} \sum_{n=M_{min}}^{M_{max}-1} \sum_{M=n+1}^{M_{max}} G(M)(M-n)(A+iB)^{k(n,M)} Spur[V][W][Q]^n
\end{aligned}
$$

Finally,

$$
\begin{aligned}
I &= \overline{M} Spur[V][W] \\
&\quad + 2\mathrm{Re} \sum_{n=1}^{M_{max}-1} \left[\overline{M} c_n^* + \sum_{M=\max(M_{min}, n+1)}^{M_{max}} G(M)(M-n-Mc_n^*)(A+iB)^{k(n,M)} \right] Spur[V][W][Q]^n .
\end{aligned}
$$

This particular model is equivalent to that proposed by Plançon (2002) if all CSD contain a single layer, that is if $\overline{N} = 1$. The total number of defects in all $(n+1)$ layer sequences is then equal to $(M-n)n$, $c_n = 0$, and $k_n = n$. As a consequence, the term $(A+iB)^n$ can be included in the $[Q]^n$ matrix, and Eqs. (2.3.80) and (2.3.79) are equivalent. All other models can be described with a single additional parameter (λ, σ, ξ_{max}) describing the distribution $W(\Delta\xi)$, which is the degree of coherence between CSD in megacrystals. It should be noted (i) that the information about CSD size distribution is kept when using this alternative model, and (ii) that there is no positional shift of the reflections if a normal distribution is used.

2.3.8 DIFFRACTION BY A POWDER SAMPLE

Clay minerals occur as finely dispersed crystals whose size within the layer plane is ~1 μm, which restricts the methods allowing their routine structure determination to powder diffraction. However, the actual experimental setting

influences the intensity distribution for a given powder sample, and this influence should be taken into account in the calculation of diffraction effects if they are to be compared with the data. The general theory of XRD by randomly oriented crystal powders was described by von Laue (1932), Warren (1941), and Wilson (1949b). XRD is conveniently described using the Ewald sphere. This geometrical construction allows identifying points in the reciprocal space that satisfy the Bragg diffraction condition. Intersection of the Ewald sphere (radius $1/\lambda$) with hk rods of a crystal rotated around the origin of reciprocal space is considered usually. The present description of mixed-layer structures is restricted to the intensity distribution of basal $00l$ reflections, and only the rod with $h=0$ and $k=0$ is to be considered. Data collection conditions for basal reflections are schematized in Fig. 2.3.9 for the θ–2θ reflection configuration routinely available on diffractometers with Bragg–Brentano geometry. For a given sample rotation θ, vector $\mathbf{s}$ connects the vector tips of the primary ($\mathbf{k_0}/\lambda$) and scattered ($\mathbf{k}/\lambda$) beams that define the diffraction angle 2θ. For this case, Fig. 2.3.9 shows the intersection of the Ewald sphere (origin in O′, radius $1/\lambda$) with the $h=0$, and $k=0$ rod, which is perpendicular to the basal surface π of a diffracting crystal and passes through the origin O of the reciprocal space. Alternatively, powder XRD can be described using a fixed crystal and the intersection of hk rods with spheres centred at the origin of the reciprocal space and of a variable radius s (Brindley and Méring, 1951). The intensity distribution $i_{00}(s)$ then corresponds to that of waves diffracted at a given angle 2θ ($s=2\sin\theta/\lambda$) by an assembly of randomly oriented crystals. For a given value of s, the intensity

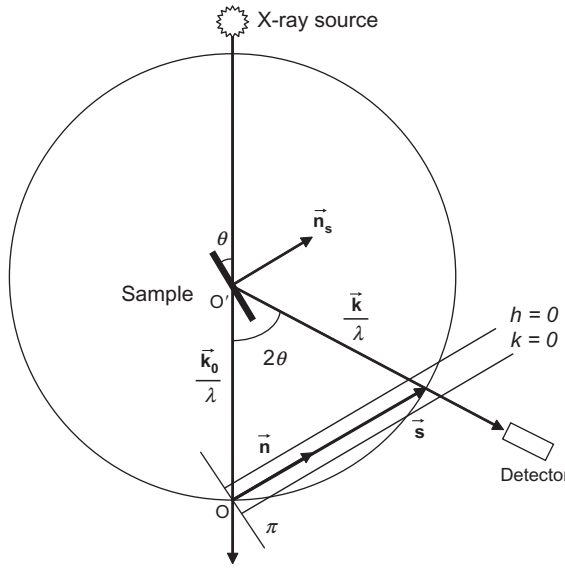

FIGURE 2.3.9 Schematic representation of the geometric configuration used for data collection in θ–2θ reflection mode. $\mathbf{n_s}$ is the normal to the sample surface, π is the basal surface of a crystal, $1/\lambda$ is the radius of the Ewald sphere, 2θ is the diffraction angle, and O is the origin in the reciprocal space.

$i_{00}(s)$ is proportional to the intersection of the rod 00 with a sphere of radius s integrated over their common surface A (Fig. 2.3.10). From Eqs. (2.3.8) and (2.3.23), this intensity can be written as

$$i_{00}(s) = \int_A I_{00}(\mathbf{s}) \frac{\mathrm{d}A}{4\pi s^2} = \frac{1}{4\pi\sigma\Omega s^2} |F_{00}(Z)|^2 G_{00}(Z) \int_A D(X,Y) D^*(X,Y)\, \mathrm{d}A \tag{2.3.81}$$

where $I_{00}(\mathbf{s})$ is the intensity within the 00 rod at the tip of vector $\mathbf{s}$, $\mathrm{d}A$ is the surface increment of the sphere of radius s, and σ and Ω are the surface areas of the layer and unit cell, respectively, in the **a**–**b** plane.

For large sizes of the layers in the **a**–**b** plane, the intersection of the 00 rod with the sphere of radius s is close to a flat cross-section, except for very small s values, and the spherical surface A can be approximated by the plane A', which is tangent to the sphere at its intersection with the Z-axis (Fig. 2.3.10). In this case

$$\int_{A'} D(X,Y) D^*(X,Y)\, \mathrm{d}X\mathrm{d}Y = \sigma, \quad \text{and} \quad i_{00}(Z) = \frac{1}{4\pi\Omega Z^2} |F_{00}(Z)|^2 G_{00}(Z) \tag{2.3.82}$$

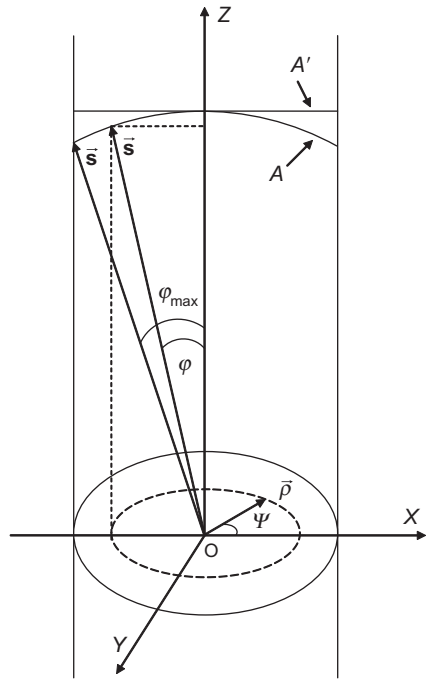

FIGURE 2.3.10 Schematic representation of the intersection of the 00 reciprocal rod by the Ewald sphere (A) of radius s. The plane A' is tangent to the sphere at its intersection with the 00 rod.

The intensity of X-rays diffracted at a given $Z = 2\sin\theta/\lambda$ value by a powder of randomly oriented crystals is thus proportional to the product of the unit-cell structure factor $[|F_{00}(Z)|^2]$ and the interference function $[G_{00}(Z)]$; it is also inversely proportional to the squared distance of the Z point from the origin $(1/Z^2)$. The latter term is the Lorentz factor and will be discussed hereafter.

Approximating the integration over the spherical surface by that over the tangent plane (Eq. 2.3.82) is valid in most practical cases. The surface area of the 00 rod intersection with the sphere of radius s and the tangent plane can be expressed as $S_A = \frac{\pi}{R^2}\left[1 + \frac{1-\cos\varphi_{\max}}{\sin\varphi_{\max}}\right]$ and $S_{A'} = \frac{\pi}{R^2}$, respectively, where R is the radius of disc-shaped layers (Fig. 2.3.10). This radius is equal to several hundreds of angstroms for most clay minerals, and the difference between the two expressions can be calculated for the 001 reflection of mica: $\frac{1-\cos\varphi_{\max}}{\sin\varphi_{\max}} = 0.025$ $(\varphi_{\max} = \arcsin(d/R) = 2.9°$ for $d_{001} = 10$ Å, and $R = 200$ Å). The planar approximation thus reduces the integration area by ~2.5%, this reduction decreasing for higher order reflections owing to the decreasing values of $\varphi_{\max}$. The underestimation of the integration area reaches ~7.5% for the super-reflection of a mixed-layer structure with $d = 30$ Å and $R = 200$ Å ($\varphi_{\max} = 8.6°$).

2.3.8.1 Effect of the Crystal Partial Orientation

Structural investigation of clay minerals is commonly restricted to the analysis of diagnostic basal reflections, and oriented preparations are thus preferred to enhance their intensity while diminishing that of *hkl* reflections (Moore and Reynolds, 1997). Crystal orientation is naturally favoured by the strong anisotropy of clay particles, whose extension within the layer plane is usually much larger than perpendicular to it. In addition, oriented preparations possess an axial symmetry of crystal orientation normal to the sample surface. The influence of partial crystal orientation on the intensity distribution was described in the literature for different experimental settings and particle shapes (Taylor and Norrish, 1966; Ruland and Tompa, 1968, 1972; Reynolds, 1976, 1986; Plançon and Tchoubar, 1977; de Courville et al., 1979; Plançon, 1980), and will be hereafter described only for basal reflections.

For this purpose, a flat sample containing Np crystals with different orientations is considered, the normal to the sample surface being $\boldsymbol{n_s}$, whereas the cylindrically symmetrical function $Np(\alpha)$ describes the relative proportion of crystals whose normal to their basal surface ($\boldsymbol{n}$) deviates from $\boldsymbol{n_s}$ by the angle α (Fig. 2.3.11). If $\mathrm{d}Np$ is the number of crystals whose normal to their basal surfaces lie in a zone of sphere $\mathrm{d}\Omega$, then $\mathrm{d}Np = Np \cdot Np(\alpha)\,\mathrm{d}\Omega$. As $\int \mathrm{d}Np = Np$ and $\mathrm{d}\Omega = 2\pi \sin\alpha\,\mathrm{d}\alpha$, $\int Np(\alpha)\,\mathrm{d}\Omega = 2\pi \int_0^{\pi} Np(\alpha)\sin\alpha\,\mathrm{d}\alpha = 1$.

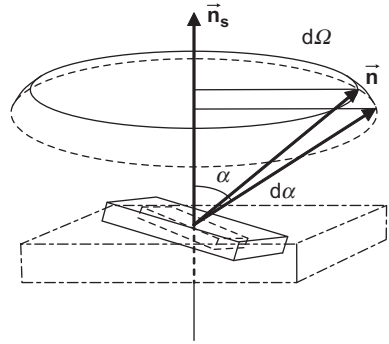

FIGURE 2.3.11 Schematic representation of diffraction by a partially oriented sample. $\mathbf{n_s}$ is the normal to sample surface, and **n** is the normal to 'misoriented' crystal basal surface, α being the 'misorientation' angle.

For a randomly oriented powder, $Np(\alpha)$ is independent of α, and $2\pi Np(\alpha)\int_0^{\pi}\sin\alpha\,d\alpha = 1$, or $Np(\alpha) = 1/4\pi$ (or $Np/4\pi$ when using absolute units). If the powder is perfectly oriented, then $Np(\alpha)$ is a Dirac function and $Np(0) = 1$ (or Np when using absolute units).

For the geometry schematized in Fig. 2.3.9, directions of vectors **s**, $\mathbf{n_s}$, and **n** are identical for crystals contributing to diffracted intensity at a given 2θ angle and for an ideally narrow and perfectly parallel beam. In this ideal case, a restricted set of crystals, corresponding to $Np(0)$, contributes to the diffracted intensity, whatever the 2θ angle. The basal surfaces of these crystals are strictly parallel to the sample surface and only their azimuthal orientation in the **a**–**b** plane may differ. As a consequence, the relative intensities of basal reflections do not depend on the orientation function $Np(\alpha)$, although the absolute intensity will depend on $Np \times Np(0)$, the number of diffracting crystals. However, the divergence of both incident and diffracted beams, coupled to partial crystal orientation, noticeably modifies the experimental intensity and profile of basal reflections (Reynolds, 1976, 1986; Drits et al., 1993). Correction factors are described for partial orientation and for the main experiment- and sample-induced modifications of the intensity distribution with the usual Bragg–Brentano geometry. To allow a quantitative comparison with the data, XRD patterns calculated for mixed-layer structures, or periodic structures, should include these corrections or the data should be corrected, if possible.

2.3.8.2 Sample Absorption

When collecting data in reflection mode with the Bragg–Brentano geometry, incident and diffracted X-ray beams form a unique angle θ with the flat sample surface. Penetration of the incident beam into the sample induces an intensity decrease because of absorption, and the same effect is observed for the

diffracted beam. For a thin element of thickness dx located at a distance x from the sample surface (Fig. 2.3.12), the intensity decrease at a diffraction angle 2θ can be written as

$$\mathrm{d}I = \frac{I_0 S_0 \,\mathrm{d}x}{\sin\theta} \exp - \frac{2\mu^* \rho x}{\sin\theta},$$

where I_0 is the incident beam intensity per volume unit, S_0 is the cross-section of the incident beam at the centre of the goniometer, μ^* is the average mass absorption coefficient of the sample and ρ is the average sample density.

The intensity diffracted by the whole volume of irradiated sample is then

$$I = \int_{x=0}^{x=d} \mathrm{d}I = \frac{I_0 S_0}{\sin\theta} \int_{x=0}^{x=d} \exp - \frac{2\mu^* \rho x}{\sin\theta} \mathrm{d}x = \frac{I_0 S_0}{2\mu^* \rho} \left[1 - \exp\left(-\frac{2\mu^* \rho d}{\sin\theta}\right)\right] \quad (2.3.83)$$

From this equation, the exponential term is infinitely small for thick (large d value) samples, and the absorption of the X-rays is proportional to $1/2\mu^*\rho$, and constant for all basal reflections. For thinner samples, the exponential term in Eq. (2.3.83) cannot be neglected, and the relative intensities of basal reflections vary with the diffraction angle 2θ. However, reliable values are difficult to obtain experimentally for both d and ρ, and it is convenient to define V as the volume of sample irradiated and to write

$$I_0^* = I_0 \quad V = I_0 \frac{S_0 d}{\sin\theta}.$$

It is then possible to deduce

$$I = \frac{I_0^* \sin\theta}{2\mu^* \rho d} \left[1 - \exp\left(-\frac{2\mu^* \rho d}{\sin\theta}\right)\right] = \frac{I_0^* \sin\theta}{2\mu^* g} \left[1 - \exp\left(-\frac{2\mu^* g}{\sin\theta}\right)\right],$$

where I_0^* is the intensity of the primary beam on the sample, and g is the experimentally available surface density of the sample, with $g = \rho d = md/V = m/S$; m, V, and S are the mass, volume, and surface area, respectively, of the sample with thickness d.

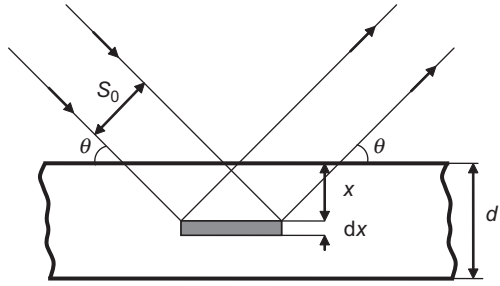

FIGURE 2.3.12 Schematic representation of X-ray absorption by a thin sample element dx when collecting XRD data in reflection mode.

2.3.8.3 Beam Overflow

Clay minerals have large (7–20 Å) unit-cell parameters perpendicular to the layer plane, and their first basal reflections thus occur at a low angle ($2\theta < 15°$ for Cu or Co radiation). However, sample availability, or experimental setting, may require the preparation of samples with a limited length L, which would induce beam overflow for low diffraction angles (Fig. 2.3.13; $2\theta_1$), while the whole cross-section S_0 of the primary beam is used for sample illumination when increasing the diffraction angle (Fig. 2.3.13; $2\theta_2$). As a consequence, the relative intensity of low-angle reflections is reduced compared to high-angle ones:

$$I = \frac{I_0 L \sin\theta}{2\mu^*\rho}\left[1 - \exp\left(-\frac{2\mu^*\rho d}{\sin\theta}\right)\right]$$
$$= \frac{I_m L \sin\theta}{2\mu^*}\left[1 - \exp\left(-\frac{2\mu^* g}{\sin\theta}\right)\right] \quad \text{if } S_0 > L\sin\theta (\text{low} - \text{angle reflections})$$

$$I = \frac{I_0 S_0}{2\mu^*\rho}\left[1 - \exp\left(-\frac{2\mu^*\rho d}{\sin\theta}\right)\right]$$
$$= \frac{I_m S_0}{2\mu^*}\left[1 - \exp\left(-\frac{2\mu^* g}{\sin\theta}\right)\right] \quad \text{if } S_0 < L\sin\theta (\text{high} - \text{angle reflections})$$

where $I_m = I_0/\rho$ is the intensity per mass unit.

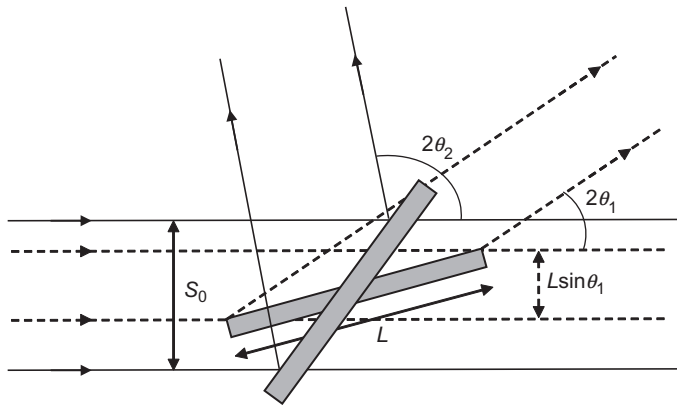

FIGURE 2.3.13 Schematic representation of sample illumination for different 2θ diffraction angles.

2.3.8.4 Polarization of the Diffracted X-ray Beam

When emitted by the tube, the X-ray beam is not polarized: that is, its intensity is independent of the angle of view, all other parameters being constant. In contrast, the intensity of the X-ray beam depends on the 2θ angle after being scattered by electrons in a crystal; the beam intensity is maximum in the direction of the primary beam and in the inverse direction, whereas it is minimum in directions perpendicular to the primary beam. The angular dependence, with respect to the primary beam, of the intensity diffracted by a crystal is called the polarization factor (Klug and Alexander, 1974) and can be expressed as

$$P(2\theta) = \frac{1 + \cos^2 2\theta}{2} \tag{2.3.84}$$

When a monochromator, flat or bent, is added in the optical pathway, this factor becomes

$$P(2\theta) = \frac{1 + \cos^2 2\theta \cos^2 2\theta_m}{1 + \cos^2 2\theta_m}$$

with θ_m being the reflection angle of the monochromator.

2.3.8.5 Lorentz Factor

The integration of the 00 rod (Eq. 2.3.81) induces further dependence of the intensity on the θ angle, the above-mentioned Lorentz factor. This factor describes the evolution of the sample volume actually diffracting as a function of the diffraction angle 2θ, and its expression depends both on the sample state (monocrystal, powder) and on the experimental geometry. The usual expressions of the Lorentz factor are $L = 1/\sin^2\theta \cos\theta$ and $L = 1/\sin\theta \cos\theta$, for randomly and perfectly oriented powders, respectively (Klug and Alexander, 1974). These expressions are valid for integrated intensities but should be modified if intensities are calculated for all 2θ angles to model XRD patterns. The modified expressions are $L = 1/\sin^2\theta$ and $L = 1/\sin\theta$ for randomly and perfectly oriented powders, respectively. Partial crystal orientation leads to values intermediate between those corresponding to the two above cases. Reynolds (1976, 1986) derived the analytical expression of a correction factor ψ (powder ring distribution factor) that accounts for both partial crystal orientation, assuming a normal distribution, and beam collimation by Soller slits:

$$\psi = \frac{s_1 s_2}{\bar{s}(\sigma^*)^2}\left[\frac{\sqrt{2\pi}\sigma^*}{2} erf(Q) - \frac{2(\sigma^*)^2 \sin\theta}{\bar{s}}\left(1 - \exp\left(-Q^2\right)\right)\right],$$

where s_1 and s_2 are the Soller slit divergence (in degrees) for the primary and the diffracted beams, respectively, $\bar{s} = \sqrt{s_1^2 + s_2^2}$, σ^* is the standard deviation of the Gaussian orientation function (in degrees), $Q = 2\sqrt{2}\sigma^* \sin\theta$, and $erf(x) = \frac{2}{\sqrt{\pi}}\int_{t=0}^{t=x} \exp(-t^2)\,dt$ is the tabulated integral.

Owing to their common dependence on the θ diffraction angle, Lorentz and polarization factors are usually combined to define the Lorentz polarization (*LP*) factor. For maximum intensities, this factor can be expressed as $\frac{1+\cos^2 2\theta}{\sin\theta}\psi$.

The powder ring distribution factor ψ is proportional to $1/\sin\theta$ for randomly oriented powders and constant for single crystals (Reynolds, 1986). In these two extreme cases, the complete correction factor is equivalent to the *LP* factor for randomly oriented powders and monocrystals, respectively. Taking into account both *LP* and powder ring distribution factors, and neglecting constant factors, Eq. (2.3.82) becomes

$$i(Z) \approx \frac{1}{\Omega} LP\psi |F(Z)|^2 G(Z). \tag{2.3.85}$$

2.3.8.6 Intensity Scaling

Analysis of XRD intensities is usually performed on a relative basis. For normalization purposes, it is, however, convenient to calculate intensities on a given basis, for example, one unit cell, a volume unit, and so on. Several possible normalizations are thus described hereafter for calculated intensities. In Eq. (2.3.85), the intensity I_{col} is calculated for a column of unit cells in a crystal, and the intensity diffracted by the whole crystal is thus proportional to

$$I_{\text{crys}} = I_{\text{col}} \frac{\sigma}{\Omega} \approx \frac{\sigma}{\Omega^2} LP\psi |F(Z)|^2 G(Z),$$

with σ the surface area of the layers in the $\mathbf{a}-\mathbf{b}$ plane.

On the other hand, the intensity calculated for one unit cell (I_c) is proportional to

$$I_c = I_{\text{col}}/N \approx \frac{1}{N\Omega} LP\psi |F(Z)|^2 G(Z), \quad \text{with } N \text{ the number of layers in a crystal.}$$

The intensity calculated for one volume unit (I_v) is proportional to $I_v = I_c/V_c \approx \frac{\xi}{NV_c^2} LP\psi |F(Z)|^2 G(Z)$, with V_c the volume of the unit cell and ξ the layer thickness.

Similarly, the intensity per mass unit (I_m) can be expressed as $I_m = I_v/\rho$, ρ being the crystal density. For thick enough crystals, the beam is totally absorbed, and absorption is proportional to $1/2\mu^*\rho$ (Eq. 2.3.83), thus leading to the following expression for I_m:

$$I_m \approx \frac{\xi}{NV_c^2 \mu^* \rho} LP\psi |F(Z)|^2 G(Z)$$

which is equivalent to the equation of Reynolds (1983–Eq. 8).

To use the above equations for mixed-layer structures, fixed parameters can be replaced by their average values subject to minor approximations. For example

$$I_m \approx \frac{\overline{\xi}}{\overline{V}_c^2 \overline{\mu}^* \overline{\rho}} LP\psi \left\{ SpurVW + 2\mathrm{Re} \frac{1}{\overline{N}} \sum_{n=1}^{N-1} \sum_{m=n+1}^{N} (m-n) F(m) SpurVW Q^n \right\} \tag{2.3.86}$$

where $\overline{N}$, $\overline{V}_c$, $\overline{\mu}^*$, $\overline{\rho}$, and $\overline{\xi}$ are the average values of the number of layers, volume of unit cells, mass absorption coefficient, density, and thickness of layers in the crystals. The above normalizations are especially useful for quantitative analysis of clay minerals including mixed-layer structures. The relative mass contribution of smectite-containing compounds obviously varies with their interlayer contents, and contrasting contributions are thus expected from XRD patterns recorded under different experimental conditions, as required for the multi-specimen technique (e.g. Drits et al., 1997b; Sakharov et al., 1999a,b). The contrast is, however, minor owing to the relative 'weights' of the 2:1 layer and of the interlayer space.

2.3.9 CONCLUSION

Drits (1997, 2003) stressed the remarkable ability of diffraction techniques to extract average structural information from the profiles and intensities of diffraction maxima arising from mixed-layer structures, and more generally from crystals deprived of 3D periodicity. He also pointed out that a reliable determination of structural and chemical heterogeneity of layered structures depends essentially on a reliable interpretation of diffraction data. Such an interpretation relies necessarily on the previously described calculation of diffraction effects from mixed-layer structures.

Because of the intrinsic complexity of the calculations, simplified methods have been proposed in the literature that take advantage of the shift of reflection position as a function of the actual composition of the mixed-layer structures predicted by the pioneering work of Méring (1949). According to this author, basal reflections corresponding to a randomly interstratified mixed-layer structure (two components) are located between neighbouring 00*l* reflections corresponding to periodic structures whose layers are interstratified. The actual position of these reflections depends on the relative proportions of the interstratified layer types and on the intensity of the neighbouring 00*l* reflections. In addition, the breadth of the mixed-layer reflections increases with the 'distance' between the 00*l* reflections corresponding to periodic structures whose layers are interstratified ('Q-rule' of Moore and Reynolds, 1997). More generally, the positions of basal reflections corresponding to an ordered mixed-layer structure containing *A* and *B* layers ($w_A > w_B$) with $S=1$ or $S=2$ are located between neighbouring 00*l* reflections corresponding to

periodic stacking sequences consisting of *A* and *AB* ($S=1$), or *AAB* ($S=2$), fragments (Reynolds, 1988; Drits et al., 1994).

In natural environments, interstratification is especially widespread among clay minerals which differ in the type of interstratified layers and in their stacking sequences. Because of the reactivity of the frequently interstratified expandable layers and of their resulting ability to evolve as a function of physicochemical conditions, these mixed-layer structures have drawn special attention for decades, and simplified peak-migration methods have been proposed over the years for the identification of illite–smectite (Srodon, 1980, 1981, 1984; Watanabe, 1981, 1988; Velde et al., 1986; Tomita et al., 1988; Inoue et al., 1989; Drits and Plançon, 1994; Drits et al., 1994; Plançon and Drits, 1994, 2000; Dudek and Srodon, 1996) and other mixed-layer structures (Drits and Sakharov, 1976; Tomita and Takashi, 1985; Drits et al., 1994; Lanson and Bouchet, 1995; Moore and Reynolds, 1997). These methods rely essentially on peak-migration curves linking the position of a given set of reflections (or of a given reflection) to the composition (relative proportion of the different layer types) and the layer stacking mode of the mixed-layer structures. The curves were derived essentially from the calculation of XRD patterns using either Newmod (Reynolds, 1985) or the program based on the matrix formalism developed by Watanabe (1981, 1988). The intensity ratio between some of these reflections, or between reflections and 'background', was used occasionally as an additional criterion to estimate the relative contents of the different layer types in the mixed-layer structures.

Despite their widespread use, these simplified identification methods have major limitations (Lanson, 2011):

- The first of these limitations is the lack of direct comparison between experimental and calculated patterns, which is intrinsic to the approach. As a result, there is no way to assess the validity of the identification by using a parameter measuring the 'goodness of fit' as is usual in structural studies. However, direct comparison of experimental XRD patterns with those calculated on the basis of the identification performed allowed refuting peak position as a valid criterion for mixed-layer structure characterization (Claret et al., 2004; McCarty et al., 2008), and thus these simplified identification methods.
- Another limitation of these methods comes from the use of a unique XRD pattern for identification purposes, which does not allow the validation of the proposed identification by independent XRD measurements on the same sample submitted to different treatments. In addition, the profiles of the diffraction lines, which are strongly affected by interstratification effects, are not taken into account by these peak-position methods. As discussed by Lanson (2011), these additional constraints are especially useful owing to the low sensitivity of diffraction to the actual nature of structural

disorder as illustrated by the common possibility of fitting the data equally well with different structure models (Drits, 1985; McCarty et al., 2008).

– Other limitations are linked to those of the programs used to calculate diffraction effects arising from mixed-layer structures, and the limited range used for variable parameters in order to (over)simplify the identification process. Intrinsic limitations of the programs include, for example, their inability to calculate diffraction effects from multi-component mixed-layer structures, when heterogeneity, rather than homogeneity, is the rule for smectite hydration even for homoionic specimens under controlled relative humidity conditions (Ferrage et al., 2005a,b, 2007, 2010; Karmous et al., 2009). Consistently, all structural characterizations of natural samples performed with calculation algorithms allowing the calculation of their XRD patterns have led to the identification of mixed-layer structures that include more than two components owing to the systematic heterogeneity of the swelling/hydration behaviour of expandable layers (Drits et al., 1997b, 2002a,b, 2004, 2007; Sakharov et al., 1999a,b, 2004a; Lindgreen et al., 2000, 2002, 2008; Claret et al., 2004; McCarty et al., 2004, 2008; Inoue et al., 2005; Aplin et al., 2006; Hubert et al., 2009; Lanson et al., 2009). It should be noted that heterogeneity is present whatever the chemistry (both Fe- and Al-rich) of expandable layers (McCarty et al., 2004). In addition, the hydration behaviour exhibited by expandable layers in smectite is not restricted to the usual 0W ($d_{001} = 9.6$–10.0 Å), 1W ($d_{001} = 12.0$–12.8 Å), and 2W ($d_{001} = 14.8$–15.6 Å) states, and 'unusual' basal spacings were reported for hydrated expandable layers (e.g. Lindgreen et al., 2002; Lanson et al., 2009) as suggested by Bailey et al. (1982). Heterogeneity is not restricted to expandable layers, and the co-existence of different mica-like layers in a given mixed-layer structure was also reported, thus substantiating the inability of these methods to provide a satisfactory identification of mixed-layer structures. In particular, the co-existence of K^+- and NH_4^+-mica layers was repeatedly demonstrated in the context of burial diagenesis in the vicinity of source rocks (Drits et al., 1997a, 2001, 2002a, 2005, 2007; Sakharov et al., 1999a; Lindgreen et al., 2000).

– In addition, most methods include calculations only for randomly interstratified mixed-layer structures ($S = 0$, $p_{ii} = w_i$) and for the sole MPDO case for higher values of the Reichweite parameter S despite the key role of junction probabilities in the profiles of XRD patterns calculated for mixed-layer structures (see Appendix A1). The high frequency of natural and synthetic mixed-layer structures exhibiting junction probabilities different from the usual $S = 0$ and MPDO cases (i.e. partial segregation or partial ordering; Drits et al., 1997b, 2002b, 2004; Sakharov et al., 1999a, b; Claret et al., 2004; Inoue et al., 2005; McCarty et al., 2008, 2009; Hubert et al., 2009, 2012; Lanson et al., 2009; Ferrage et al., 2011b)

clearly demonstrates that XRD profile modelling is the unique tool that can provide an accurate structure characterization of mixed-layer structures, as peak migration curves are not available for junction probabilities different from the 'ideal' cases.

– Finally, essential adjustable parameters that are insufficiently varied include the size and distribution of the CSD, as the calculations are most often restricted to a single mean value, and the crystal chemistry (layer thickness, coordinates and occupancies of the different sites, chemistry, etc.) of elementary layers.

Although the systematic calculation of XRD patterns for a variety of mixed-layer models allows an improved prediction of these complex diffraction effects, such a description is not included in this chapter. The effect on calculated XRD patterns of junction probability parameters and of various defects described in the previous sections to emphasize their potential importance for the XRD identification of mixed-layer structures is rather illustrated in the Appendix. As discussed by Lanson (2011), the modelling approach represents, indeed, the optimum, and at present the sole, quantitative method allowing a thorough structure determination of mixed-layer structures, even on polyphasic and/or natural samples. This approach allowed revealing the intrinsic complexity of defective lamellar structures and improving their structural characterization.

Available calculation routines thoroughly renewed the description of mixed-layer structures, and a key point when using these tools is thus IMAGINATION: the search for possible structure models should not be restricted to what has been reported previously in the literature but should include all models with realistic crystal chemistry.

This approach requires a quantitative comparison of XRD data with calculated patterns and benefits from additional constraints to assess the validity of structure models in an effort to overcome the major intrinsic limitation of the XRD identification of clay minerals resulting from the tendency of XRD to average parameters describing crystal structure. The resulting low sensitivity of XRD to variation in local disorder can allow for the existence of several structure models giving rise to similar diffraction effects for a given set of experimental conditions. To determine the actual structure model, additional constraints obtained from the analysis of different XRD patterns collected from the same sample after different treatments are thus essential (multi-specimen approach; Drits et al., 1997b; Sakharov et al., 1999a,b; McCarty et al., 2004). Complementary computational or experimental (microscopies, spectroscopies, chemical and thermal analyses, etc.) approaches may also be used to obtain unambiguous and comprehensive structure models (Drits, 1983, 2003; Ferrage et al., 2011a,b; Lanson, 2011).

APPENDIX INFLUENCE OF VARIOUS ADJUSTABLE PARAMETERS ON XRD PATTERNS CALCULATED FOR MIXED-LAYER STRUCTURES

A1 XRD Patterns Calculated for two-Component Mixed-Layer Structures with Contrasting Junction Probabilities

XRD patterns shown in Fig. 2.3.14 were all calculated for a 0.7:0.3 ratio between illite and smectite with two planes of ethylene glycol (EG) molecules and $S=1$, but with different junction probability parameters (p_{SS}). Basal reflections systematically exhibit non-rational series of d values. Depending on the junction probability parameters, XRD patterns calculated for a unique composition (w_I:w_S=0.7:0.3) differ considerably by the number, positions, profiles, and relative intensities of the basal reflections. The positions of these reflections are reminiscent of a rectorite-like structure (a regular illite–smectite with a 50:50 illite:smectite ratio) when the degree of ordering is maximum ($S=1$ with MPDO, $p_{SS}=0$; Fig. 2.3.14A), or of a physical mixture of finely dispersed smectite and mica for the highly segregated model ($p_{SS}=0.6$; Fig. 2.3.14E), despite their identical w_I:w_S ratios. The pattern corresponding to random interstratification ($S=0$, $p_{SS}=0.3$; Fig. 2.3.14C) is only weakly modulated in the low-angle region ($2\theta<10^\circ$ Cu Kα).

XRD patterns shown in Fig. 2.3.15 were calculated for the same w_I:w_S ratio (0.7:0.3) and different junction probability parameters at $S=2$, and MPDO at $S=1$ ($p_{SS}=p_{SSS}=p_{ISS}=p_{SSI}=0$). XRD patterns differ only by their value of the p_{SIS} coefficient that may take any value from 0 to 1, but systematically exhibit non-rational series of d values for basal reflections. Similar to Fig. 2.3.14, the first two patterns exhibit a tendency to ordering at $S=2$ ($p_{SIS}=0.0$ and 0.2 for Fig. 2.3.15A and B, respectively), and reflection positions are close to that of the periodic IISIIS... stacking when the degree of ordering is maximum ($S=2$ with MPDO, $p_{SS}=p_{SSS}=p_{SIS}=0$; Fig. 2.3.15A). Random layer stacking at $S=2$ is obtained for $p_{SIS}=p_{IS}=0.429$, and corresponds to the $S=1$ with MPDO case (Figs. 2.3.14A and 2.3.15C). Segregation of I layers and of IS pairs is illustrated in Fig. 2.3.15D and E ($p_{SIS}=0.5$ and 0.7, respectively), the latter pattern being similar to that of a mixture of mica- and rectorite-like structures.

Similar calculations can be performed as a function of p_{SIS} for mixed-layer structures with $S=2$ and the same w_I:w_S ratio (0.7:0.3) but with junction probability parameters differing from the MPDO case at $S=1$ (i.e. with $p_{SS}>0$). XRD patterns displayed in Fig. 2.3.16 were calculated for $p_{SS}=p_{SSS}=0.15$; their resolution within the low-angle region ($2\theta<10^\circ$ Cu Kα) is strongly degraded compared to the case with MPDO at $S=1$ (Fig. 2.3.15), especially when the tendency to ordering of I layers and of IS pairs is high. This effect is significantly enhanced when the occurrence probability of smectite layer pairs and triplets is increased (Figs. 2.3.17 and 2.3.18 were calculated for

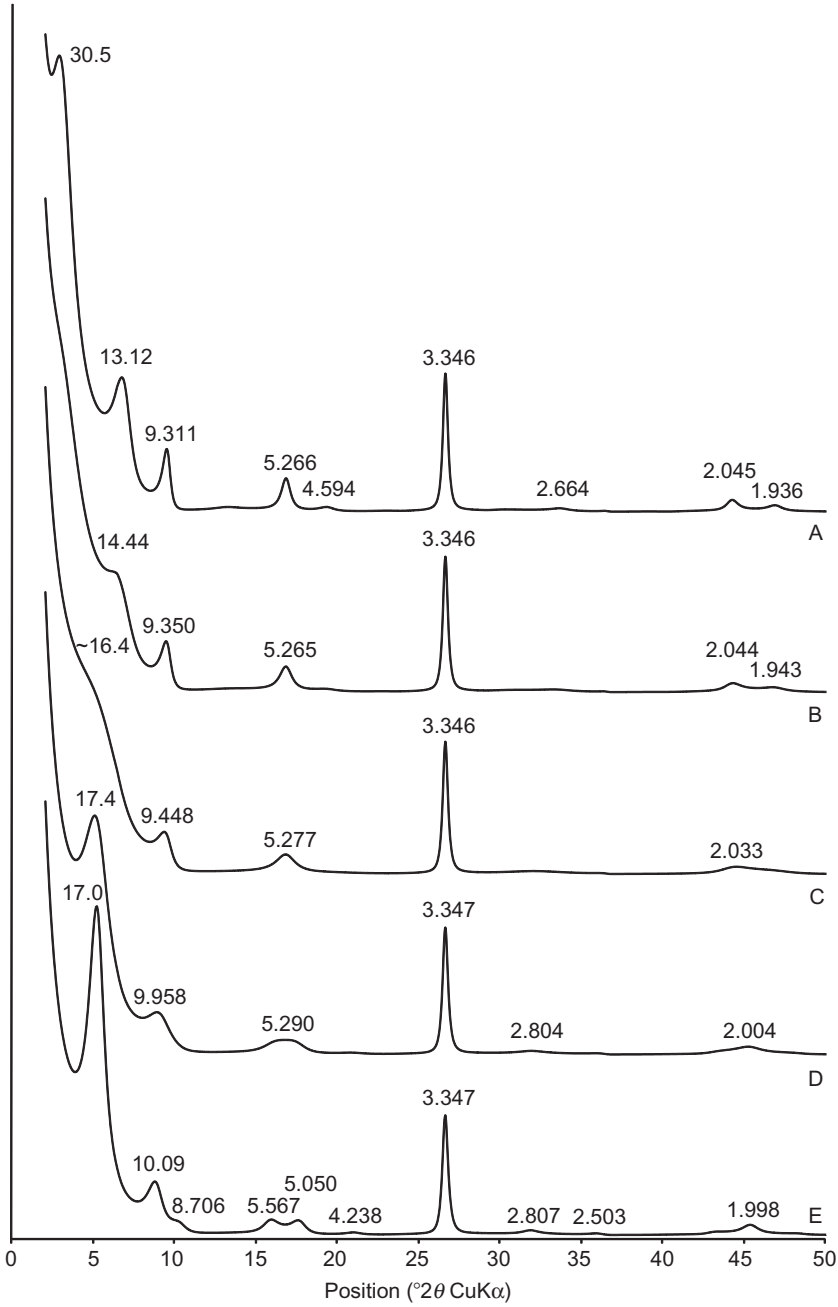

FIGURE 2.3.14 XRD patterns calculated for two-component illite–smectite having a unique composition (w_I:w_S = 0.7:0.3) and contrasting degrees of ordering at $S = 1$. (A) Maximum possible degree of ordering, $p_{SS} = 0$; (B) partial ordering, $p_{SS} = 0.15$; (C) random interstratification, $p_{SS} = w_S = 0.3$ ($S = 0$); (D) partial segregation, $p_{SS} = 0.45$; (E) partial segregation, $p_{SS} = 0.60$. Layer thicknesses of illite and smectite (with two sheets of interlayer ethylene glycol molecules) layers are 9.98 and 16.9 Å, respectively. Peak positions are given in angstroms (Å).

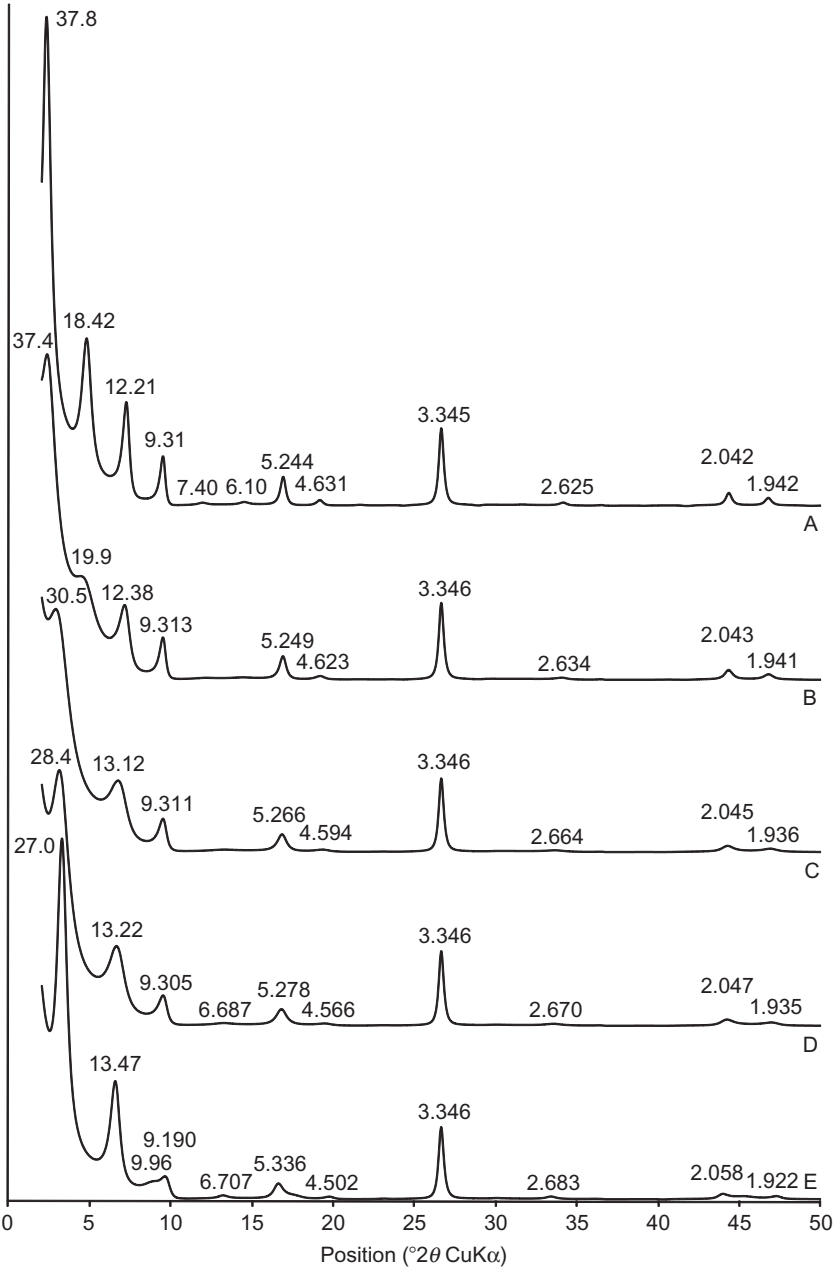

FIGURE 2.3.15 XRD patterns calculated for two-component illite–smectite with identical composition (w_I:w_S = 0.7:0.3) and junction probability at $S = 1$ (MPDO; $p_{SS} = 0$) but contrasting degrees of ordering at $S = 2$. In all cases, $p_{ISS} = p_{SS} = 0$. (A) Maximum possible degree of ordering, $p_{SIS} = 0$; (B) partial ordering, $p_{SIS} = 0.20$; (C) random interstratification, $p_{SIS} = 0.429$ (equivalent to the $S = 1$ with MPDO case; Fig. 2.3.14A); (D) partial segregation, $p_{SIS} = 0.50$; (E) partial segregation, $p_{SIS} = 0.70$. Other parameters as in Fig. 2.3.14.

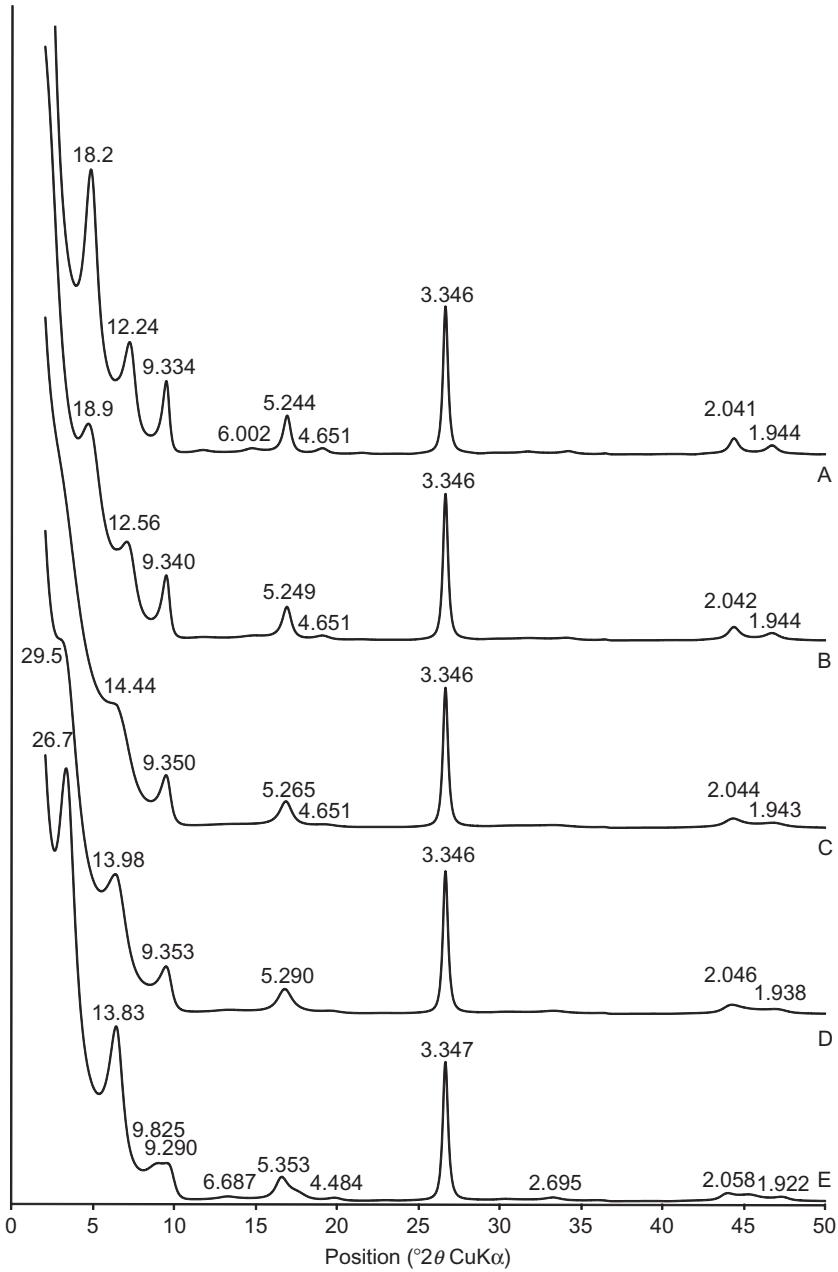

FIGURE 2.3.16 XRD patterns calculated for two-component illite–smectite having identical composition (w_I:w_S = 0.7:0.3) and junction probability at $S = 1$ ($p_{SS} = 0.15$) but contrasting degrees of ordering at $S = 2$. In all cases, $p_{ISS} = p_{SS} = 0.15$. (A) Maximum possible degree of ordering, $p_{SIS} = 0$; (B) partial ordering, $p_{SIS} = 0.15$; (C) random interstratification, $p_{SIS} = 0.364$ (equivalent to the $S = 1$ case; Fig. 2.3.14B); (D) partial segregation, $p_{SIS} = 0.45$; (E) partial segregation, $p_{SIS} = 0.60$. Other parameters are as in Fig. 2.3.14.

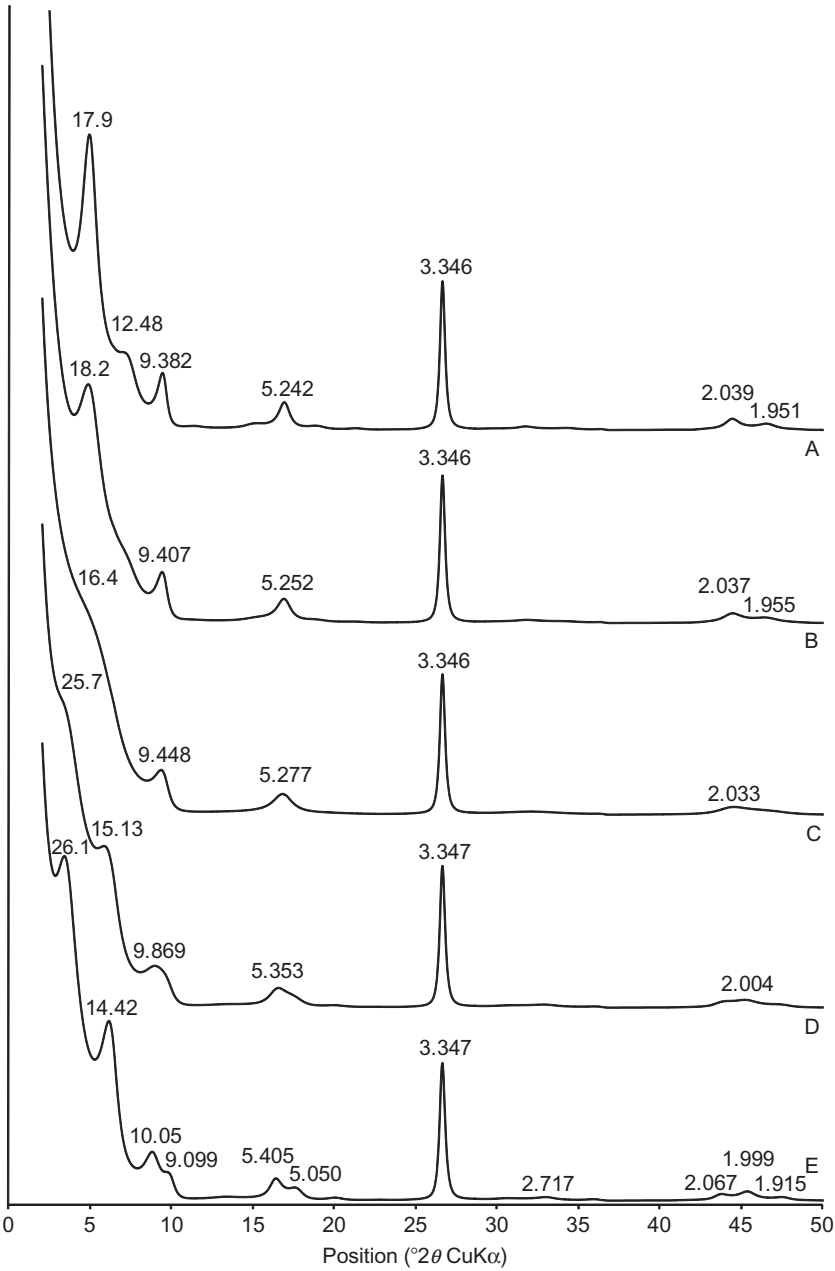

FIGURE 2.3.17 XRD patterns calculated for two-component illite–smectite having identical composition (w_I:w_S = 0.7:0.3) and junction probability at $S = 1$ ($p_{SS} = 0.30$) but contrasting degrees of ordering at $S = 2$. In all cases, $p_{ISS} = p_{SS} = 0.30$. (A) Maximum possible degree of ordering, $p_{SIS} = 0$; (B) partial ordering, $p_{SIS} = 0.15$; (C) random interstratification, $p_{SIS} = 0.364$ (equivalent to the $S = 0$ case; Fig. 2.3.14C); (D) partial segregation, $p_{SIS} = 0.45$; (E) partial segregation, $p_{SIS} = 0.60$. Other parameters are as in Fig. 2.3.14.

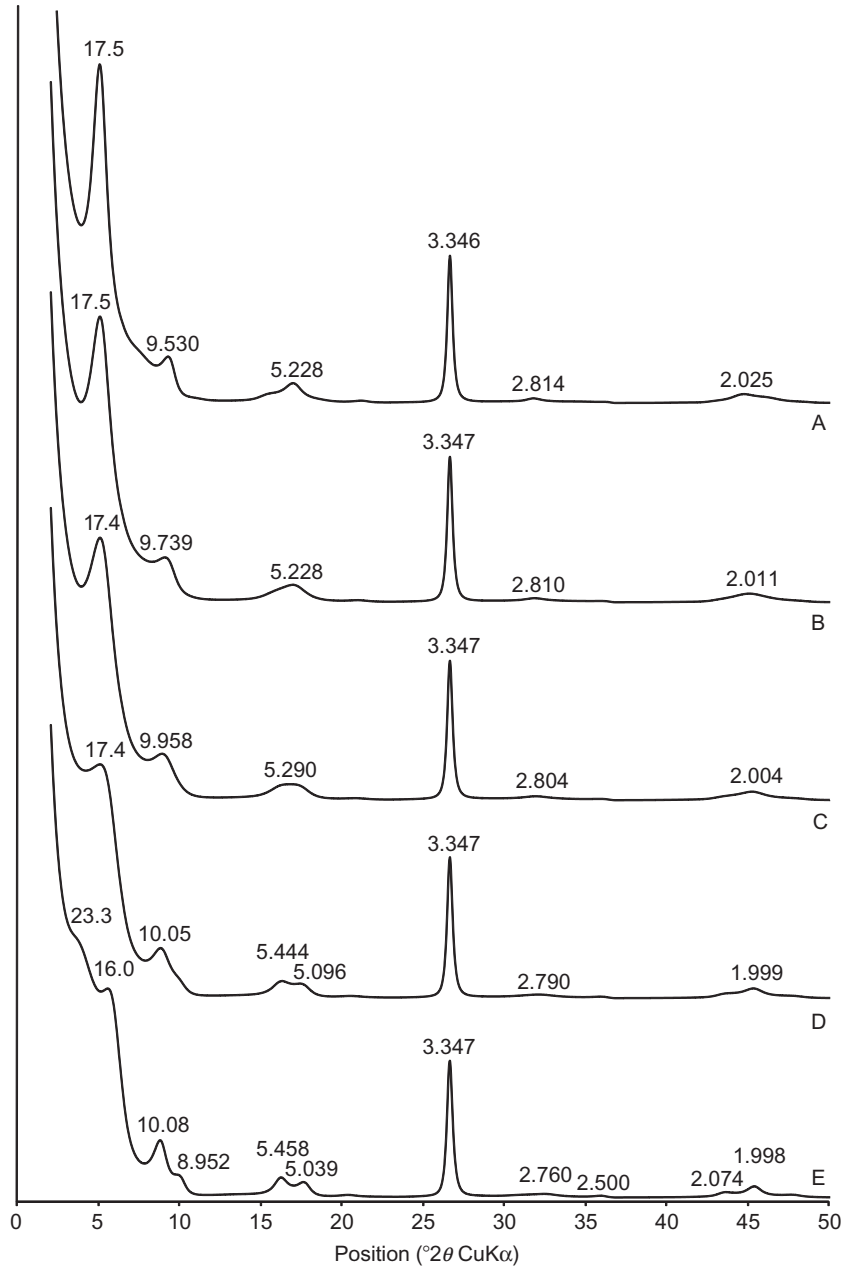

FIGURE 2.3.18 XRD patterns calculated for two-component illite–smectite having identical composition (w_I:w_S = 0.7:0.3) and junction probability at $S = 1$ ($p_{SS} = 0.45$) but contrasting degrees of ordering at $S = 2$. In all cases, $p_{ISS} = p_{SS} = 0.45$. (A) Maximum possible degree of ordering, $p_{SIS} = 0$; (B) partial ordering, $p_{SIS} = 0.15$; (C) random interstratification, $p_{SIS} = 0.236$ (equivalent to the $S = 1$ case; Fig. 2.3.14D); (D) partial segregation, $p_{SIS} = 0.35$; (E) partial segregation, $p_{SIS} = 0.45$. Other parameters are as in Fig. 2.3.14.

mixed-layer structures with $S=2$, the same w_I:w_S ratio (0.7:0.3), and $p_{SS}=p_{SSS}=0.30$ and 0.45, respectively). Additional XRD patterns can be calculated for mixed-layer structures with $S=2$ and the same w_I:w_S ratio (0.7:0.3) by varying the junction probability parameter p_{SSS} for a given set of p_{SS} and p_{SIS} parameters. One such series of calculated patterns is shown in Fig. 2.3.19 for $p_{SS}=0.30$ and $p_{SIS}=0.15$, with a significant impact on peak position, profile, and relative intensity, except for the low-angle reflections. In all XRD patterns calculated for a mixed-layer structures with the same w_I:w_S ratio (0.7:0.3), neither the position nor the profile of the reflection with $d=3.346$–3.347 Å seems to be affected by modification of junction probability parameters, owing to the close basal spacings of reflections corresponding to illite [$d_I(003)=3.327$ Å] and smectite [$d_S(005)=3.380$ Å] in this region.

A2 XRD Patterns Calculated for Multi-Component Mixed-Layer Structures

The co-existence of K^+- and $NH_4{}^+$-mica layers in mica–smectite was repeatedly evidenced in the context of burial diagenesis in the vicinity of source rocks. In addition to tobelite ($NH_4{}^+$-mica), paragonite, margarite, or aluminoceladonite may also occur in mica-containing mixed-layer structures. The contrasting layer-to-layer distance of these mica varieties (~10.33, ~9.65, ~9.56, and ~9.86 Å, respectively) compared to illite (9.98 Å) induces a subtle but significant peak shift. The co-existence of different types of mica layers in mica–smectite (e.g. illite–tobelite–smectite) is best evidenced after saturation of the sample with K^+ ions and subsequent heating at ~300 °C (Drits et al., 1997a, 2005). Such treatment decreases the layer-to-layer distance of smectite layers to that of illite layers (9.98 Å), and the relative abundance of tobelite (e.g.) layers can be estimated from the accurate modelling of reflection positions. This ability is illustrated in Fig. 2.3.20, which compares the XRD patterns calculated for illite–smectite and illite–tobelite–smectite having the same mica:smectite ratio and differing by the composition and thickness of mica layers. Experimentally, the addition of Si powder (NIST SRM 640c) as an internal standard is helpful for the accurate determination of experimental d values.

When adapted calculation routines were used, mixed-layer structures containing expandable layers were described systematically as multi- (three- or four-) component mixed-layer structures owing to the intrinsic hydration/swelling heterogeneity of expandable layers. Saturation with polar organic compounds such as EG likely reduces this heterogeneity but the actual behaviour of expandable interlayer spaces in mixed-layer structures remains poorly constrained (Bailey et al., 1982). The impact of swelling heterogeneity on XRD patterns is illustrated in Fig. 2.3.21, which compares the XRD patterns calculated for illite—expandable with a 0.7:0.3 w_I:w_{Exp} ratio. Compared to the calculations performed with no swelling heterogeneity (Fig. 2.3.14), the presence of 8% smectite layers swelling to 12.9 Å (one plane of interlayer EG

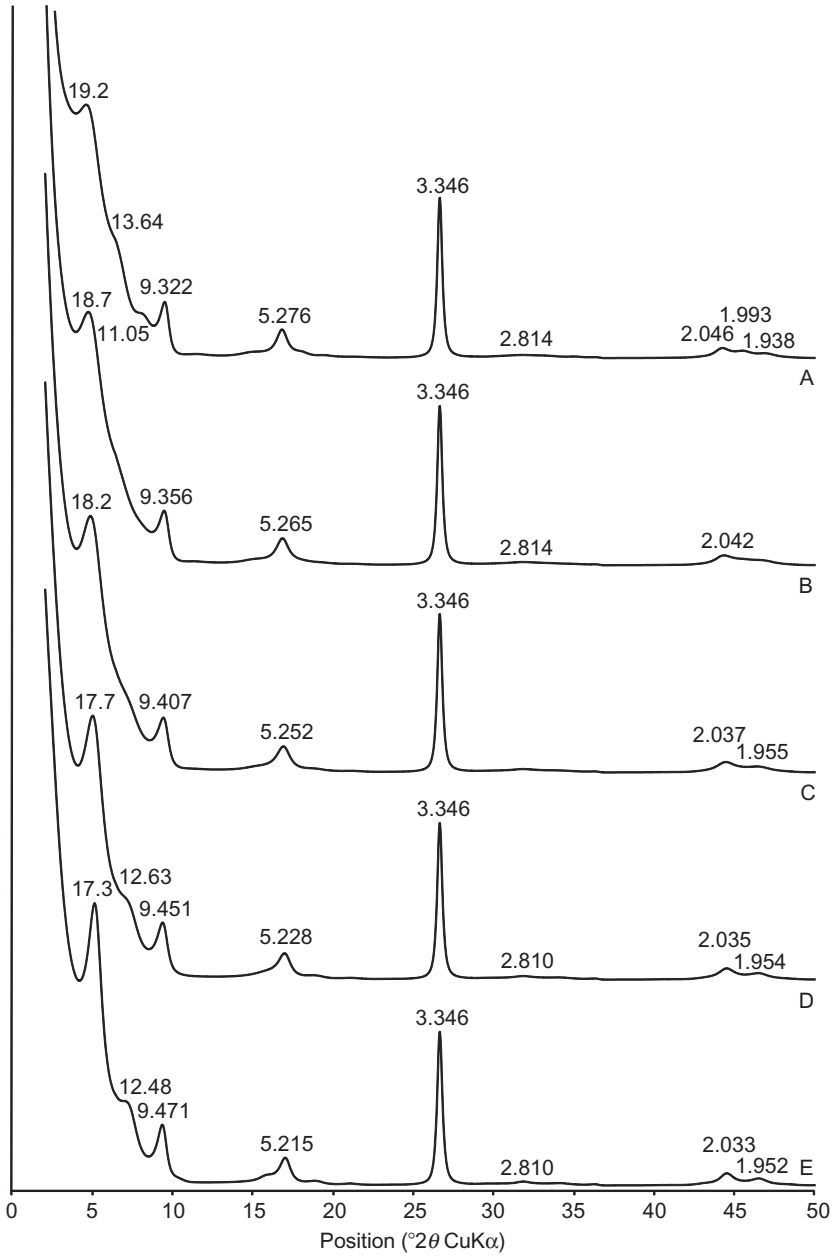

FIGURE 2.3.19 XRD patterns calculated for two-component illite–smectite having identical composition (w_I:w_S = 0.7:0.3) and junction probability at $S = 1$ ($p_{SS} = 0.30$) but contrasting degrees of ordering at $S = 2$. In all cases, $p_{SIS} = 0.15$. (A) $p_{SSS} = 0$; (B) $p_{SSS} = 0.15$; (C) $p_{SSS} = 0.30$; (D) $p_{SSS} = 0.45$; (E) $p_{SSS} = 0.60$. Other parameters are as in Fig. 2.3.14.

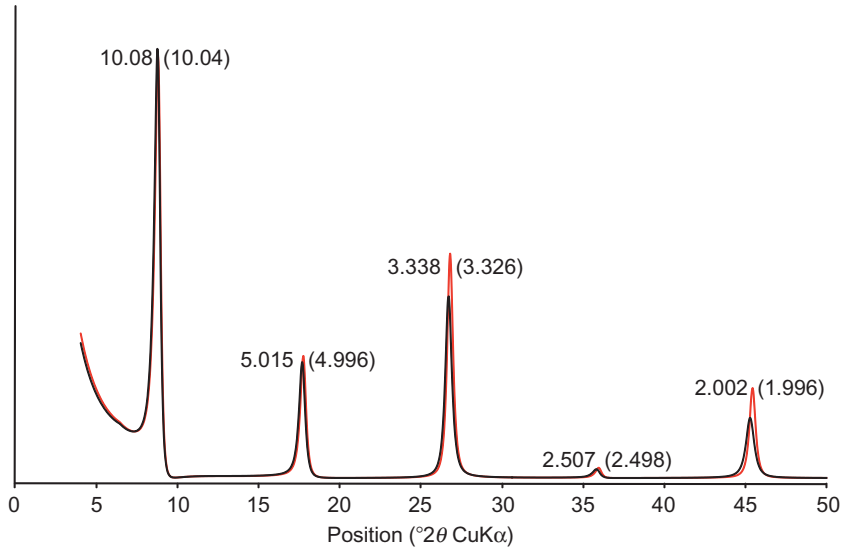

FIGURE 2.3.20 XRD patterns calculated for mica–smectite having identical composition (w_M: $w_S = 0.95{:}0.05$) but different interlayer composition for the mica interlayers. The black and grey lines are calculated for 85:10 and 95:0 ratios between K-(illite) and NH_4-(tobelite) micas, respectively. Layer thicknesses of tobelite (NH_4-mica), illite, and smectite (following K-saturation and heating to 300 °C) layers are 10.35, 9.98, and 9.98 Å, respectively. In all cases, interstratification is random ($S = 0$). Other parameters are as in Fig. 2.3.14.

molecules) together with 22% smectite layers hosting two planes of interlayer EG (d value: 16.9 Å) induces major modifications of the calculated profiles, especially in the low-angle region ($2\theta < 10°$ Cu Kα).

A3 XRD Patterns Calculated for Mixed-Layer Structures with Different Types of Defects

Figure 2.3.22 compares XRD patterns calculated for illite–smectite in which all 'core' expandable layers host two planes of interlayer EG. The occurrence of different types of layers (either 'naked' 2:1 layers as in Newmod, or 2:1 layers with one interlayer plane of EG) on the external edges of the crystals (OSL) significantly modifies the diffraction pattern over the low-angle region ($2\theta < 10°$ Cu Kα).

The influence of layer thickness fluctuations is illustrated in Fig. 2.3.23 and is visible essentially over the high-angle region ($2\theta > 20°$ Cu Kα). From the diffraction point of view, defects of the first type are similar to atomic thermal motion. For a similar $\Delta\xi$ value, the intensity reduction, compared to a defect-free model, within the high-angle region appears stronger for defects of the second type compared to defects of the first type (see Section 2.3.5 for

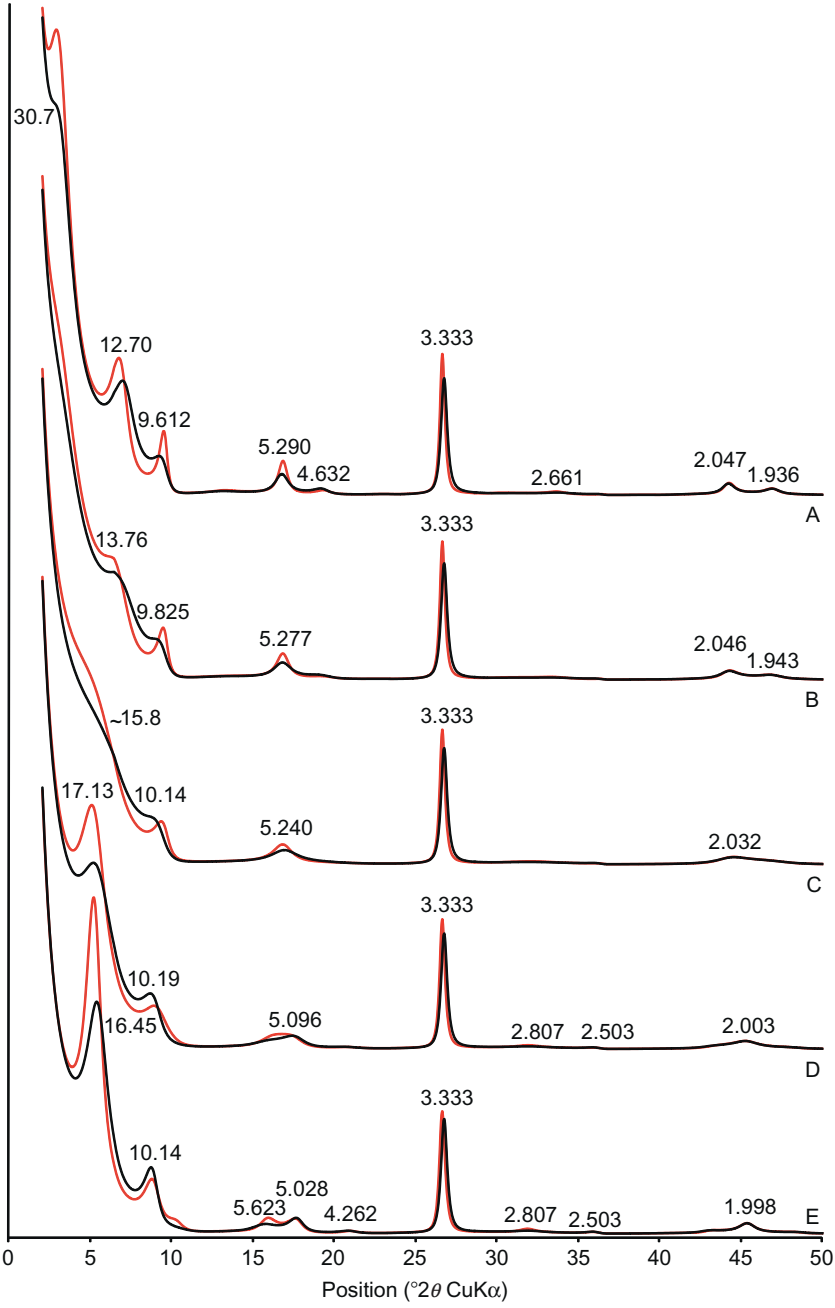

FIGURE 2.3.21 XRD patterns calculated for illite-expandable having identical composition (w_I:$w_{Exp1:Exp2}$ = 0.70:0.22:0.08) but contrasting junction probabilities at $S = 1$. The grey patterns are systematically calculated with homogeneous smectite interlayers (w_I:$w_{Exp1:}$

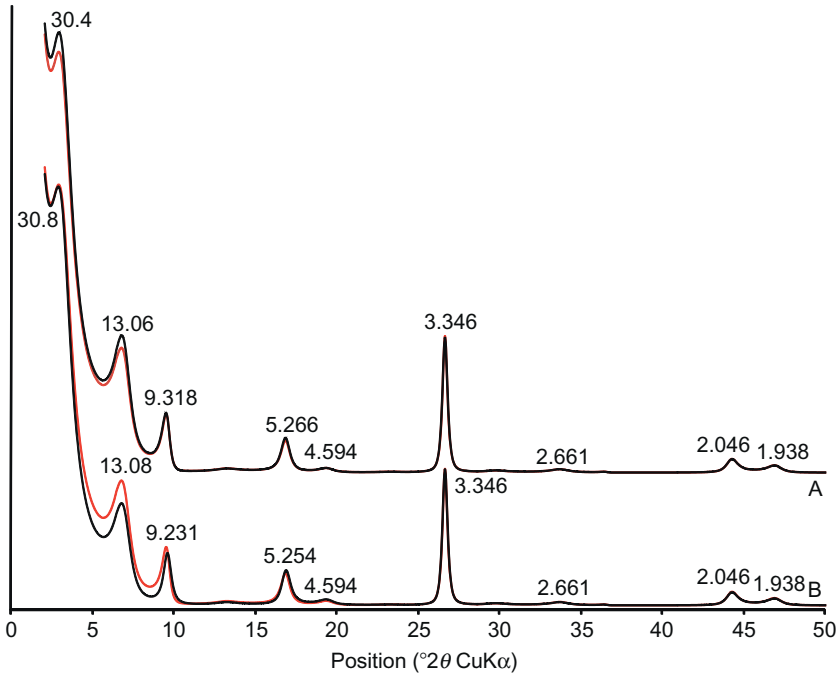

FIGURE 2.3.22 XRD patterns calculated for two-component illite–smectite with identical composition (w_I:w_S = 0.7:0.3) and junction probability at $S = 1$ (MPDO; $p_{SS} = 0$) but different outer surface layers. The grey pattern is systematically calculated with an asymmetrical model with a naked 2:1 layer on the crystal bottoms, and two sheets of ethylene glycol molecules or K-mica interlayers on crystal tops. (A) The black line is calculated with naked 2:1 layers on both crystal bottoms and tops. (B) The black line is calculated with one sheet of ethylene glycol molecules on both crystal bottoms and tops.

a description; Fig. 2.3.23A and B). In addition, defects of the second type induce peak broadening that increases with increasing θ values, compared to a defect-free model. For a similar $\Delta\xi$ value, peak broadening is lower for defects of the first type. Finally, if the distribution of layer thicknesses is not symmetrical with respect to the average value, for example, if layer thickness can only take values larger than the 'usual' d-spacings, reflections are

---

$_{Exp2}$ = 0.70:0.30:0.00) and correspond to the patterns shown in Fig. 2.3.14. (A) Maximum possible degree of ordering (MPDO), $p_{Exp1Exp1} = p_{Exp2Exp1} = p_{Exp1Exp2} = p_{Exp2Exp2} = 0$; (B) $p_{Exp1Exp1} = p_{Exp2Exp1} = 0.11$, $p_{Exp1Exp2} = p_{Exp2Exp2} = 0.04$; (C) $p_{Exp1Exp1} = p_{Exp2Exp1} = 0.22$, $p_{Exp1Exp2} = p_{Exp2Exp2} = 0.08$; (D) $p_{Exp1Exp1} = p_{Exp2Exp1} = 0.33$, $p_{Exp1Exp2} = p_{Exp2Exp2} = 0.12$; (E) $p_{Exp1Exp1} = p_{Exp2Exp1} = 0.44$, $p_{Exp1Exp2} = p_{Exp2Exp2} = 0.16$. Peak positions are indicated for mixed-layer structures with heterogeneous smectite behaviour (w_I:$w_{Exp1:Exp2}$ = 0.70:0.22:0.08).

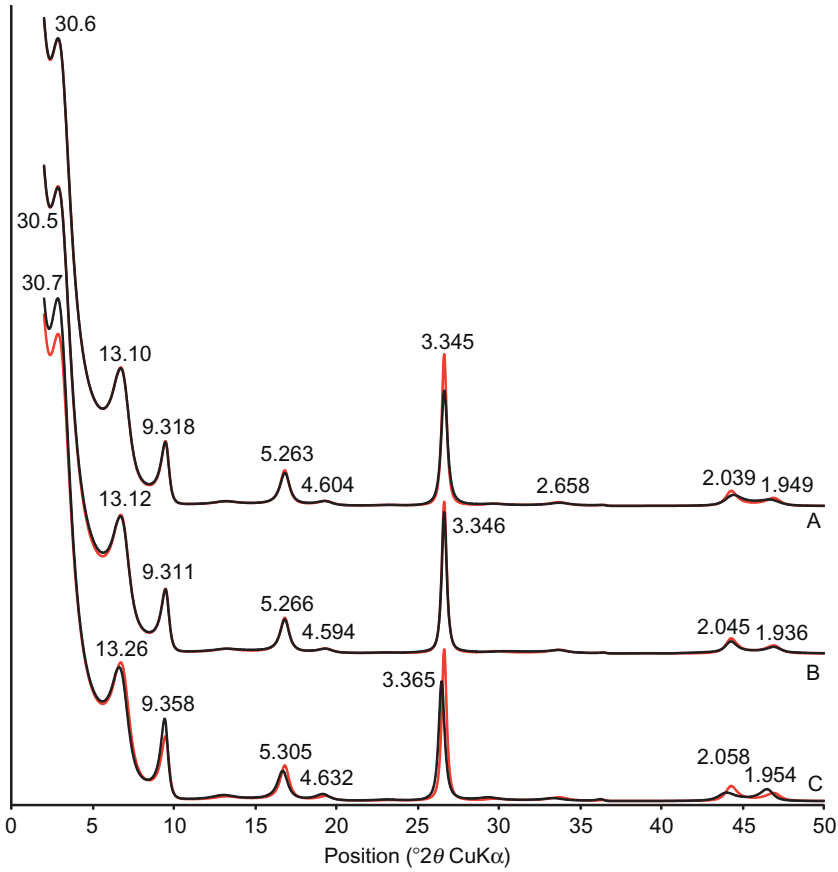

FIGURE 2.3.23 XRD patterns calculated for two-component illite–smectite with identical composition (w_I:w_S = 0.7:0.3) and junction probability at $S = 1$ (MPDO; $p_{SS} = 0$) but contrasting fluctuations of layer thickness (see Section 2.3.5 for details). The grey pattern is systematically calculated with no fluctuation of layer-to-layer distances. (A) The black line is calculated with a Gaussian distribution of defects of the second type for S layers ($\Delta(\xi) = 0.3$). (B) The black line is calculated with a Gaussian distribution of defects of the first type for S layers ($\Delta(\xi) = 0.3$). (C) The black line is calculated with a semi-normal distribution of defects of the second type for S layers ($\Delta(\xi) = +0.3$).

shifted (in this case towards larger d values and lower diffraction angles) compared to the position calculated for defect-free layers (Fig. 2.3.23C).

Figure 2.3.24 shows that XRD patterns calculated for the same average CSD size but different distributions are essentially similar. However, a minor effect may be observed on the relative intensity of the different reflections. In particular, reflection intensity decreases faster with increasing diffraction angle when a lognormal distribution is used compared to Ergun's model (see Section 2.3.4 for details regarding the different distributions).

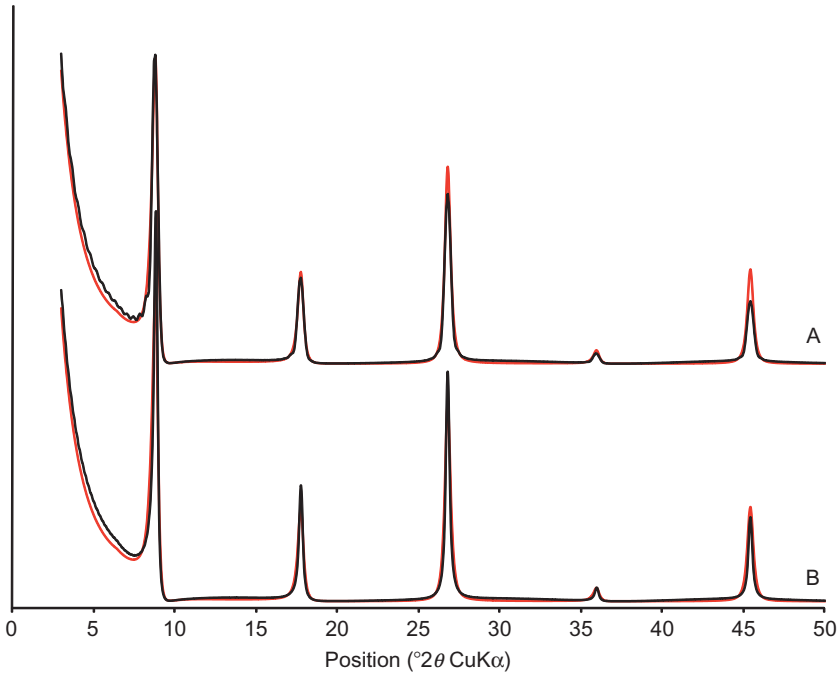

FIGURE 2.3.24 XRD patterns calculated for discrete illite with different distributions of coherent scattering domain sizes (see Section 2.3.4 for details). The grey pattern is systematically calculated for lognormal distribution of CSD sizes ($\overline{N} = 12$ layers). (A) The black line is calculated for a uniform distribution of CSD sizes ($\overline{N} = 12$ layers). (B) The black line is calculated for a Ergun distribution of CSD sizes ($\delta = 15$ layers).

REFERENCES

Allegra, G., 1961. A simplified formula for the calculation of the X-ray intensity diffracted by a monodimensionally disordered structure. Acta Crystallogr. 14, 535.

Allegra, G., 1964. The calculation of the intensity of X-rays diffracted by monodimensionally disordered structures. Acta Crystallogr. 14, 579–586.

Aplin, A.C., Matenaar, I.F., McCarty, D.K., van Der Pluijm, B.A., 2006. Influence of mechanical compaction and clay mineral diagenesis on the microfabric and pore-scale properties of deep-water Gulf of Mexico Mudstones. Clays Clay Miner. 54, 500–514.

Bailey, S.W., 1982. Nomenclature for regular interstratifications. Am. Mineral. 67, 394–398.

Bailey, S.W., Brindley, G.W., Kodama, H., Martin, R.T., 1982. Report of the Clay Minerals Society Nomenclature Committee for 1980–1981: nomenclature for regular interstratifications. Clays Clay Miner. 30, 76–78.

Besson, G., 1980. Structures des smectites dioctaédriques. Paramètres conditionnant les fautes d'empilement des feuillets. Ph.D. Thesis, Université d'Orléans, France.

Bethke, C.G., Altaner, S.P., 1986. Layer-by-layer mechanism of smectite illitization and application to a new rate law. Clays Clay Miner. 34, 136–145.

Brindley, G.W., Méring, J., 1951. Diffraction des Rayons X par les Structures en Couches Désordonnées. Acta Crystallogr. 4, 441–447.

Cesari, M., Allegra, G., 1967. The intensity of X-rays diffracted by monodimensionally disordered structures: case of identical layers and three different translation vectors. Acta Crystallogr. 23, 200–205.

Cesari, M., Morelli, G.L., Favretto, L., 1965. The determination of the type of stacking in mixed-layer clay minerals. Acta Crystallogr. 18, 189–196.

Claret, F., Sakharov, B.A., Drits, V.A., Velde, B., Meunier, A., Griffault, L., Lanson, B., 2004. Clay minerals in the Meuse-Haute marne underground laboratory (France): possible influence of organic matter on clay mineral evolution. Clays Clay Miner. 52, 515–532.

de Courville, J., Tchoubar, D., Tchoubar, D., 1979. Détermination expérimentale de la fonction d'orientation, son application dans le calcul des bandes de diffractions. J. Appl. Crystallogr. 12, 332–338.

Drits, V.A., 1983. Some aspects of the study of the real crystal structure of clay minerals. In: Konta, J. (Ed.), Proceedings of the 5th Meeting of the European Clay Groups, Prague, Univerzita Karlova, pp. 33–42.

Drits, V.A., 1985. Mixed-layer minerals: diffraction methods and structural features. In: Schultz, L.G., Van Olphen, H., Mumpton, F.A. (Eds.), Proceedings of the International Clay Conference, Denver, Clay Minerals Society, pp. 33–45.

Drits, V.A., 1997. Mixed-layer minerals. In: Merlino, S. (Ed.), Modular aspects of minerals. EMU Notes in Mineralogy, vol. 1. Eötvös University Press, Budapest, pp. 153–190.

Drits, V.A., 2003. Structural and chemical heterogeneity of layer silicates and clay minerals. Clay Miner. 38, 403–432.

Drits, V.A., Plançon, A., 1994. Expert system for structural characterization of phyllosilicates. II. Application to mixed-layer minerals. Clay Miner. 29, 39–45.

Drits, V.A., Sakharov, B.A., 1976. X-ray Structure Analysis of Mixed-Layer Minerals. Nauka, Moscow.

Drits, V.A., Tchoubar, C., 1990. X-ray Diffraction by Disordered Lamellar Structures: Theory and Applications to Microdivided Silicates and Carbons. Springer-Verlag, Berlin.

Drits, V.A., Kameneva, M.Y., Sakharov, B.A., Dainyak, L.G., Tsipursky, S.I., Smoliar-Zviagina, B.B., Bookin, A.S., Salyn, A.L., 1993. The Actual Structure of Glauconites and Related Mica-Like Minerals. Nauka, Novosibirsk.

Drits, V.A., Varaxina, T.V., Sakharov, B.A., Plançon, A., 1994. A simple technique for identification of one-dimensional powder X-ray diffraction patterns for mixed-layer illite-smectites and other interstratified minerals. Clays Clay Miner. 42, 382–390.

Drits, V.A., Lindgreen, H., Salyn, A.L., 1997a. Determination of the content and distribution of fixed ammonium in illite-smectite by X-ray diffraction: application to North sea illite-smectite. Am. Mineral. 82, 79–87.

Drits, V.A., Sakharov, B.A., Lindgreen, H., Salyn, A., 1997b. Sequential structure transformation of illite-smectite-vermiculite during diagenesis of Upper Jurassic shales from the North Sea and Denmark. Clay Miner. 32, 351–371.

Drits, V.A., Srodon, J., Eberl, D.D., 1997c. XRD measurement of mean crystallite thickness of illite and illite/smectite: reappraisal of the Kubler index and the Scherrer equation. Clays Clay Miner. 45, 461–475.

Drits, V.A., Eberl, D.D., Srodon, J., 1998. XRD measurement of mean thickness, thickness distribution and strain for illite and illite-smectite crystallites by the Bertaut-Warren-Averbach technique. Clays Clay Miner. 46, 38–50.

Drits, V.A., Ivanovskaya, T.A., Sakharov, B.A., Gor'kova, N.V., Karpova, G.V., Pokrovskaya, E.V., 2001. Pseudomorphous replacement of globular glauconite by mixed-layer chlorite-berthierine in the outer contact of dike: evidence from the Lower Riphean Ust'Il'ya Formation, Anabar uplift. Lithol. Miner. Resour. 36, 337–352.

Drits, V.A., Lindgreen, H., Sakharov, B.A., Jakobsen, H.J., Salyn, A.L., Dainyak, L.G., 2002a. Tobelitization of smectite during oil generation in oil-source shales. Application to North Sea illite-tobelite-smectite-vermiculite. Clays Clay Miner. 50, 82–98.

Drits, V.A., Sakharov, B.A., Dainyak, L.G., Salyn, A.L., Lindgreen, H., 2002b. Structural and chemical heterogeneity of illite-smectites from Upper Jurassic mudstones of East Greenland related to volcanic and weathered parent rocks. Am. Mineral. 87, 1590–1606.

Drits, V.A., Lindgreen, H., Sakharov, B.A., Jakobsen, H.J., Zviagina, B.B., 2004. The detailed structure and origin of clay minerals at the cretaceous/tertiary boundary, Stevns Klint (Denmark). Clay Miner. 39, 367–390.

Drits, V.A., Sakharov, B.A., Salyn, A.L., Lindgreen, H., 2005. Determination of the content and distribution of fixed ammonium in illite-smectite using a modified X-ray diffraction technique: application to oil source rocks of western Greenland. Am. Mineral. 90, 71–84.

Drits, V.A., Lindgreen, H., Sakharov, B.A., Jakobsen, H.J., Fallick, A.E., Salyn, A.L., Dainyak, L.G., Zviagina, B.B., Barfod, D.N., 2007. Formation and transformation of mixed-layer minerals by tertiary intrusives in cretaceous mudstones, West Greenland. Clays Clay Miner. 55, 260–283.

Dudek, T., Srodon, J., 1996. Identification of illite/smectite by X-ray powder diffraction taking into account the lognormal distribution of crystal thickness. Geol. Carpath. 5, 21–32.

Eberl, D.D., Srodon, J., Kralik, M., Taylor, B.E., Peterman, Z.E., 1990. Ostwald ripening of clays and metamorphic minerals. Science 248, 474–477.

Eberl, D.D., Drits, V.A., Srodon, J., 1998. Deducing growth mechanisms for minerals from the shapes of crystal size distributions. Am. J. Sci. 298, 499–533.

Ergun, S., 1970. X-ray scattering by very defective lattices. Phys. Rev. B 1, 3371–3380.

Ewald, P.P., 1940. X- ray diffraction by finite and imperfect crystal lattices. Proc. Phys. Soc. 52, 167–174.

Ferrage, E., Lanson, B., Malikova, N., Plançon, A., Sakharov, B.A., Drits, V.A., 2005a. New insights on the distribution of interlayer water in bi-hydrated smectite from X-ray diffraction profile modeling of 00l reflections. Chem. Mater. 17, 3499–3512.

Ferrage, E., Lanson, B., Sakharov, B.A., Drits, V.A., 2005b. Investigation of smectite hydration properties by modeling experimental X-ray diffraction patterns: part I. Montmorillonite hydration properties. Am. Mineral. 90, 1358–1374.

Ferrage, E., Lanson, B., Sakharov, B.A., Geoffroy, N., Jacquot, E., Drits, V.A., 2007. Investigation of dioctahedral smectite hydration properties by modeling of X-ray diffraction profiles: influence of layer charge and charge location. Am. Mineral. 92, 1731–1743.

Ferrage, E., Lanson, B., Michot, L.J., Robert, J.L., 2010. Hydration properties and interlayer organization of water and ions in synthetic Na-smectite with tetrahedral layer charge. Part 1. Results from X-ray diffraction profile modeling. J. Phys. Chem. C 114, 4515–4526.

Ferrage, E., Sakharov, B.A., Michot, L.J., Delville, A., Bauer, A., Lanson, B., Grangeon, S., Frapper, G., Jimenez-Ruiz, M., Cuello, G.J., 2011a. Hydration properties and interlayer organization of water and ions in synthetic Na-smectite with tetrahedral layer charge. Part 2. Towards a precise coupling between molecular simulations and diffraction data. J. Phys. Chem. C 115, 1867–1881.

Ferrage, E., Vidal, O., Mosser-Ruck, R., Cathelineau, M., Cuadros, J., 2011b. A reinvestigation of smectite illitization in experimental hydrothermal conditions: results from X-ray diffraction and transmission electron microscopy. Am. Mineral. 96, 207–223.

Fogg, A.M., Dunn, J.S., O'Hare, D., 1998. Formation of second-stage intermediates in anion-exchange intercalation reactions of the layered double hydroxide $[LiAl_2(OH)_6]Cl{\cdot}H_2O$ as observed bu time-resolved, *in situ* X-ray diffraction. Chem. Mater. 10, 356–360.

Guggenheim, S., Adams, J.M., Bain, D.C., Bergaya, F., Brigatti, M.F., Drits, V.A., Formoso, M.L.L., Galan, E., Kogure, T., Stanjek, H., 2006. Summary of recommendations of nomenclature committees relevant to clay mineralogy: report of the Association Internationale pour l'Etude des Argiles (AIPEA) Nomenclature Committee for 2006. Clay Miner. 41, 863–877.

Guinier, A., 1964. Théorie et technique de la radiocristallographie. Dunod, Paris.

Hendricks, S., Teller, E., 1942. X-ray interference in partially ordered layer lattices. J. Chem. Phys. 10, 147–167.

Hubert, F., Caner, L., Meunier, A., Lanson, B., 2009. Advances in characterization of soil clay mineralogy using X-ray diffraction: from decomposition to profile fitting. Eur. J. Soil Sci. 60, 1093–1105.

Hubert, F., Caner, L., Meunier, A., Ferrage, E., 2012. Unraveling complex <2 μm clay mineralogy from soils using X-ray diffraction profile modeling on particle-size sub-fractions: implications for soil pedogenesis and reactivity. Am. Mineral. 97, 384–398.

Ijdo, W.L., Pinnavaia, T.J., 1998. Staging of organic and inorganic gallery cations in layered silicate heterostructures. J. Solid State Chem. 139, 281–289.

Inoue, A., Bouchet, A., Velde, B., Meunier, A., 1989. Convenient technique for estimating smectite layer percentage in randomly interstratified illite/smectite minerals. Clays Clay Miner. 37, 227–234.

Inoue, A., Lanson, B., Marques Fernandes, M., Sakharov, B.A., Murakami, T., Meunier, A., Beaufort, D., 2005. Illite-smectite mixed-layer minerals in the hydrothermal alteration of volcanic rocks: I. One-dimensional XRD structure analysis and characterization of component layers. Clays Clay Miner. 53, 423–439.

Jagodzinski, H., 1949a. Eindimensionale Fehlordnung in Kristallen und ihr Einfluss auf die Röntgeninterferenzen: I. Berechnung des Fehlordnungsgrades aus der Röntgenintensitaten. Acta Crystallogr. 2, 201–207.

Jagodzinski, H., 1949b. Eindimensionale Fehlordnung in Kristallen und ihr Einfluss auf die Röntgeninterferenzen. II. Berechnung der fehlgeordneten dichtesten Kugelpackungen mit Wechselwirkungen der Reichweite 3. Acta Crystallogr. 2, 208–214.

Jagodzinski, H., 1949c. Eindimensionale Fehlordnung in Kristallen und ihr Einfluss auf die Röntgeninterferenzen. III. Vergleich der Berechnungen mit experimentellen Ergebnissen. Acta Crystallogr. 2, 298–304.

Jagodzinski, H., 1954. Der Symmetrieeinfluss Auf Den Allgemeinen Losungsansatz Eindimensionaler Fehlordnungsprobleme. Acta Crystallogr. 7, 17–25.

Kakinoki, J., Komura, Y., 1952. Intensity of X-ray diffraction by one dimensionally disordered crystal: I. General derivation in cases of the "Reichweit" S=0 and 1. J. Physical Soc. Japan 7, 30–35.

Kakinoki, J., Komura, Y., 1954a. Intensity of X-ray diffraction by one dimensionally disordered crystal: II. General derivation in the case of the correlation range $S \geq 2$. J. Physical Soc. Japan 9, 169–176.

Kakinoki, J., Komura, Y., 1954b. Intensity of X-ray diffraction by one dimensionally disordered crystal: III. The close-packed structure. J. Physical Soc. Japan 9, 177–183.

Karmous, M.S., Ben Rhaiem, H., Robert, J.L., Lanson, B., Amara, A.B.H., 2009. Charge location effect on the hydration properties of synthetic saponite and hectorite saturated by Na^{+}, Ca^{2+} cations: XRD investigation. Appl. Clay Sci. 46, 43–50.

Klug, H.P., Alexander, L.E., 1974. X-ray Diffraction Procedures for Polycrystalline and Amorphous Materials. Wiley, New York.

Kodama, H., Gatineau, L., Méring, J., 1971. An analysis of X-ray diffraction line profiles of microcrystalline muscovites. Clays Clay Miner. 19, 405–413.

Kogure, T., Hybler, J., Durovic, S., 2001. A HRTEM study of cronstedtite: determination of polytypes and layer polarity in trioctahedral 1:1 phyllosilicates. Clays Clay Miner. 49, 310–317.

Lanson, B., 2011. Modelling of X-ray diffraction profiles: Investigation of defective lamellar structure crystal chemistry. In: Brigatti, M.F., Mottana, A. (Eds.), Bulk and surface structures of layer silicates and oxides: theoretical aspects and applications. EMU Notes in Mineralogy, vol. 11. European Mineralogical Union and the Mineralogical Society of Great Britain, London, pp. 151–202.

Lanson, B., Bouchet, A., 1995. Identification des minéraux argileux par diffraction des rayons X: Apport du traitement numérique. Bull. Centres Rech. Elf Aqu. Product. 19, 91–118.

Lanson, B., Sakharov, B.A., Claret, F., Drits, V.A., 2009. Diagenetic smectite-to-illite transition in clay-rich sediments: a reappraisal of X-ray diffraction results using the multi-specimen method. Am. J. Sci. 309, 476–516.

Lindgreen, H., Drits, V.A., Sakharov, B.A., Salyn, A.L., Wrang, P., Dainyak, L.G., 2000. Illite-smectite structural changes during metamorphism in black Cambrian Alum shales from the Baltic area. Am. Mineral. 85, 1223–1238.

Lindgreen, H., Drits, V.A., Sakharov, B.A., Jakobsen, H.J., Salyn, A.L., Dainyak, L.G., Kroyer, H., 2002. The structure and diagenetic transformation of illite-smectite and chlorite-smectite from North Sea Cretaceous-Tertiary chalk. Clay Miner. 37, 429–450.

Lindgreen, H., Drits, V.A., Jakobsen, F.C., Sakharov, B.A., 2008. Clay mineralogy of the central North Sea Upper Cretaceous-Tertiary chalk and the formation of clay-rich layers. Clays Clay Miner. 56, 693–710.

Ma, C., Eggleton, R.A., 1999. Surface layer types of kaolinite: a high-resolution transmission electron microscope study. Clays Clay Miner. 47, 181–191.

MacEwan, D.M.C., 1958. Fourier transform methods for studying X-ray scattering from lamellar systems: II. The calculation of X-ray diffraction effects for various types of interstratification. Kolloidzeitschrift 156, 61–67.

McCarty, D.K., Drits, V.A., Sakharov, B., Zviagina, B.B., Ruffell, A., Wach, G., 2004. Heterogeneous mixed-layer clays from the Cretaceous greensand, Isle of Wight, southern England. Clays Clay Miner. 52, 552–575.

McCarty, D.K., Sakharov, B.A., Drits, V.A., 2008. Early clay diagenesis in Gulf Coast sediments: new insights from XRD profile modeling. Clays Clay Miner. 56, 359–379.

McCarty, D.K., Sakharov, B.A., Drits, V.A., 2009. New insights into smectite illitization: a zoned K-bentonite revisited. Am. Mineral. 94, 1653–1671.

Méring, J., 1949. L'interférence des rayons-X dans les systèmes à stratification désordonnée. Acta Crystallogr. 2, 371–377.

Méring, J., 1950. Les réflections des rayons X par les minéraux argileux interstratifiés. Proceedings of the 4th International Congress of Soil Science, Amsterdam, 1950, pp. 21–26.

Moore, D.M., Reynolds Jr., R.C., 1997. X-ray Diffraction and the Identification and Analysis of Clay Minerals. Oxford University Press, Oxford.

Plançon, A., 1980. The calculation of intensities diffracted by a partially oriented powder with a layer structure. J. Appl. Crystallogr. 13, 524–528.

Plançon, A., 1981. Diffraction by layer structures containing different kinds of layers and stacking faults. J. Appl. Crystallogr. 14, 300–304.

Plançon, A., 2002. New modeling of X-ray diffraction by disordered lamellar structures, such as phyllosilicates. Am. Mineral. 87, 1672–1677.

Plançon, A., Drits, V.A., 1994. Expert system for structural characterization of phyllosilicates. I. Description of the expert system. Clay Miner. 29, 33–38.

Plançon, A., Drits, V.A., 2000. Phase analysis of clays using an expert system and calculation programs for X-ray diffraction by two- and three-component mixed-layer minerals. Clays Clay Miner. 48, 57–62.

Plançon, A., Tchoubar, C., 1977. Determination of structural defects in phyllosilicates by X-ray powder diffraction. I. Principle of calculation of the diffraction phenomenon. Clays Clay Miner. 25, 430–435.

Pons, C.H., 1980. Mise en évidence des relations entre la texture et la structure dans les systèmes eau-smectites par diffusion aux petits angles du rayonnement-X synchrotron. Ph.D. Thesis. University of Orléans, France.

Reynolds Jr., R.C., 1967. Interstratified clay systems: calculation of the total one-dimensional diffraction function. Am. Mineral. 52, 661–672.

Reynolds Jr., R.C., 1976. The Lorentz factor for basal reflections from micaceous minerals in oriented powder aggregates. Am. Mineral. 61, 484–491.

Reynolds Jr., R.C., 1980. Interstratified clay minerals. In: Brindley, G.W., Brown, G. (Eds.), Crystal Structures of Clay Minerals and Their X-ray Identification. The Mineralogical Society, London, pp. 249–359.

Reynolds Jr., R.C., 1983. Calculation of absolute diffraction intensities for mixed-layered clays. Clays Clay Miner. 31, 233–234.

Reynolds Jr., R.C., 1985. NEWMOD: A Computer Program for the Calculation of One-Dimensional Patterns of Mixed-Layered Clays. Hanover, NH.

Reynolds Jr., R.C., 1986. The Lorentz-polarization factor and preferred orientation in oriented clay aggregates. Clays Clay Miner. 34, 359–367.

Reynolds Jr., R.C., 1988. Mixed layer chlorite minerals. In: Bailey, S.W. (Ed.), Hydrous Phyllosilicates (Exclusive of Micas). Reviews in Mineralogy, vol. 19. Mineralogical Society of America, Washington, DC, pp. 601–630.

Ruland, W., Tompa, H., 1968. Effect of preferred orientation on intensity distribution of *hk* interferences. Acta Crystallogr. A 24, 93–99.

Ruland, W., Tompa, H., 1972. Influence of preferred orientation on line width and peak shift of *hk* interferences. J. Appl. Crystallogr. 5, 225–230.

Sakharov, B.A., 2005. Improved model for simulation of experimental XRD patterns for clays including mixed-layer clay minerals. Proceedings of the Clay Minerals Society 42nd Annual Meeting, Burlington, Vermont, pp. 95.

Sakharov, B.A., Naumov, A.S., Drits, V.A., 1982a. X-ray diffraction by mixed-layer structures with random distribution of stacking faults. Dokl. Akad. Nauk 265, 339–343 (in Russian).

Sakharov, B.A., Naumov, A.S., Drits, V.A., 1982b. X-ray intensities scattered by layer structures with short-range ordering parameters $S \geq 1$ and $G \geq 1$. Dokl. Akad. Nauk 265, 871–874 (in Russian).

Sakharov, B.A., Naumov, A.S., Drits, V.A., 1983. X-ray scattering by defect layer structures. Kristallografia 28, 951–958 (in Russian).

Sakharov, B.A., Lindgreen, H., Salyn, A., Drits, V.A., 1999a. Determination of illite-smectite structures using multispecimen X-ray diffraction profile fitting. Clays Clay Miner. 47, 555–566.

Sakharov, B.A., Lindgreen, H., Salyn, A.L., Drits, V.A., 1999b. Mixed-layer kaolinite-illite-vermiculite in North Sea shales. Clay Miner. 34, 333–344.

Sakharov, B.A., Dubinska, E., Bylina, P., Kozubowski, J.A., Kapron, G., Frontczak Baniewicz, M., 2004a. Serpentine-smectite interstratified minerals from Lower Silesia (SW Poland). Clays Clay Miner. 52, 55–65.

Sakharov, B.A., Plançon, A., Lanson, B., Drits, V.A., 2004b. Influence of the outer surface layers of crystals on the X-ray diffraction intensity of basal reflections. Clays Clay Miner. 52, 680–692.

Sato, M., 1965. Structure of interstratified (mixed-layer) minerals. Nature 208, 70–71.

Sato, M., 1969a. Interstratified structures. Z. Kristallogr. 129, 388–395.

Sato, M., 1969b. Interstratified structures with Reichweite g = 2 and its X-ray diffraction pattern. In: Heller, L. (Ed.), Proceedings of the International Clay Conference, Tokyo. Israel University Press, Jerusalem, pp. 207–214.

Srodon, J., 1980. Precise identification of illite/smectite interstratifications by X-ray powder diffraction. Clays Clay Miner. 28, 401–411.

Srodon, J., 1981. X-Ray identification of randomly interstratified illite-smectite in mixtures with discrete illite. Clay Miner. 16, 297–304.

Srodon, J., 1984. X-ray powder diffraction of illitic materials. Clays Clay Miner. 32, 337–349.

Srodon, J., Eberl, D.D., Drits, V.A., 2000. Evolution of fundamental-particle size during illitization of smectite and implications for reaction mechanism. Clays Clay Miner. 48, 446–458.

Taylor, R.M., Norrish, K., 1966. The measurement of orientation distribution and it sapplication to quantitative X-ray diffraction analysis. Clay Miner. 6, 127–141.

Tomita, K., Takashi, H., 1985. Curves for the quantification of mica/smectite and chlorite/smectite interstratifications by X-ray powder diffraction. Clays Clay Miner. 33, 379–390.

Tomita, K., Takashi, H., Watanabe, T., 1988. Quantification curves for mica/smectite interstratifications by X-ray powder diffraction. Clays Clay Miner. 36, 258–262.

Tsipursky, S.J., Eberl, D.D., Buseck, P.R., 1992. Unusual tops (bottoms ?) of particles of 1M illite from the Silverton caldera (CO). In: Proceedings of the American Society of Agronomy annual meeting, American Society of Agronomy, Madison, WI, pp. 381–382.

Velde, B., Suzuki, T., Nicot, E., 1986. Pressure-temperature-composition of illite/smectite mixed-layer minerals: Niger delta mudstones and other examples. Clays Clay Miner. 34, 435–441.

von Laue, M., 1932. Spectra of square lattices. Z. Kristallogr. 82, 127–141.

Warren, B.E., 1941. X-ray diffraction in random layer lattices. Phys. Rev. 59, 693–698.

Watanabe, T., 1981. Identification of illite/montmorillonite interstratification by X-ray powder diffraction. J. Mineral. Soc. Jpn. 15, 32–41 (Special issue).

Watanabe, T., 1988. The structural model of illite/smectite interstratified mineral and the diagram for their identification. Clay Sci. 7, 97–114.

Wilson, A.J.C., 1942. Imperfections in the structure of cobalt. II. Mathematical treatment of proposed structure. Proc. R. Soc. Lond. Ser. A Math. Phys. Sci. 180, 0277–0285.

Wilson, A.J.C., 1949a. X-ray optics: the diffraction of X-rays by finite and imperfect crystals. Methuen's Monographs on Physical Subjects. Methuen & Co Ltd., London, UK.

Wilson, A.J.C., 1949b. X-ray diffraction by random layers: ideal line profiles and determination of structure amplitudes from observed line profiles. Acta Crystallogr. 2, 245–251.

Yuan, H.J., Bish, D.L., 2010. NEWMOD+, a new version of the NEWMOD program for interpreting X-ray powder diffraction patterns from interstratified clay minerals. Clays Clay Miner. 58, 318–326.